

Universidade Federal do Rio Grande - FURG
Instituto de Oceanografia
Programa de Pós-Graduação em Oceanologia

**Variabilidade Espaço-Temporal da
fugacidade do CO₂ no sudoeste do oceano
Atlântico Sul**

Ciro Cataneo Liutti

Dissertação apresentada ao
Programa de Pós-Graduação em
Oceanologia, como parte dos
requisitos para a obtenção do
Título de Mestre.

Orientador: Prof. Dr. Rodrigo Kerr Duarte Pereira

Rio Grande, RS, Brasil

Junho de 2019

Variabilidade Espaço-Temporal da fugacidade do CO₂ no sudoeste do oceano Atlântico Sul

Dissertação apresentada ao Programa de Pós-Graduação em Oceanologia,
como parte dos requisitos para a obtenção do Título de Mestre

por

Ciro Cataneo Liutti

Rio Grande, RS, Brasil

Junho de 2019

© A cópia parcial e a citação de trechos desta tese são permitidas sobre a condição de que qualquer pessoa que a consulte reconheça os direitos autorais do autor. Nenhuma informação derivada direta ou indiretamente desta obra deve ser publicada sem o consentimento prévio e por escrito do autor.

Liutti, Ciro Cataneo

Variabilidade Espaço-Temporal da fugacidade do CO₂ no sudoeste do oceano Atlântico Sul / Ciro Cataneo Liutti. – Rio Grande: FURG, 2019.

Número de páginas p. 75

Dissertação (Mestrado) – Universidade Federal do Rio Grande. Mestrado em Oceanologia. Área de Concentração: Física dos Oceanos e Clima.

1. Dióxido de carbono.
 2. Parâmetros do sistema carbonato.
 3. Algoritmos de $f\text{CO}_2$.
 4. Oceano Atlântico Sul.
 5. Tendência anual da $f\text{CO}_2$.
 6. Forçantes da $f\text{CO}_2$.
- I. Titulo. Variabilidade Espaço-Temporal da fugacidade do CO₂ no sudoeste do oceano Atlântico Sul.



UNIVERSIDADE FEDERAL DO RIO GRANDE - FURG
IO - INSTITUTO DE OCEANOGRAFIA
PROGRAMA DE PÓS-GRADUAÇÃO EM OCEANOLOGIA
E-mail: ccpofqg@furg.br – home-page: www.pgo.furg.br



ATA ESPECIAL DE DEFESA DE DISSERTAÇÃO DE MESTRADO – 07/2019

Às nove horas do dia dezoito de junho do ano de dois mil e dezenove, na Sala de Reuniões - IO - FURG/Carreiros, reuniu-se a Comissão Examinadora da Dissertação de MESTRADO intitulada "**Variabilidade Espaço-Temporal da Fugacidade do CO₂ no Sudoeste do Oceano Atlântico Sul**", do Acad. Ciro Cataneo Liutti. A Comissão Examinadora foi composta pelos seguintes membros: Prof. Dr. Rodrigo Kerr - Orientador / Presidente - (IO-FURG), Prof. Dr. Mauricio Mata – (IO-FURG) e Prof. Dr. Humberto Marotta – (UFF). Dando início à reunião, o Coordenador do Programa de Pós-Graduação em Oceanologia, e presidente da sessão, Prof. Dr. Rodrigo Kerr, agradeceu a presença de todos, e fez a apresentação da Comissão Examinadora. Logo após, esclareceu que o Candidato teria de 45 a 60 min para explanação do tema, e cada membro da Comissão Examinadora, um tempo máximo de 30 min para perguntas. A seguir, passou à palavra ao Candidato, que apresentou o tema e respondeu às perguntas formuladas. Após ampla explanação, a Comissão Examinadora reuniu-se em reservado para discussão do conceito a ser atribuído ao Candidato. Foi estabelecido que as sugestões de todos os membros da Comissão Examinadora, que seguem em pareceres em anexo, foram aceitas pelo Orientador/Candidato para incorporação na versão final da Dissertação. Finalmente, a Comissão Examinadora considerou o candidato **APROVADO**, por unanimidade. Nada mais havendo a tratar, foi lavrada a presente ATA, que após lida e aprovada, será assinada pela Comissão Examinadora, pelo Candidato e pelo Coordenador do Programa de Pós-Graduação em Oceanologia.

Prof. Dr. Rodrigo Kerr
Presidente

Prof. Dr. Mauricio Mata

Prof. Dr. Humberto Marotta

Acad. Ciro C. Liutti

**“I am the master of my fate:
I am the captain of my soul.”**

Invictus – William E. Henley

Agradecimentos

Tenho a obrigação de agradecer à minha família pelo apoio que me deram nessa maratona, que foi minha carreira acadêmica até esse momento. Principalmente aos meus pais, que confiaram nas minhas escolhas e sempre me ajudaram a perseguir meus objetivos. E a minha irmã, que por mais que briguemos, consegue dizer que tem orgulho de mim.

Agradeço à Universidade Federal do Rio Grande – FURG por ser minha casa nos últimos 8 anos, ao Instituto de Oceanografia por ter me ensinado o significado de ser um Oceanólogo e, principalmente, ao Laboratório de Estudos dos Oceanos e Clima – LEOC por ter me dado ótimas experiências e amigos.

A Mariah, por ter me levantado quando eu caia e ter me acalmado nos momentos de estresse.

A Iole, que mesmo quando estava distante, não deixou de me mostrar o caminho certo quando estava perdido.

Ao professor Rodrigo Kerr, pela orientação desde a graduação e por ter me aturado todo esse tempo.

Aos amigos que o Cassino me deu, pelos melhores momentos dos últimos anos.

E, por fim, ao Programa de Pós-Graduação em Oceanologia e a Coordenação de Aperfeiçoamento de Pessoal de Nível Superior – CAPES, pela oportunidade e suporte para o desenvolvimento desse trabalho.

Índice

Agradecimentos.....	vi
Lista de Figuras da Dissertação	x
Lista de Figuras do Artigo.....	xi
Lista de Tabelas da Dissertação.....	xiii
Lista de Tabelas do Artigo.....	xiv
Lista de Acrônimos, Abreviações e Símbolos.....	xv
Resumo.....	xvii
Abstract.....	xviii
Capítulo I: Introdução.....	1
I.I – Introdução.....	1
I.II – Objetivos.....	6
Capítulo II: Dados e Métodos.....	7
II.I – Área de Estudo.....	7
II.II – Dados utilizados para desenvolvimento e teste dos algoritmos para $f\text{CO}_2$ na água do mar	10
II.III – Banco de dados na reconstrução da distribuição da $f\text{CO}_2$ na água do mar.....	13
II.IV – Algoritmos da $f\text{CO}_2$ na água do mar.....	14
II.V - Avaliação da distribuição espacial e comportamento temporal da $f\text{CO}_2$ na água do mar.....	15
II.VI - As forçantes da variabilidade da $f\text{CO}_2$ na água do mar.....	16
Capítulo III: Artigo Científico.....	19
1. Introduction.....	20

2. Data and Methods.....	24
2.1. <i>Study area</i>	24
2.2. <i>Database used to develop and assess the seawater fCO₂ algorithms</i>	26
2.3. <i>Database used to reconstruct the distribution of seawater fCO₂</i>	29
2.4. <i>Seawater fCO₂ algorithms</i>	29
2.5. <i>Evaluation of the spatial distribution and temporal behavior of seawater fCO₂</i>	30
2.6. <i>Drivers of the variability of seawater fCO₂</i>	31
3. Results.....	32
3.1. <i>Assessment of the seawater fCO₂ algorithms</i>	32
3.2. <i>Spatial distribution and temporal behavior of seawater fCO₂</i>	35
3.3. <i>Spatial distribution of Alk and DIC</i>	40
3.4. <i>Drivers of the variability in seawater fCO₂</i>	41
4. Discussion.....	47
4.1. <i>The performance of the seawater fCO₂ algorithms</i>	47
4.2. <i>Spatiotemporal distribution of the seawater fCO₂ in the southwestern South Atlantic Ocean</i>	49
4.3. <i>What are the main drivers of seawater fCO₂ in the biogeochemical provinces of the southwestern South Atlantic Ocean?</i>	52
5. Summary and conclusions.....	54
Acknowledgements.....	55
Supplementary Material.....	56

Capítulo IV: Síntese dos resultados e discussão.....	63
IV.I – Algoritmos da $f\text{CO}_2$ na água do mar.....	63
IV.II – Distribuição espacial e comportamento temporal da $f\text{CO}_2$ na água do mar.....	64
IV.III – Quais são as principais forçantes que controlam a variabilidade da $f\text{CO}_2$ na água do mar na região?.....	65
Capítulo V: Perspectivas Futuras.....	67
Referências Bibliográficas.....	68

Listas de Figuras da Dissertação

Figura 1. Províncias biogeoquímicas do sudoeste do oceano Atlântico Sul: região de Abrolhos-Campos (ACR), *South Brazil Bight* (SBB), *Southern Brazilian Shelf* (SBS) e região offshore. A região em branco, que é delimitada pelas linhas pontilhadas, mostra a região de ressurgência na ACR, enquanto as setas brancas na SBS mostram os sentidos da intrusão de água provenientes da pluma do Rio da Plata e do sistema Patos-Mirim. A Corrente do Brasil (*Brazil Current*) tem seu sentido e área de influência mostrada pela seta preta. O limite entre a plataforma continental (o limite das áreas ACR, SBB e SBS) e a região offshore foi definido seguindo a linha batimétrica de 200 metros.....pág. 5

Figura 2. A distribuição espacial do banco de dados usado para desenvolver e testar os algoritmos de $f\text{CO}_2$. O dado usado para desenvolver o algoritmo para Outono-Inverno (*Fall-Winter*; pontos vermelhos) e Primavera-Verão (*Spring-Summer*; pontos verdes), enquanto a seção do cruzeiro FORSA (pontos azuis) foi usada para validar o algoritmo. A divisão das regiões (ACR, SBB, SBS e Offshore) é representada pelos pontos pretos e a batimetria é mostrada em tons de cinza.....pág. 11

Lista de Figuras do Artigo

Figure 2. Regional biogeochemical provinces of the southwestern South Atlantic Ocean: Abrolhos-Campos Region (ACR), South Brazil Bight (SBB), Southern Brazilian Shelf (SBS), and offshore regions. The white region within dotted lines highlights the upwelling zone of the ACR, while the white arrows at the SBS depict the inflow of continental waters from the La Plata River and the Patos-Mirim Lagoon plumes. The Brazil Current is depicted by black straight arrows. The border between the continental shelf (defining the areas of ACR, SBB, and SBS) and offshore regions is defined by the 200 m isobaths.....pág. 24

Figure 2. Spatial distribution of the dataset used to create and assess the $f\text{CO}_2$ algorithms. The data used to develop the Fall-Winter (red lines) and Spring-Summer algorithms (black lines), while the FORSA cruise section (blue line) was used to validate the algorithm. The bathymetry is expressed on gray shades.....pág. 27

Figure 3. The seawater $f\text{CO}_2$ (μatm) reconstruction along the FORSA cruise section (Fig. 2 in blue dots) using the Fall-Winter algorithm: modeled (black) and observed (gray) data. The values shown are the coefficient of determination (r^2), p-value and root-mean-square error (RMSE) between the predicted and the modeled $f\text{CO}_2$ data.....pág. 34

Figure 4. Spatial distribution of the difference in seawater $f\text{CO}_2$ (μatm) between both developed algorithms (i.e., the results obtained with the Spring-Summer algorithm minus the results obtained with the Fall-Winter algorithm) in the two last months of each seasonal period (i.e., February and August). The map (a) shows the absolute seawater $f\text{CO}_2$ difference for February and (b) August, the last months of the Spring-Summer and Fall-Winter periods, respectively.....pág. 35

Figure 5. Spatial distribution of the seawater $f\text{CO}_2$ (μatm) in the study region for each month of the year. The panels show the averaged maps from 2011-2015. The exception is July, which was compiled for the period 2012-2015.....pág. 37

Figure 6. Interannual variability in the seawater $f\text{CO}_2$ (μatm) during the analyzed period (August 2011 to June 2015) for the (a) entire studied region, (b) Abrolhos-Campos Region (ACR), (c) South Brazil Bight (SBB), (d) Southern Brazilian Shelf (SBS), and (e) offshore region. The black line depicts the monthly $f\text{CO}_2$, and the gray dashed lines depict one standard deviation from the monthly averaged $f\text{CO}_2$pág. 39

Figure 7. Averaged spatial distribution of the hydrographic and marine carbonate system parameters between 2011-2015: (a) seawater $f\text{CO}_2$ (μatm), (b) SST ($^{\circ}\text{C}$), (c) SSS, (d) Alk ($\mu\text{mol kg}^{-1}$), and (e) DIC ($\mu\text{mol kg}^{-1}$).....pág. 41

Figure 8. Spatial distribution of the seawater $f\text{CO}_2$ anomalies and parameter drivers of the seawater $f\text{CO}_2$ in the southwestern South Atlantic Ocean (μatm). The panels show the spatial distribution of (a) the seawater $f\text{CO}_2$ anomalies and the driver effect of (b) sea surface temperature (SST), (c) sea surface salinity (SSS), (d) salinity-normalized total alkalinity (Alkn) and (e) salinity-normalized total dissolved inorganic carbon (DICn).....pág. 43

Figure 9. Drivers' influence on the seawater $f\text{CO}_2$ variability in μatm for each biogeochemical province in the southwestern South Atlantic Ocean: (a) entire studied region, (b) Abrolhos-Campos Region (ACR), (c) South Brazil Bight (SBB), (d) Southern Brazilian Shelf (SBS), and (e) offshore region. The bars represent the influence of sea surface temperature (SST, blue), sea surface salinity (SSS, orange), salinity-normalized total alkalinity (Alkn, gray), and salinity-normalized total dissolved inorganic carbon (DICn; yellow) on the spatial distribution of the seawater $f\text{CO}_2$. The black bar represents the sum of the $f\text{CO}_2$ anomalies (i.e., seawater $f\text{CO}_2$ – regional mean $f\text{CO}_2$).....pág. 44

Figure 10. Seasonal cycle of the parameter drivers of the seawater $f\text{CO}_2$ in the (a) entire studied region and each subregion analyzed in this study: (b) Abrolhos-Campos Region (ACR), (c) South

Brazil Bight (SBB), (d) Southern Brazilian Shelf (SBS), and (e) offshore region. Temporal anomaly of the seawater $f\text{CO}_2$ (μatm ; black) and the drivers of the seawater $f\text{CO}_2$ (μatm ; in color). The drivers evaluated are sea surface temperature (SST, blue), sea surface salinity (SSS, orange), salinity-normalized total alkalinity (Alkn, gray), and salinity-normalized total dissolved inorganic carbon (DICn, yellow).....pág. 46

Figure S1. Spatial distribution of the SST ($^{\circ}\text{C}$) of the study region. The panels show the averaged maps for each month from 2011-2015. The exception is July, which was compiled for the period 2012-2015pág. 57

Figure S2. Spatial distribution of the SSS of the study region. The panels show the averaged maps for each month from 2011-2015. The exception is July, which was compiled for the period 2012-2015.....pág. 58

Figure S3. Spatial distribution of the Chla (mg m^{-3}) of the study region. The panels show the averaged maps for each month from 2011-2015. The exception is July, which was compiled for the period 2012-2015.....pág. 59

Figure S4. Seasonal cycle of the regional seawater $f\text{CO}_2$ (μatm) during the analyzed period (August 2011 to June 2015) for the (a) entire studied region in the southwestern South Atlantic Ocean, (b) Abrolhos-Campos Region (ACR), (c) South Brazil Bight (SBB), (d) Southern Brazilian Shelf (SBS) and (e) offshore region.....pág. 60

Figure S5. The annual seawater $f\text{CO}_2$ trend (μatm) based on the difference between the $f\text{CO}_2$ in each month and the respective monthly average (gray line) for the (a) entire studied region, (b) Abrolhos-Campos Region (ACR), (c) South Brazil Bight (SBB), (d) Southern Brazilian Shelf (SBS), and (e) offshore region. The annual trend for each biogeochemical province is shown in each panel. The trend is represented by a black dotted line.....pág. 61

Figure S6. Spatial distribution of the $f\text{CO}_2$ anomalies and $f\text{CO}_2$ drivers in the Plata River Plume region (μatm). Map a) is the spatial distribution of the $f\text{CO}_2$ anomaly; map b) is the spatial distribution of the effect of SST as a driver of $f\text{CO}_2$; map c) is the spatial distribution of the effect of SSS as a driver of $f\text{CO}_2$; map d) is the spatial distribution of the effect of Alk on $f\text{CO}_2$; and map e) is the spatial distribution of the effect of DIC as a driver of $f\text{CO}_2$pág. 62

Listas de Tabelas da Dissertação

Tabela 1. As médias e desvios padrões do banco de dados utilizados para desenvolvimento dos algoritmos sazonais da $f\text{CO}_2$ na água do mar: Primavera-Verão (setembro até fevereiro) e Outono-Inverno (março até agosto). A tabela mostra a $f\text{CO}_2$ na água do mar (μatm), temperatura superficial da água do mar (SST, $^{\circ}\text{C}$), salinidade superficial da água do mar (SSS) e concentração de clorofila- α (Chla, mg m^{-3}) para toda a área de estudo, no sudoeste do oceano Atlântico Sul, e para as divisões regionais e sazonais. Região de Abrolhos-Campos (ACR), *South Brazil Bight* (SBB), *Southern Brazilian Shelf* (SBS) e região offshore (offshore).....pág. 12

Lista de Tabelas do Artigo

Table 2. Average and standard deviation values of the dataset used to develop the seasonal algorithms for seawater carbon dioxide fugacity ($f\text{CO}_2$): Spring-Summer (September to February) and Fall-Winter (March to August). The table shows seawater $f\text{CO}_2$ (μatm), sea surface temperature (SST, $^{\circ}\text{C}$), sea surface salinity (SSS), and chlorophyll-a concentration (Chla, mg m^{-3}) for the entire study area in the southwestern South Atlantic Ocean and each regional and seasonal division. Abrolhos-Campos Region (ACR), South Brazil Bight (SBB), Southern Brazilian Shelf (SBS), and offshore region (offshore).....pág. 28

Table 2. Correlation coefficients (r) between $f\text{CO}_2$ and the other parameters (SST, SSS and Chla) for Spring-Summer (September to February) and Fall-Winter (March to August). All p -values are <0.05pág. 33

Table 3. Algorithms obtained for each seasonal division following Eq. 1: Spring-Summer (September to February); Fall-Winter (March to August). Each β has a specific unit, where β_0 is μatm , β_1 is μatm per $^{\circ}\text{C}$, β_2 is μatm per salinity unit, and β_3 μatm per mg m^{-3} of chlorophyll a. Also shown are the coefficient of determination (r^2), root-mean-squared error (RMSE) and number of stations (n) used to develop each algorithm.....pág. 33

Table 4. Regional averages and deviations of Alk ($\mu\text{mol kg}^{-1}$) and DIC ($\mu\text{mol kg}^{-1}$) for each region and the region affected by the Plata River's plume. The Plata plume region was excluded from the other regions.....pág. 42

Table 5. List of previous studies that used seawater CO_2 algorithms developed for the southwestern South Atlantic Ocean and their respective performances, sampling periods, evaluated parameters (i.e., $p\text{CO}_2$, $Np\text{CO}_2$, $f\text{CO}_2$, $Nf\text{CO}_2$), correlation coefficient values (r^2), associated errors (i.e., *Root-mean-square error or **Standard Error; μatm), and sample numbers (n). $Np\text{CO}_2$ and $Nf\text{CO}_2$ are the forms of $p\text{CO}_2$ and $f\text{CO}_2$ normalized by the mean sampled temperature, respectively.....pág. 48

Lista de Acrônimos, Abreviações e Símbolos

A

ACR - região Abrolhos-Campos
(*Abrolhos-Campos region*)

Alk - alcalinidade total (*total alkalinity*)

Alkn - Alk normalizada pela salinidade (*Alk normalized by the salinity*)

C

Chla - concentração de clorofila-a
(*chlorophyll-a concentration*)

CO₂ - dióxido de carbono (*carbon dioxide*)

D

DIC - carbono inorgânico dissolvido
(*total dissolved inorganic carbon*)

DICn - DIC normalizado pela salinidade (*DIC normalized by the salinity*)

F

fCO₂ - fugacidade do CO₂ (*carbon dioxide's fugacity*)

FORSA - *Following Ocean Rings in the South Atlantic*

G

GOAL - Grupo Brasileiro de Oceanografia de Altas Latitudes

H

H₂CO₃ - ácido carbônico (*carbonic acid*)

HCO₃⁻ - bicarbonato (*bicarbonate*)

HSO₄⁻ - sulfato de hidrogênio
(*hydrogen sulfate*)

K

K₁ - constante de dissolução do H₂CO₃ (*H₂CO₃ dissociation constant*)

K₂ - constante de dissolução do HCO₃⁻ (*HCO₃⁻ dissociation constant*)

km - quilômetros (*kilometers*)

L

LDEO v2017 - Global Surface pCO₂ Database v2017

M

m - metros (*meters*)

mg/m³ - miligramas por metro cúbico
(*milligrams per cubic meter*)

MLR - regressão multilinear (*multiple linear regression*)

MODIS Aqua - *The Moderate Resolution Imaging Spectroradiometer Aqua*

O

°C - Graus Celsius (*Celsius degrees*)

ODV - Ocean Data View

P

pCO₂ - pressão parcial do CO₂ (*CO₂ partial pressure*)

R

r² - coeficiente de determinação
(*coefficient of determination*)

RMSE - erro médio quadrático (*root-mean-squared error*)

S

SBB - *South Brazil Bight*

SBS - *Southern Brazilian Shelf*

SOCATv5 - Surface Ocean CO₂ Atlas v.5

SSS - salinidade superficial do mar
(*sea surface salinity*)

SST - temperatura superficial do mar
(*sea surface temperature*)

STSF - Frente Subtropical de Plataforma (*Subtropical Shelf Front*)

Símbolos

β - coeficiente de multiplicação
(*multiplier coefficient*)

µatm - microatmosfera
(*microatmosphere*)

µmol kg⁻¹ - micromol por quilograma
(*micromol per kilogram*)

Resumo

O oceano Atlântico tem uma função importante no ciclo global do dióxido de carbono (CO_2), contudo o Atlântico Sul é menos amostrado em comparação ao Atlântico Norte. Para entender o comportamento da fugacidade do CO_2 ($f\text{CO}_2$) no sudoeste do oceano Atlântico Sul, foram desenvolvidos dois modelos sazonais (representando períodos de Primavera-Verão e Outono-Inverno no hemisfério sul) para reproduzir a variabilidade espaço-temporal da $f\text{CO}_2$ entre 2011-2015. Os modelos de $f\text{CO}_2$ foram produzidos usando modelos de regressão multilinear a partir de dados *in situ* provenientes dos bancos de dados do SOCATv5, LDEO v2017, e GOAL. A avaliação espaço-temporal da $f\text{CO}_2$ foi investigada nos regimes de oceano aberto e plataforma continental, sendo que a última foi dividida nas províncias biogeoquímicas de Abrolhos-Campos (ACR), South Brazil Bight (SBB) e Southern Brazilian Shelf (SBS). Ambos os modelos reproduziram bem a distribuição espacial da $f\text{CO}_2$ na região de estudo, com melhor reprodução do regime da plataforma nas margens brasileiras. O modelo para Primavera-Verão apresentou um coeficiente de determinação (r^2) de 0.71 e um erro médio quadrático (RMSE) de 13.81 μatm , enquanto o modelo para Outono-Inverno apresentou um r^2 de 0.64 e um RMSE de 10.05 μatm . Os modelos foram testados utilizando o banco de dados provenientes do cruzeiro FORSA, que ocorreu durante o inverno de 2015. Este teste apresentou bons resultados na comparação entre as saídas do modelo de $f\text{CO}_2$ e os dados observados no FORSA ($r^2=0.95$ e RMSE=16.22 μatm). Em geral, a variabilidade sazonal da $f\text{CO}_2$ sobre a plataforma é controlada pelas dinâmicas da Corrente do Brasil e pela oscilação da posição da Frente Subtropical de Plataforma (STSF). A ressurgência costeira na ACR também apresentou influência sobre variações da $f\text{CO}_2$ na região. As oscilações sazonais no sudoeste do Atlântico Sul são controladas por variações entre as principais forçantes, com a temperatura superficial do oceano controlando as variações entre dezembro e maio, e a distribuição do carbono inorgânico dissolvido total controlando as alterações entre junho e novembro. As regiões influenciadas pelas oscilações da STSF (i.e., SBS e SBB) mostraram que a distribuição da alcalinidade apresenta a maior influência da $f\text{CO}_2$ durante o outono.

Palavras-chaves: Dióxido de carbono, Parâmetros do sistema carbonato, Algoritmos de $f\text{CO}_2$, Oceano Atlântico Sul, Tendência anual da $f\text{CO}_2$, Forçantes da $f\text{CO}_2$.

Abstract

The Atlantic Ocean plays an important role on the global carbon dioxide (CO_2) cycle, however the South Atlantic is comparatively less sampled than the North Atlantic. In order to understand the behaviour of the seawater CO_2 fugacity ($f\text{CO}_2$) in the southwestern South Atlantic Ocean, we developed two seasonal algorithms (representing the periods of Spring-Summer and Fall-Winter in the Southern Hemisphere) to reproduce the spatiotemporal variability of the seawater $f\text{CO}_2$ between 2011-2015. The $f\text{CO}_2$ algorithms were developed using multilinear regression with *in situ* data from SOCATv5, LDEO v2017, and Brazilian GOAL databases. Thus, allowing to include the continental shelf regime in the algorithms. The spatiotemporal variability of the seawater $f\text{CO}_2$ was investigated on the open ocean and continental shelf regimes, with the latter subdivided into the biogeochemical provinces of the Abrolhos-Campos region (ACR), the South Brazil Bight (SBB), and the Southern Brazilian Shelf (SBS). Both seasonal algorithms well reproduced the seawater $f\text{CO}_2$ spatial distribution in the study region, with an improved representation on the continental shelves of the south and southeast Brazilian margins. The Spring-Summer algorithm had a coefficient of determination (r^2) of 0.71 and a root-mean-squared error (RMSE) of 13.81 μatm , while the Fall-Winter algorithm had a $r^2=0.64$ and RMSE=10.05 μatm . The algorithms were assessed using the FORSA cruise dataset conducted during the winter of 2015, achieving a good agreement between modelled $f\text{CO}_2$ outputs and observations ($r^2=0.95$ and RMSE=16.22 μatm). In general, the seawater $f\text{CO}_2$ seasonal variability on the continental shelf regime was controlled by the dynamics of the Brazilian Current and oscillations of the Subtropical Shelf Front position. The coastal upwelling on the ACR also influences the seawater $f\text{CO}_2$ variations in the region. In general, the seawater $f\text{CO}_2$ seasonal oscillation in the southwestern South Atlantic Ocean is driven by swings between the main drivers, with sea surface temperature controlling the changes between December-May and total dissolved inorganic carbon between June-November. The regions influenced by displacements of the Subtropical Shelf Front (i.e., SBS and SBB) show that distribution of total alkalinity also have a major influence on seawater $f\text{CO}_2$ control during Fall.

Key words: Carbon dioxide, Carbonate system parameters, $f\text{CO}_2$'s algorithm, Brazilian Continental Shelf, Annual $f\text{CO}_2$ trends, $f\text{CO}_2$ drivers.

Capítulo I: Introdução

I.I - Introdução

O dióxido de carbono (CO_2) é conhecido como um dos principais gases do efeito estufa ([Millero, 2007](#)) e a concentração deste gás na atmosfera vem sofrendo um aumento constante desde a Revolução Industrial ([Le Quéré et al., 2018](#)). O oceano é responsável tanto pela captura do excedente do CO_2 quanto pelo aprisionamento deste por longos períodos temporais (e.g., [Takahashi et al., 2009](#); [Le Quéré et al., 2018](#)). Por exemplo, na última década o oceano Atlântico foi responsável pela captura média de $0.49 \pm 0.11 \text{ Pg}$ de carbono ao ano ([Shuster et al., 2013](#)). Porém, devido à grande variabilidade espacial e temporal dos parâmetros físicos, químicos e biológicos que controlam essa dinâmica de fluxos entre o oceano e atmosfera, algumas regiões do oceano podem apresentar variabilidade nos padrões de liberação e captura do CO_2 (e.g. [Mahadevan et al., 2004](#); [Takahashi et al., 2009](#)).

Os processos responsáveis pela liberação ou captura do CO_2 da atmosfera são chamados de bomba de solubilidade e bomba biológica ([Howes](#)

et al., 2015). A primeira consiste na interação química do CO₂ com a água e a formação de ácido carbônico, que devida a sua instabilidade se dissocia formando os íons bicarbonato e carbonato. Essa bomba é dependente da solubilidade do CO₂ na água, que aumenta com a diminuição da temperatura superficial da água do mar (SST) e a diminuição da salinidade superficial da água do mar (SSS). Com o aumento da solubilidade ocorre redução da pressão parcial do CO₂ ($p\text{CO}_2$) ou fugacidade¹ ($f\text{CO}_2$) na água do mar, que se tratam da pressão exercida pelo CO₂ em um volume específico de água do mar (Sarmiento e Gruber, 2006). A segunda bomba é diretamente relacionada com a atividade fotossintética, onde os organismos absorvem o carbono inorgânico da superfície pela fotossíntese e transformam esse carbono em carbono orgânico para a formação das carapaças e outras estruturas (Mucci et al., 2000). Uma forma de identificar e quantificar a atividade dessa bomba é observar a concentração de clorofila- α (Chla) nas águas superficiais. Quanto maior Chla, maior a captura do CO₂ pelos organismos e menor serão os valores de $f\text{CO}_2$ (e.g., Bianchi et al., 2009).

Outros dois parâmetros que podem ser relacionados com a $f\text{CO}_2$ são a alcalinidade total (Alk) e carbono inorgânico dissolvido (DIC). Ambos os parâmetros são influenciados por processos físico-químicos e biológicos. A Alk é definida por Broecker (1974) como sendo o balanço da contribuição de carga dos principais cátions e ânions conservativos da água do mar. Dessa forma, mudanças só ocorrem em escalas de tempo muito grandes, geológicas, sendo a Alk considerada então uma propriedade conservativa. Esta apresenta uma relação inversa com a $f\text{CO}_2$ (Sarmiento e Gruber, 2006). Já o DIC se trata da

¹ Pressão parcial do gás corrigida pelo comportamento de um gás ideal;

somatória de todas as espécies carbonáticas (Broecker, 1974) e tem uma relação direta com a $f\text{CO}_2$. Porém, quanto maior o DIC menor é a solubilidade do CO₂ na água do mar, ou seja, o DIC apresenta uma relação contrária a SST (Sarmiento e Gruber, 2006).

É muito bem conhecido que o sudoeste do oceano Atlântico Sul (Fig. 1) é uma região que apresenta baixa amostragem dos parâmetros do sistema carbonato marinho e ainda não tem sua dinâmica da $f\text{CO}_2$ completamente entendida (Kerr et al., 2016). Ito et al. (2005) estudou a variabilidade sazonal da $f\text{CO}_2$ e os fluxos do CO₂ na plataforma continental, quebra de plataforma e região de oceano aberto na parte sudoeste do oceano Atlântico subtropical durante três diferentes estações, entre 1997 e 1998. Os autores encontraram que a plataforma continental e o talude se comportaram como fontes de CO₂ para a atmosfera durante o inverno, fim do outono e verão, enquanto o oceano aberto oscilou entre fonte de CO₂ (1997) e sorvedouro (1998). Contudo, suas investigações foram concentradas em resultados obtidos em uma ou duas seções perpendiculares à plataforma continental em uma área confinada do *South Brazil Bight*. Por outro lado, a partir do uso de dados de 14 cruzeiros entre 2000 e 2008, Padin et al. (2010) analisaram a distribuição da $f\text{CO}_2$ na água do mar e os fluxos ar-água do CO₂ no oceano aberto e áreas da plataforma continental do oceano Atlântico, incluindo o sudoeste do oceano Atlântico Sul. Esse trabalho apontou que o oceano se comportou como fonte do CO₂ na primavera e sorvedouro do CO₂ durante o outono, com áreas da plataforma continental se comportando tanto como fonte e sorvedouro durante as duas estações. Mais recentemente, Arruda et al. (2015) investigaram os fluxos do CO₂ e os controles da variabilidade sazonal do $p\text{CO}_2$ na água do mar por meio do uso

de um modelo biogeoquímico para o sudoeste do oceano Atlântico Sul. Esses autores encontraram que a parte mais interna da plataforma continental se comporta como uma fonte fraca de CO₂ e com as regiões média e externa da plataforma continental se comportando como sorvedouro de CO₂ para a atmosfera. Com um estudo mais compreensivo e usando a vantagem de medições sinóticas do CO₂ no sudoeste do oceano Atlântico Sul, tanto na região de *South Brazil Bight*, quanto na *Southern Brazilian Shelf*, [Ito et al. \(2016\)](#) documentaram que a plataforma continental se comportou como fonte do CO₂ durante o fim do outono de 2010 e no início do verão de 2011. Os autores também encontram que regiões influenciadas por ressurgência e por processos físicos de submesoescala, como frentes e vórtices, apresentam grande influência na distribuição espacial do *pCO₂* na água do mar na região. [Lencina-Avila et al. \(2016\)](#) investigaram a distribuição da *fCO₂* na água do mar na seção transatlântica entre a plataforma continental Sul Africana e Sul Americana e percorrendo a linha latitudinal de 35°S durante a primavera e o início do verão de 2011. Esses autores encontraram que toda a região se comportou como zona de sorvedouro de CO₂ durante todo o cruzeiro. Um comportamento parecido também foi reportado por [Orselli et al. \(2019\)](#) em seu estudo sobre o impacto dos vórtices das Agulhas nos fluxos de CO₂ no oceano Atlântico Sul. Esses autores encontraram que a região ao longo do caminho percorrido pelos vórtices das Agulhas se comportou como sorvedouro de CO₂ durante julho de 2015. Apesar de muitos estudos terem investigado como o CO₂ se comporta no sudoeste do oceano Atlântico Sul, a maioria se baseou em cruzeiros específicos ou/e são limitados espacial ou temporalmente. Assim, dificultando uma imagem mais ampla da distribuição da *fCO₂* (ou da *pCO₂*) na água do mar, bem como das

forçantes físico-químicas e biológicas que são responsáveis pela variabilidade deste parâmetro.

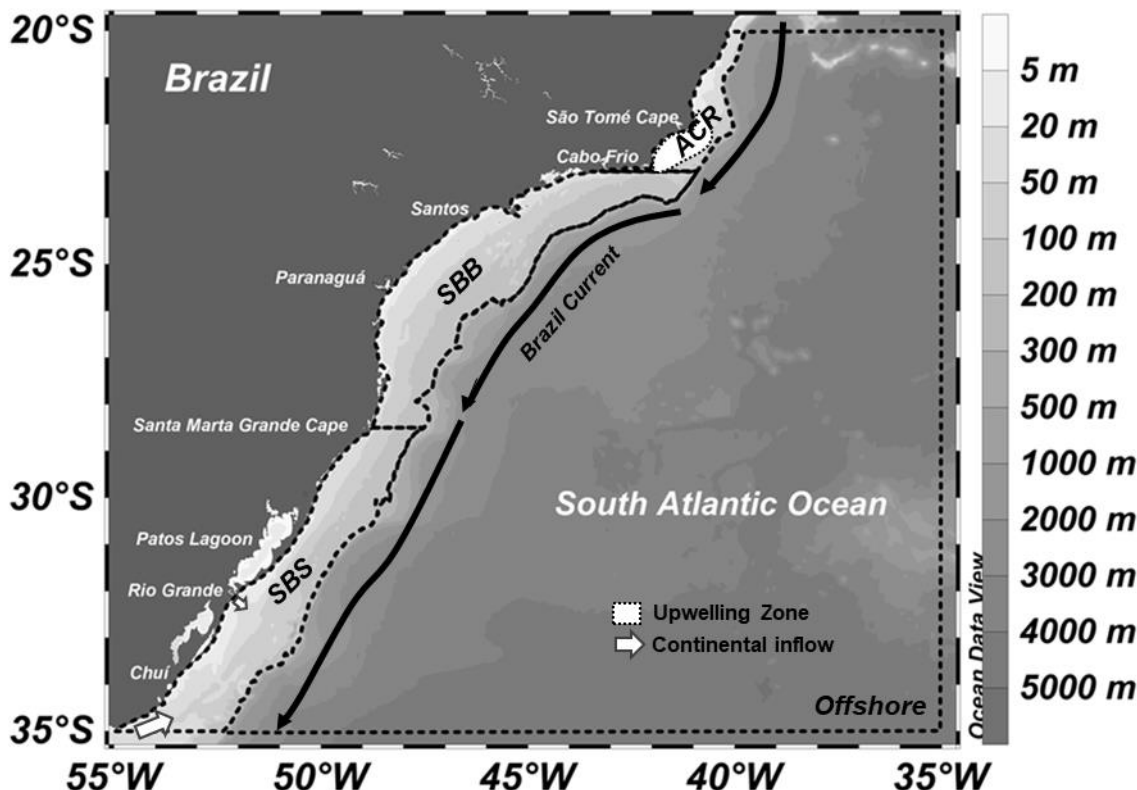


Figura 3. Províncias biogeoquímicas do sudoeste do oceano Atlântico Sul: região de Abrolhos-Campos (ACR), South Brazil Bight (SBB), Southern Brazilian Shelf (SBS) e região offshore. A região em branco, que é delimitada pelas linhas pontilhadas, mostra a região de ressurgência na ACR, enquanto as setas brancas na SBS mostram os sentidos da intrusão de água provenientes da pluma do Rio da Plata e do sistema Patos-Mirim. A Corrente do Brasil (*Brazil Current*) tem seu sentido e área de influência mostrada pela seta preta. O limite entre a plataforma continental (o limite das áreas ACR, SBB e SBS) e a região offshore foi definido seguindo a linha batimétrica de 200 metros.

Nesse contexto, esse estudo investigou a distribuição espacial e a sazonalidade e interanualidade da $f\text{CO}_2$ na água do mar no sudoeste do oceano Atlântico Sul entre o meio de 2011 e o meio de 2015. Utilizando da relação existente entre SST, SSS e Chla com a $f\text{CO}_2$, essa investigação foi baseada no desenvolvimento de dois algoritmos de $f\text{CO}_2$, considerando as divisões sazonais de Primavera-Verão e Outono-Inverno, e o uso de dados derivados de satélite. Também foram investigadas as forçantes biogeoquímicas (i.e., SST, SSS, Alk e

DIC) que controlam as variações regionais tanto na escala espacial quanto temporal da $f\text{CO}_2$.

I.II – Objetivos

O objetivo geral deste estudo é reconstruir a distribuição espacial, sazonal e interanual da $f\text{CO}_2$ na água do mar para a região de plataforma continental e oceano aberto do sudoeste do oceano Atlântico Sul. Como objetivos específicos, este estudo pretende: (i) desenvolver algoritmos para a reconstrução da distribuição da $f\text{CO}_2$ na água do mar, determinados a partir de parâmetros físicos e biológicos medidos *in situ*, a serem utilizados na reconstrução da distribuição da $f\text{CO}_2$ na água do mar, e (ii); avaliar as principais forçantes biogeoquímicas responsáveis pela variabilidade espaço-temporal na distribuição do $f\text{CO}_2$ na água do mar na área de estudo.

Capítulo II: Dados e Métodos

II.I - Área de Estudo

A região de estudo deste trabalho engloba parte da porção sudoeste do oceano Atlântico Sul, definida pelos limites latitudinais de 20°S até 35°S e longitudinais de 35°W até 55°W, ou seja, cobrindo grande parte da costa sul e sudeste brasileira e parte da desembocadura do Rio da Prata. Esta área foi dividida em quatro províncias biogeocíquímicas distintas ([Fig. 1](#)) devido à grande dinâmica oceânica e a alta variabilidade da $f\text{CO}_2$ na água do mar existente na região (e.g., [Castro e Miranda, 1998](#); [Ito et al. 2016](#)). O regime da plataforma continental foi subdividido considerando a região de Abrolhos-Campos (ACR), a *South Brazil Bight* (SBB) e *Southern Brazilian Shelf* (SBS). O limite batimétrico entre regimes de plataforma continental e oceano aberto (*offshore region*) foi determinado pela batimetria média de 200 m, enquanto os limites latitudinais foram definidos entre 20°S e 35°S.

A ACR, área situada entre 20°S e 23°S, apresenta como características uma plataforma continental estreita e uma zona de ressurgência onde ascende a Água Central do Atlântico Sul (Zembruscki 1979; Rodrigues and Lorenzetti 2001). O sistema de ressurgência de Cabo Frio, que está associado com a intensificação dos ventos vindos de nordeste na região, apresenta maior intensidade e frequência durante a primavera e o verão (Castelão e Barth 2006; Calado et al. 2008). A SBB, localizada entre 23°S e 28.5°S, é um largo embaiamento da plataforma continental, que sofre influência dos ventos locais em sua porção mais interna e da Corrente do Brasil em suas porções média e externa (Palma e Matano 2009; Matano et al. 2010). Na porção sul da plataforma na região de estudo ocorre intrusão de água com baixa salinidade proveniente da desembocadura do Rio da Prata e do sistema da lagoa Patos-Mirim (Piola et al. 2000). Na porção norte da região ocorre intrusão de água relativamente mais gelada proveniente do sistema de ressurgência da ACR. Durante o verão, devido à influência do regime de ventos e presença da Água Central do Atlântico Sul, a zona sudoeste da região apresenta ressurgência de águas relativamente mais frias próximas à costa (Matano et al. 2010). A SBS se estende entre 28.5°S e 35°S e, sendo amplamente influenciada pelo deságue do Rio da Prata e da lagoa Patos-Mirim, sofre mudanças na hidrografia e nas propriedades do sistema carbonato da água de plataforma (Ciotti et al. 1995; Piola et al. 2000; Odebrecht e Castello 2001; Braga et al. 2008; Carvalho-Borges et al. 2018). A advecção das águas costeiras provenientes do continente é fortemente influenciada pela oscilação sazonal da posição da Frente Subtropical de Plataforma (STSF²), que tem sua origem na transição entre a Água Subantártica de Plataforma,

² Do inglês *Subtropical Shelf Front*

proveniente da plataforma patagônica, e da Água Subtropical de Plataforma, que é advectada de baixas latitudes. Durante o inverno, essas águas costeiras de baixa salinidade podem atingir posições superiores a 28°S, enquanto no verão essas águas são presas ao sul de 32°S ([Piola et al. 2000](#); [Palma et al. 2008](#)).

Na região de oceano aberto, próximo à zona de quebra de plataforma, flui a Corrente do Brasil, que é uma corrente de contorno oeste. Essa corrente transporta águas relativamente mais quentes e salinas, de baixas para altas latitudes, com uma velocidade de fluxo baixa, em comparação com outras correntes de contorno oeste ([Castro e Miranda 1998](#)). Essa corrente segue para sul até encontrar a Corrente da Malvinas vindo em sentido oposto, formando uma área com alta energia cinética, conhecida como Confluência Brasil-Malvinas ([Gordon, 1989](#)). A posição da confluência varia sazonalmente, com incursões da Corrente das Malvinas a posições mais ao norte de 33°S durante o inverno, e avanço da Corrente do Brasil a posições próximas a 43°S durante o verão ([Legeckis e Gordon 1982](#); [Olson et al. 1988](#); [Provost et al. 1992](#); [Piola et al. 2000](#)). Devido as mudanças sazonais em seu fluxo e pela intrusão da Água Central do Atlântico Sul na coluna d'água da plataforma continental, a Corrente do Brasil exerce grande influência sobre a hidrodinâmica e as propriedades da água do mar sobre a plataforma continental de toda a região de estudo ([Stramma e Peterson 1990](#); [Matano et al. 2010](#)).

II.II - Dados utilizados para desenvolvimento e teste dos algoritmos para fCO₂ na água do mar

Neste estudo foram utilizados dois conjuntos de dados, uma coleção de dados *in situ* e uma coleção de dados derivados de satélites. O primeiro grupo de dados tem como principal característica serem dados de SST, SSS e fCO₂ na água do mar provenientes de coletas discretas feitas a partir de embarcações de pesquisas oceanográficas e embarcações de oportunidade. Esses dados foram extraídos dos seguintes bancos de dados: (i) Surface Ocean CO₂ Atlas (SOCAT) versão 5 ([Bakker et al. 2016](#)); (ii) Global Surface pCO₂ (LDEO) Database v2017 ([Takahashi et al. 2017](#)); e o (iii) banco de dados do Grupo Brasileiro de Oceanografia de Altas Latitudes (GOAL; [Ito et al. 2016](#); [Lencina-Avila et al. 2016](#); [Kerr et al. 2016](#); [Carvalho-Borges et al. 2018](#); [Orselli et al. 2019](#)). Destes bancos de dados foram obtidos dados de SST (°C), SSS e fCO₂ ou pCO₂ na água do mar (μatm). Sendo que o último, quando usado, foi convertido para fCO₂ utilizando a ferramenta de cálculo fornecida pelo programa Ocean Data View (ODV; <https://odv.awi.de/>; [Schlitzer et al. 2018](#)). Os bancos de dados do SOCAT, LDEO e uma parte dos dados provenientes do banco do GOAL foram usados apenas para o desenvolvimento dos algoritmos. A outra parte dos dados do GOAL, a que não foi utilizada para o desenvolvimento dos algoritmos, se refere aos dados provenientes do projeto *Following Ocean Rings in the South Atlantic* (FORSA; [Orselli et al. 2019](#); [Carvalho et al. 2019](#)), que foram utilizados apenas para o teste de desempenho dos algoritmos. A distribuição espacial e temporal destes dados está representada na [Figura 2](#).

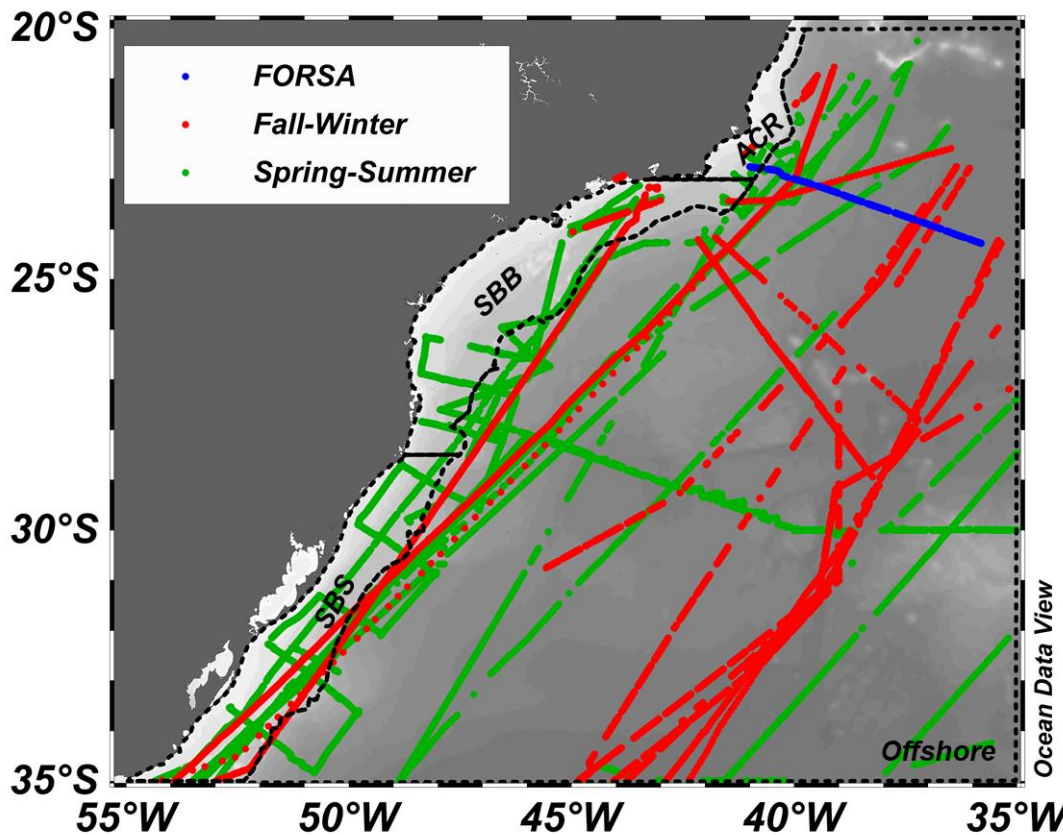


Figura 2. A distribuição espacial do banco de dados usado para desenvolver e testar os algoritmos de $f\text{CO}_2$. O dado usado para desenvolver o algoritmo para Outono-Inverno (*Fall-Winter*, pontos vermelhos) e Primavera-Verão (*Spring-Summer*, pontos verdes), enquanto a seção do cruzeiro FORSA (pontos azuis) foi usada para validar o algoritmo. A divisão das regiões (ACR, SBB, SBS e *Offshore*) é representada pelos pontos pretos e a batimetria é mostrada em tons de cinza.

Os produtos derivados de satélites foram utilizados para melhorar o desempenho dos algoritmos com a inclusão da Chla (mg/m^3) e, com isso, adicionar um proxy biológico para os cálculos de $f\text{CO}_2$ na água do mar. Com a intenção de obter essa variável, foram usados dados mapeados e diários de Chla derivados a partir do algoritmo GSM-merged, que tem resolução espacial de 4 km. Esses dados são disponibilizados pelo GlobColour Project (<http://globcolour.info>) e foram desenvolvidos, validados e distribuídos pela ACRI-ST da França (Maritorena et al. 2010; Fanton d'Andon et al. 2009). Destes mapas foram extraídos dados de Chla para o período e posição específicos das observações *in situ* (i.e., SOCATv5, LDEOv2007 e GOAL). Isso possibilitou que

para cada dado de $f\text{CO}_2$ na água do mar obtido pela coleta *in situ*, nós obtivéssemos um valor específico de Chla extraído dos produtos mapeados de satélite. Nas situações em que os produtos de satélite se tornaram indisponíveis por cobertura de nuvens no período ou não existiam na posição desejada, foram utilizadas médias de mapas que variavam de ± 1 dia até ± 2 dias dependendo da persistência das nuvens sobre a região. As médias e os desvios padrões de cada parâmetro usado para desenvolver os algoritmos com suas divisões sazonais e regionais são mostrados na [Tabela 1](#).

Tabela 3. As médias e desvios padrões do banco de dados utilizados para desenvolvimento dos algoritmos sazonais da $f\text{CO}_2$ na água do mar: Primavera-Verão (setembro até fevereiro) e Outono-Inverno (março até agosto). A tabela mostra a $f\text{CO}_2$ na água do mar (μatm), temperatura superficial da água do mar (SST, $^{\circ}\text{C}$), salinidade superficial da água do mar (SSS) e concentração de clorofila-a (Chla, mg m^{-3}) para toda a área de estudo, no sudoeste do oceano Atlântico Sul, e para as divisões regionais e sazonais. Região de Abrolhos-Campos (ACR), *South Brazil Bight* (SBB), *Southern Brazilian Shelf* (SBS) e região offshore (*offshore*).

	Período médio	$f\text{CO}_2$ (μatm)	SST ($^{\circ}\text{C}$)	SSS	Chla (mg m^{-3})
Toda a área de estudo 20°-35°S 35°-55°O	2011-2015	372.7 ± 28.3	23.09 ± 2.46	35.75 ± 1.50	1.1 ± 1.1
	Primaveira-Verão	375.2 ± 31.9	22.55 ± 2.44	35.54 ± 1.70	1.4 ± 1.2
	Outono-Inverno	368.5 ± 19.9	24.21 ± 2.08	36.16 ± 0.81	0.6 ± 0.4
ACR	2011-2015	392.9 ± 34.1	24.29 ± 0.83	35.32 ± 2.22	1.6 ± 0.8
	Primaveira-Verão	401.0 ± 11.6	23.94 ± 0.50	36.37 ± 0.32	1.5 ± 0.9
	Outono-Inverno	370.5 ± 57.7	25.54 ± 0.58	31.28 ± 1.71	1.7 ± 0.4
SBB	2011-2015	397.3 ± 25.1	24.54 ± 1.56	35.53 ± 0.87	1.1 ± 0.8
	Primaveira-Verão	395.8 ± 24.9	24.49 ± 1.54	35.49 ± 0.87	1.1 ± 0.8
	Outono-Inverno	412.2 ± 22.0	25.31 ± 1.65	36.12 ± 0.64	0.9 ± 0.3
SBS	2011-2015	384.2 ± 34.3	22.03 ± 2.37	33.11 ± 1.97	0.8 ± 0.8
	Primaveira-Verão	385.2 ± 36.6	21.79 ± 2.30	32.89 ± 1.89	0.9 ± 0.8
	Outono-Inverno	378.2 ± 12.0	23.92 ± 2.00	34.81 ± 1.71	0.5 ± 0.4
Offshore	2011-2015	365.9 ± 23.9	22.99 ± 2.50	36.36 ± 0.56	1.2 ± 1.2
	Primaveira-Verão	367.1 ± 17.9	23.76 ± 2.31	36.26 ± 0.47	0.7 ± 0.8
	Outono-Inverno	352.7 ± 7.6	22.51 ± 1.17	36.18 ± 0.24	0.4 ± 0.3

II.III - Banco de dados na reconstrução da distribuição da fCO₂ na água do mar

Foram utilizados três diferentes produtos de média mensal provenientes de satélites. Cada um fornecendo um dos três parâmetros principais para os algoritmos de fCO₂ na água do mar (i.e., SST, SSS e Chla). O produto utilizado para obter a SST possui a resolução espacial de 4 km, sendo disponibilizado pelo *The Moderate Resolution Imaging Spectro-radiometer Aqua* (MODIS Aqua), enquanto o produto utilizado para obter os dados de SSS possui resolução espacial de 1 grau (~111 km) e é disponibilizado pelo *Aquarius*. Ambos são produtos disponibilizados pelo site da NASA Ocean Color (<http://oceancolor.gsfc.nasa.gov/>). Para obter os dados de média mensal de Chla foram utilizados os produtos de resolução de 4 km disponibilizados pelo GlobColour Project, o mesmo utilizado para a elaboração dos algoritmos, porém com resolução temporal mensal. Devido ao fato dos mapas de SST, SSS e Chla apresentarem diferentes resoluções espaciais, os produtos de SSS tiveram o tamanho de seus pixels ajustados para o mesmo tamanho de pixels dos produtos de SST e Chla. Esse ajuste ocorreu pelo recorte dos pixels de ~111 km de SSS em pixels de 4 km utilizando os pixels dos produtos de SST e Chla como base. A modificação no tamanho dos pixels de SSS foi feito de forma que não houvesse nenhuma alteração de dados ou uso de interpolação.

II.IV - Algoritmos da $f\text{CO}_2$ na água do mar

Para o desenvolvimento dos algoritmos da $f\text{CO}_2$ na água do mar foi utilizada a técnica de regressão multilinear (MLR³; e.g., [Ito et al. 2016](#); [Lencina-Avila et al. 2016](#); [Orselli et al. 2019](#)). Foram obtidos dois algoritmos, considerando os períodos sazonais de Primavera-Verão (de setembro até fevereiro) e Outono-Inverno (de março até agosto) no hemisfério sul. Os coeficientes β ($\beta_0, \beta_1, \beta_2, \beta_3$) definem a relação existente entre a $f\text{CO}_2$ na água do mar (parâmetro de saída do algoritmo) e SST, SSS e Chla (parâmetros de entrada do algoritmo). Os valores de Chla foram utilizados na forma logarítmica (Log (Chla)) para obter melhores correlações com a $f\text{CO}_2$ na água do mar em ambos os períodos sazonais. O método de mínimos quadrados foi utilizado para encontrar valores de β pela minimização das diferenças entre as observações e a linha de regressão, o que em outras palavras significa, que houve a soma dos quadrados dos resíduos. Ambos os algoritmos podem ser expressos de forma simplificada pela [Equação 1](#),

$$f\text{CO}_2(\mu\text{atm}) = \beta_0 + \beta_1(\text{SST}) + \beta_2(\text{SSS}) + \beta_3(\log(\text{Chla})), \quad (1)$$

onde $f\text{CO}_2$ é fugacidade do CO_2 na água do mar em μatm , SST é a temperatura da superfície do mar em graus Celsius, SSS é a salinidade da superfície do mar em unidade prática de salinidade, e Chla é a concentração superficial de clorofila a em mg m^{-3} . Para avaliar a representatividade dos algoritmos, foram inseridos dados *in situ* de SST, SSS e Chla (obtido pelos produtos de satélite) em cada um dos algoritmos e os resultados foram comparados com os respectivos dados *in situ* da $f\text{CO}_2$ na água do mar. A comparação entre os resultados obtidos pelo

³ Do inglês *multiple linear regression*.

algoritmo e os dados *in situ* da $f\text{CO}_2$ foi realizada pela obtenção do coeficiente de determinação (r^2) e pelo erro médio quadrático (RMSE). Em adição a essa comparação, nós aplicamos o algoritmo desenvolvido para Outono-Inverno para determinar a distribuição da $f\text{CO}_2$ na água do mar ao longo do cruzeiro FORSA, usando os dados *in situ* de SST e SSS e os respectivos dados derivados de satélite para Chla.

II.V - Avaliação da distribuição espacial e comportamento temporal da $f\text{CO}_2$ na água do mar

A distribuição espacial e as séries temporais da $f\text{CO}_2$ na água do mar no sudoeste do oceano Atlântico Sul foram feitas pela aplicação dos algoritmos desenvolvidos com o *input* de produtos de satélite de SST, SSS e Chla em cada um dos períodos sazonais definidos. Com isso, foram produzidos 47 mapas com a distribuição média mensal da $f\text{CO}_2$ na água do mar, sendo um mapa para cada mês do período entre agosto de 2011 até junho de 2015. Para cada mês de um ano médio foram obtidos mapas de cada um dos parâmetros utilizados de *input* nos algoritmos (SST, SSS e Chla) e mapas da $f\text{CO}_2$ na água do mar. Isso possibilitou um melhor entendimento de como cada parâmetro *input* influencia na distribuição espacial da $f\text{CO}_2$ na água do mar na região. Para construir as séries temporais da $f\text{CO}_2$ na água do mar entre 2011 e 2015, foram utilizados os 47 mapas médios para obter os valores médios da $f\text{CO}_2$ para cada uma das regiões investigadas. Esses valores médios de cada região foram utilizados para obter os padrões sazonais de oscilação da $f\text{CO}_2$ na água do mar e tendências anuais para a análise temporal.

II.VI - As forçantes da variabilidade da $f\text{CO}_2$ na água do mar

A distribuição da $f\text{CO}_2$ na água do mar é altamente influenciada pela distribuição espacial de SST, SSS, composição e concentração de produtores primários, e mudanças na distribuição de Alk e DIC. As distribuições dessas forçantes são específicas para cada região do oceano e estação do ano. Porém, antes de identificar como cada uma dessas forçantes influenciam na distribuição espacial e modificam sazonalmente a $f\text{CO}_2$ na água do mar, foram obtidos os dados de Alk e DIC. A Alk ($\mu\text{mol kg}^{-1}$) foi obtida pela utilização de dois algoritmos dependentes de SST e SSS que foram desenvolvidos e apresentados por [Lee et al. \(2006\)](#), com cada um dos algoritmos utilizados seguindo as especificações dos autores para a faixa latitudinal de aplicação de cada algoritmo e faixas de SST e SSS. Um dos algoritmos foi desenvolvido para as regiões Subtropicais e outro para o oceano Austral (ver as equações para Zonas 1 e 5 na [Tabela 1](#) disponibilizada no trabalho de [Lee et al. 2006](#)). A distribuição de DIC ($\mu\text{mol kg}^{-1}$) foi calculada utilizando o programa CO₂Sys v.1.1 ([van Heuven et al. 2011](#)) com a inserção de parâmetros de Alk, $f\text{CO}_2$, SSS e SST como *input* no programa, a seleção do “*Mehrbach refit*” para as constantes de dissolução do H₂CO₃ e HCO₃⁻ (K₁ e K₂; [Dickson and Millero 1987](#)), a seleção da constante de dissolução do HSO₄⁻ proposta por [Dickson \(1990\)](#) e da relação entre borato total e salinidade proposta por [Uppström \(1974\)](#).

Para evitar a interferência de baixos valores de SSS, Alk e DIC encontrados na região sob influência da pluma do Rio da Prata nas médias regionais de cada parâmetro, os dados dessa região foram retirados da região de estudo durante a análise das forçantes espaciais da $f\text{CO}_2$ na água do mar. Essa separação foi feita encontrando os dados de SSS com valores inferiores a

34 (Piola et al. 2005) e excluindo esses dados das sub-regiões analisadas. Já que a pluma tem influência localizada a uma parte específica da região de estudo, as análises das forçantes espaciais nessa região em particular é mostrada na sessão de Material Suplementar.

O método utilizado para a análise das forçantes que controlam a distribuição espacial e oscilações temporais da $f\text{CO}_2$ na água do mar seguiram o proposto por Signorini et al. (2013), porém com a normalização dos dados de Alk e DIC pelo valor médio da SSS, produzindo Alkn e DICn. Essa normalização remove o efeito da diluição sobre esses dois parâmetros. Uma vez que obtivemos todos os parâmetros, a análise foi dividida em dois caminhos: a distribuição espacial e a evolução temporal.

Para a primeira, nós obtivemos um mapa médio de distribuição para cada parâmetro em toda a região, os valores de cada pixel nesse mapa foram considerados nossas variáveis (e.g. SST', SSS', Alkn', DICn' e $f\text{CO}_2'$). Deste mapa, foram extraídos os valores espaciais médios de cada parâmetro, que forma definidos como nossas constantes (e.g., $\overline{\text{SST}}$, $\overline{\text{SSS}}$, $\overline{\text{Alkn}}$, $\overline{\text{DICn}}$ e $\overline{f\text{CO}_2}$). Já para a análise temporal, foram obtidas as médias mensais de cada parâmetro por região (e.g., valores médios de SST para ACR em janeiro). Cada uma dessas médias mensais foi considerada como uma variável (e.g., SST', SSS', Alkn', DICn' e $f\text{CO}_2'$) e da média entre os valores dos parâmetros nesse ano médio, foram obtidas nossas constantes (e.g., $\overline{\text{SST}}$, $\overline{\text{SSS}}$, $\overline{\text{Alkn}}$, $\overline{\text{DICn}}$ e $\overline{f\text{CO}_2}$).

Para identificar a sensibilidade da $f\text{CO}_2$ as mudanças em cada um dos parâmetros (e.g., SST, SSS, Alkn e DICn), três desses parâmetros são identificados como constantes (\bar{X}) e o quarto é identificado como a variável (X').

Esses valores foram inseridos no programa CO₂Sys v.1.1, com as mesmas especificações utilizadas para obter os valores de DIC, e foram obtidos valores de $f\text{CO}_2$ associados a mudanças espaciais ou temporais de apenas um desses parâmetros. Por exemplo, para obter a influência de SST sobre $f\text{CO}_2$, nós operamos o CO₂Sys v.1.1 como:

$$f\text{CO}_2^{\text{SST}} = f\text{CO}_2(\text{SST}', \overline{\text{SSS}}, \overline{\text{Alkn}}, \overline{\text{DICn}}) \quad (2)$$

onde $f\text{CO}_2^{\text{SST}}$ nos dará valores de fugacidade do CO₂ levando em conta apenas as variações da SST. SST' são as variáveis espaciais ou temporais de SST, e $\overline{\text{SSS}}$, $\overline{\text{Alkn}}$ e $\overline{\text{DICn}}$ são as constantes espaciais ou temporais de salinidade superficial da água do mar, Alk normalizada pela salinidade, e DIC normalizado pela salinidade, respectivamente. Essa operação foi realizada 4 vezes para cada uma das análises de forçantes e desta forma foram obtidos valores de $f\text{CO}_2^{\text{SST}}$, $f\text{CO}_2^{\text{SSS}}$, $f\text{CO}_2^{\text{Alk}}$ e $f\text{CO}_2^{\text{DIC}}$. Para quantificar os desvios da $f\text{CO}_2$ em relação ao valor médio causado por cada variável, foi feita a seguinte operação:

$$\delta^{\text{SST}} = f\text{CO}_2^{\text{SST}} - \overline{f\text{CO}_2}, \quad (3)$$

onde δ^{SST} representa o desvio da fugacidade do CO₂ causado pela variação espacial ou temporal da temperatura superficial da água do mar, $f\text{CO}_2^{\text{SST}}$ representa a fugacidade do CO₂ em relação a variações espaciais ou temporais apenas na temperatura superficial da água do mar, e $\overline{f\text{CO}_2}$ representa a média espacial ou temporal da fugacidade do CO₂. Dessa forma foram obtidos valores de δ^{SST} , δ^{SSS} , δ^{Alk} e δ^{DIC} para cada uma das análises de forçantes.

Capítulo III: Artigo Científico

Para a obtenção do título de Mestre pelo Programa de Pós-Graduação em Oceanologia, é requerido que o discente realize a submissão de pelo menos um artigo científico como primeiro autor em periódico com corpo indexado. Desse modo, os resultados da pesquisa desenvolvida durante o período de mestrado e a discussão dos resultados serão apresentados em forma de artigo neste Capítulo. O manuscrito, de autoria de Ciro Cataneo Liutti, Rodrigo Kerr, Iole Beatriz Marques Orselli, Rosane Gonçalves Ito e Carlos Alberto Eiras Garcia, é intitulado “***Spatiotemporal variability of the seawater CO₂ fugacity on the southwestern South Atlantic Ocean***” e foi submetido para publicação no periódico “***Continental Shelf Research***”.

1. Introduction

Carbon dioxide (CO_2) is known as an important gas contributing to the greenhouse effect (e.g., [Millero 2007](#)), and oceans play a key role in the uptake or release of gases from or to the atmosphere (e.g., [Takahashi et al. 2009](#); [Le Quéré et al. 2018](#)). [Broecker and Peng \(1982\)](#) proposed a formulation to estimate the CO_2 fluxes between ocean and atmosphere considering sea–air differences in CO_2 partial pressure ($p\text{CO}_2$) or fugacity ($f\text{CO}_2$; i.e., the partial pressure of the gas corrected for the real gas behavior), the CO_2 transfer coefficient (K_T) based on measurements of wind, and the CO_2 solubility coefficient (K_s). The difference in $f\text{CO}_2$ between the two reservoirs (i.e., ocean and atmosphere) is highly variable, mainly because of the great spatial and temporal variability of CO_2 in the ocean (e.g., [Mahadevan et al. 2004](#); [Takahashi et al. 2009](#)). In particular, each region of the ocean has its own $f\text{CO}_2$ variability, dynamics and controls, which depend on many factors, such as changes in seawater parameters and biological activity ([Cai et al. 2003](#)).

The dynamics and drivers of CO_2 in some regions of the oceans, such as the South Atlantic Ocean, have not yet been comprehensively investigated, mainly due to low sample resolution at both spatial and temporal scales ([Takahashi et al. 2009](#); [Schuster et al. 2013](#)). This lack of information and data is usually associated with the necessity of vessels to obtain *in situ* oceanic $p\text{CO}_2$ or $f\text{CO}_2$, which generally present a low resolution, and the inherent safety limitations of vessels. To tackle this issue, existing data on hydrography and marine carbonate properties from a specific region can be an alternative to *in situ* sampling to develop seawater $p\text{CO}_2$ or $f\text{CO}_2$ regional climatologies ([Takahashi et al. 2018](#)) or algorithms (e.g., [Ito et al. 2016](#); [Lencina-Avila et al. 2016](#); [Benallal et al. 2018](#)).

al. 2017; Orselli et al. 2019). These algorithms are developed by using the relationship between available sets of parameters, such as sea surface temperature (SST), sea surface salinity (SSS), chlorophyll-a concentration (Chla), and related values of seawater $p\text{CO}_2$ or $f\text{CO}_2$. Regional algorithms can be used in association with satellite-derived products to produce high spatial and temporal resolution information on the seawater $f\text{CO}_2$ distribution in a region (e.g., Stephens et al. 1995; McNeil et al. 2007; Zhu et al. 2009; Moussa et al. 2016; Benallal et al. 2017).

One way to understand the drivers of the spatial or temporal variability of seawater $f\text{CO}_2$ in a certain oceanic region is based on the investigation of the variability of SST, SSS, total alkalinity (Alk), and total dissolved inorganic carbon (DIC) (e.g., Signorini et al. 2013). Changes in seawater $f\text{CO}_2$ by physical processes are usually associated with changes in all four of the parameters cited above, while changes in biological processes are identified by changes in Alk and DIC (Takahashi et al. 1993; Lenton et al. 2012).

It is well known that the southwestern South Atlantic Ocean (Fig. 1) is an under-sampled region of marine carbonate parameters, and the dynamics of CO_2 in this region are still not completely understood (Kerr et al. 2016). In this context, Ito et al. (2005) studied the seasonal variability of the seawater $f\text{CO}_2$ and sea-air CO_2 fluxes on the continental shelf, shelf break, and open ocean areas of the southwestern subtropical Atlantic during three different seasons between 1997 and 1998. They found that the continental shelf and shelf-break zones behaved as a CO_2 source to the atmosphere during winter, late spring, and summer, while the open ocean oscillated between a CO_2 source (1997) or sink (1998). However, their investigation was concentrated on results obtained in one or two sections

perpendicular to the continental shelf in a confined area of the South Brazil Bight (SBB). On the other hand, through the use of data obtained from 14 cruises between 2000 and 2008, [Padin et al. \(2010\)](#) analyzed the seawater $f\text{CO}_2$ distribution and sea-air CO_2 fluxes on the open ocean and continental shelf regions of the Atlantic Ocean, including the southwestern South Atlantic Ocean. Their work showed that the ocean behaved as a CO_2 source (sink) in spring (fall), whereas the continental shelf behaved as a source of CO_2 in both seasons. More recently, [Arruda et al. \(2015\)](#) investigated the CO_2 fluxes and controls of the seasonal variability of seawater $p\text{CO}_2$ using a biogeochemical model in the southwestern South Atlantic Ocean. The authors found that the inner continental shelf acted as a weak CO_2 source, in contrast to the mid- and outer shelf, which acted as a CO_2 sink. In a more comprehensive study taking advantage of the synoptic measurements of the CO_2 in the southwestern South Atlantic Ocean on both the SBB and Southern Brazilian Shelf (SBS), [Ito et al. \(2016\)](#) documented that the continental shelf behaved as a CO_2 source during late spring 2010 and early summer 2011. In addition, they found that both regional upwelling and mesoscale physical processes, such as fronts and eddies, had a great influence on the spatial distribution of the seawater $p\text{CO}_2$ over the region. Furthermore, [Lencina-Avila et al. \(2016\)](#) investigated the seawater $f\text{CO}_2$ distribution in a trans-Atlantic section at 35°S between the continental shelves of South Africa and South America during spring and early summer of 2011. The authors found that the entire region acted as a CO_2 sink zone during the entire cruise. Similar behavior was found by [Orselli et al. \(2019\)](#) in their study of the impact of Agulhas eddies on CO_2 fluxes in the South Atlantic Ocean. The authors found that the entire region along the Agulhas corridor in the South Atlantic Ocean acted as a

CO₂ sink during July 2015 (austral winter). Although several earlier studies have investigated the behavior of CO₂ in the southwestern South Atlantic Ocean, the majority of these studies are based on single cruises (i.e., snapshots of moments) and/or are too spatially or temporally limited to allow a broader picture of the seawater CO₂ distribution and drivers. Additionally, few studies have investigated how seawater *f*CO₂ oscillates at seasonal scales.

In this context, this study investigated the spatial distribution and seasonal variability of seawater *f*CO₂ in the southwestern South Atlantic Ocean between mid-2011 and mid-2015. The investigation was based on the development of two seawater *f*CO₂ algorithms, considering the Spring-Summer and Fall-Winter seasons and the use of satellite-derived data. We also investigated the temporal behavior of the seawater *f*CO₂ and the seawater *f*CO₂ drivers that control the CO₂ variations in the region.

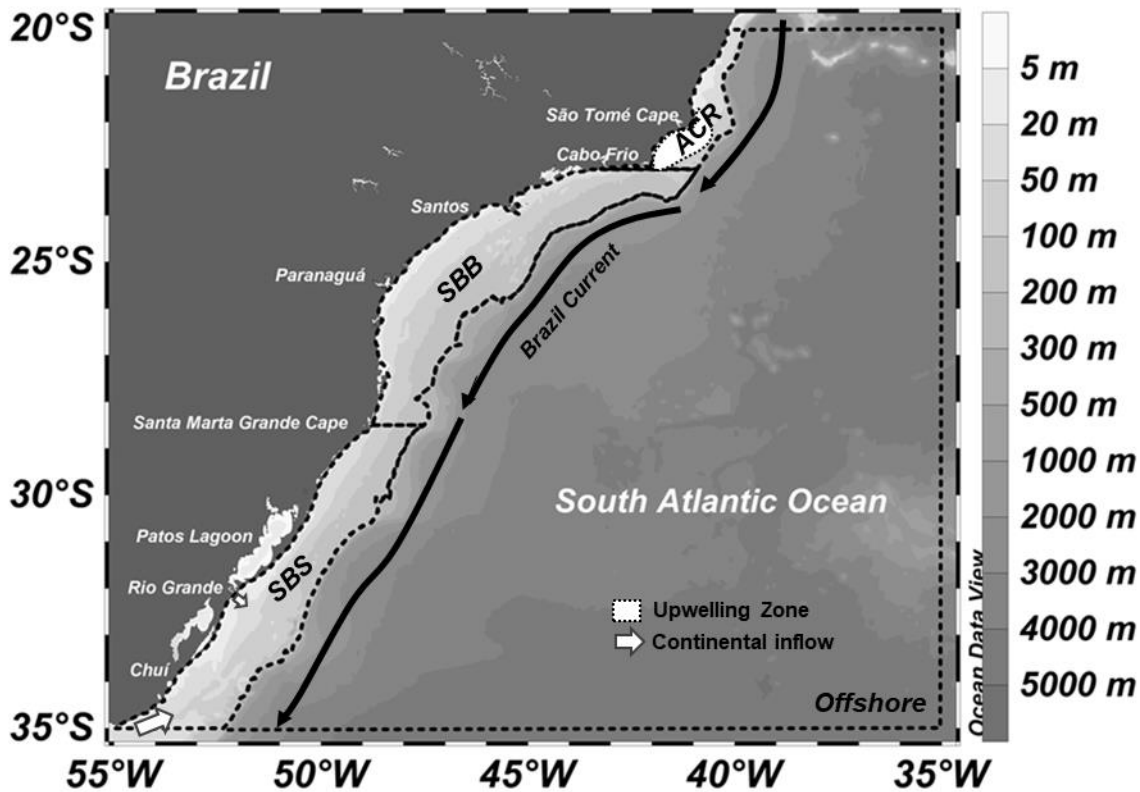


Figure 4. Regional biogechemical provinces of the southwestern South Atlantic Ocean: Abrolhos-Campos Region (ACR), South Brazil Bight (SBB), Southern Brazilian Shelf (SBS), and offshore regions. The white region within dotted lines highlights the upwelling zone of the ACR, while the white arrows at the SBS depict the inflow of continental waters from the La Plata River and the Patos-Mirim Lagoon plumes. The Brazil Current is depicted by black straight arrows. The border between the continental shelf (defining the areas of ACR, SBB, and SBS) and offshore regions is defined by the 200 m isobaths.

2. Data and Methods

2.1. Study area

We split the study area in the southwestern South Atlantic Ocean into distinct biogechemical provinces (Fig. 1). This approach was necessary because of the high ocean dynamics and seawater $f\text{CO}_2$ variability in the region (e.g., Castro and Miranda, 1998; Ito et al. 2016). The continental shelf regime was subdivided (Fig. 1) into the Abrolhos-Campos region (ACR), the SBB, and the SBS. The bathymetric limit between the continental shelf and the open ocean

was set by the 200 m isobaths; the latter is hereafter referred to as the offshore region and encompasses the area between 20°S and 35°S (Fig. 1).

The ACR is situated between 20°S and 23°S and has a narrow continental shelf where upwelling of South Atlantic Central Water (SACW) occurs near the coast (Zembruski 1979; Rodrigues and Lorenzetti 2001). The Cabo Frio upwelling system, which is associated with the intensification of northeasterly winds in the region, has a higher frequency and intensity during spring and summer (Castelão and Barth 2006; Calado et al. 2008). The SBB (23°S to 28.5°S) is a wide continental shelf embayment influenced by local winds on the inner continental shelf and the Brazil Current on the mid and outer regions of the shelf (Palma and Matano 2009; Matano et al. 2010). The southern portion of this region experiences the intrusion of low-salinity waters from the La Plata River and runoff from the Patos-Mirim Lagoon, which are driven by shelf circulation (Piola et al. 2000), and the intrusion of colder oceanic water from the persistent upwelling at the ACR occurs in the northern portion of this region. During the summer period, due to local winds and the presence of the SACW, the northwest zone of the region presents the coastal upwelling of colder water (Matano et al. 2010). The SBS extends from 28.5°S to 35°S and is largely influenced by continental inflow from the La Plata River and the Patos-Mirim Lagoon, which changes the shelf water hydrography and carbonate properties (Ciotti et al. 1995; Piola et al. 2000; Odebrecht and Castello 2001; Braga et al. 2008; Carvalho-Borges et al. 2018; Orselli et al. 2018). The advection of coastal waters derived from the continent is strongly affected by the seasonal oscillation of the Subtropical Shelf Front (STSF), which is formed by the transition between the Subantarctic Shelf Water flowing from the Patagonian Shelf and the Subtropical Shelf Water advected from

low latitudes. During the winter, these low-salinity waters can reach up to 28°S, while they are trapped south of 32°S during the summer ([Piola et al. 2000; Palma et al. 2008](#)).

In the offshore region near the continental shelf break, the Brazil Current, a westward boundary current that transports warm and relatively salty waters, flows from low to high latitudes with a weak velocity ([Castro and Miranda 1998](#)). This current goes south until meeting the Malvinas Current coming from the opposite direction and forming a highly energetic zone known as the Brazil-Malvinas Confluence ([Gordon, 1989](#)). The region of the confluence varies seasonally, with incursions of the Malvinas Current up to 33°S during winter and an advance of the Brazil Current down to 43°S during summer (e.g., [Legeckis and Gordon 1982; Olson et al. 1988; Provost et al. 1992; Piola et al. 2000](#)). In the entire study area, the Brazil Current has an important role in hydrodynamics and seawater property changes over the continental shelf because of seasonal changes in the flow of this current and the intrusion of the SACW ([Stramma and Peterson 1990; Matano et al. 2010](#)).

2.2. Database used to develop and assess the seawater fCO₂ algorithms

First, we characterize the *in situ* ocean data used, which were obtained by oceanographic vessels and ships of opportunity and are composed of measurements of SST, SSS and fCO₂. These data were extracted from the following databases: (i) Surface Ocean CO₂ Atlas (SOCAT) version 5 ([Bakker et al. 2016](#)); (ii) Global Surface pCO₂ (LDEO) Database v2017 ([Takahashi et al. 2018](#)); and (iii) Brazilian High Latitude Oceanographic Group (GOAL) Database ([Ito et al. 2016; Lencina-Avila et al. 2016; Kerr et al. 2016; Carvalho-Borges et al.](#)

2018; Orselli et al. 2019). We obtained SST ($^{\circ}\text{C}$), SSS, and seawater $f\text{CO}_2$ or $p\text{CO}_2$ (μatm) from these data. When used, $p\text{CO}_2$ was converted to $f\text{CO}_2$ using Ocean Data View (ODV; <https://odv.awi.de/>; Schlitzer, 2018). The SOCAT and LDEO datasets were used only to develop the $f\text{CO}_2$ algorithms. The same analysis was performed on part of the GOAL dataset, but the *in situ* data from *Following Ocean Rings in the South Atlantic* (FORSA; Orselli 2019; Carvalho et al. 2019) were used only to test and validate the algorithms. The spatial and temporal distributions of these datasets are presented in Fig. 2.

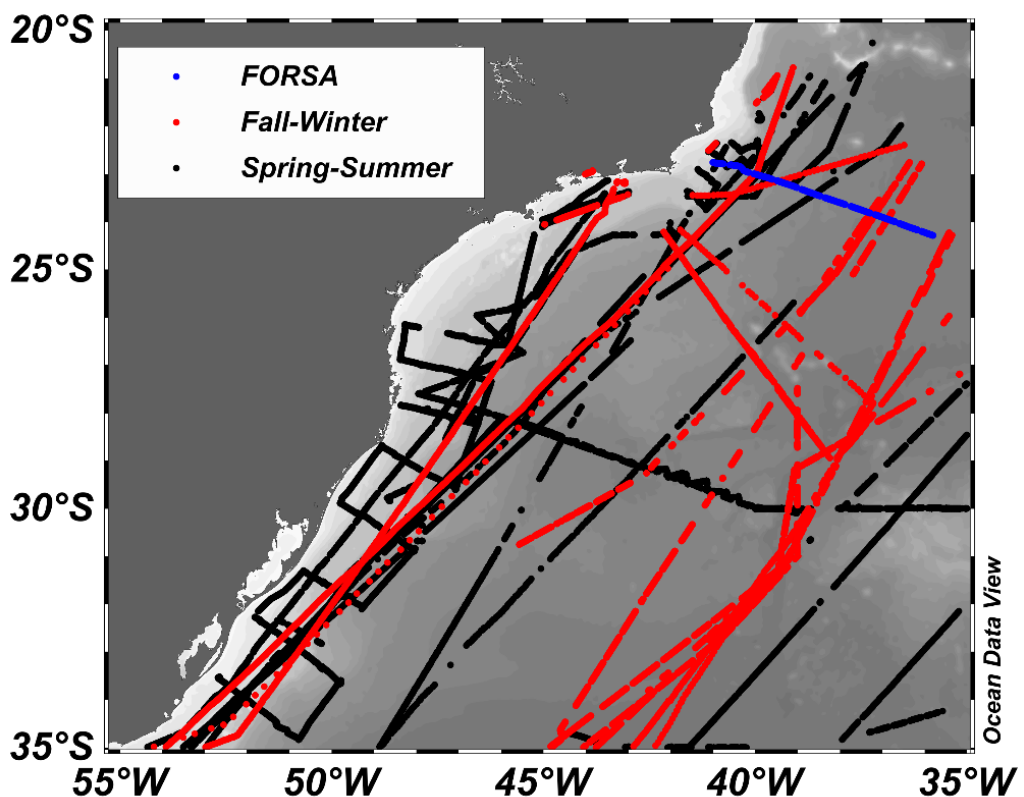


Figure 2. Spatial distribution of the dataset used to create and assess the $f\text{CO}_2$ algorithms. The data used to develop the Fall-Winter (red lines) and Spring-Summer algorithms (black lines), while the FORSA cruise section (blue line) was used to validate the algorithm. The bathymetry is expressed on gray shades.

Then, the satellite-derived product was used to develop algorithms considering the inclusion of Chla (mg/m^3). This variable was added to improve the algorithm's development through the inclusion of a biological component. In order to obtain Chla, daily mapped GSM-merged Chla data with a 4 km resolution

from the GlobColour project (<http://globcolour.info>) were used as the Chla data for the periods of *in situ* observations (i.e., sampling periods of SOCATv5, LDEOv2007 and GOAL). These products were developed, validated, and distributed by ACRI-ST, France (Maritorena et al. 2010; Fanton d'Andon et al. 2009). Thus, for each measurement of seawater $f\text{CO}_2$, a specific Chla value from the corresponding measurement position and date was extracted from the satellite-mapped product. In the presence of clouds, averages of ± 1 day or ± 2 days were used, depending on the cloudiness persistence. The average values and standard deviations of each parameter used to develop the algorithms, with seasonal and regional divisions, are shown in [Table 1](#).

Table 4. Average and standard deviation values of the dataset used to develop the seasonal algorithms for seawater carbon dioxide fugacity ($f\text{CO}_2$): Spring-Summer (September to February) and Fall-Winter (March to August). The table shows seawater $f\text{CO}_2$ (μatm), sea surface temperature (SST, $^{\circ}\text{C}$), sea surface salinity (SSS), and chlorophyll-a concentration (Chla, mg m^{-3}) for the entire study area in the southwestern South Atlantic Ocean and each regional and seasonal division. Abrolhos-Campos Region (ACR), South Brazil Bight (SBB), Southern Brazilian Shelf (SBS), and offshore region (offshore).

	Averaged period	$f\text{CO}_2$ (μatm)	SST ($^{\circ}\text{C}$)	SSS	Chla (mg m^{-3})
Entire region	2011-2015	372.7 ± 28.3	23.09 ± 2.46	35.75 ± 1.50	1.1 ± 1.1
	Spring-Summer	375.2 ± 31.9	22.55 ± 2.44	35.54 ± 1.70	1.4 ± 1.2
	Fall-Winter	368.5 ± 19.9	24.21 ± 2.08	36.16 ± 0.81	0.6 ± 0.4
ACR	2011-2015	392.9 ± 34.1	24.29 ± 0.83	35.32 ± 2.22	1.6 ± 0.8
	Spring-Summer	401.0 ± 11.6	23.94 ± 0.50	36.37 ± 0.32	1.5 ± 0.9
	Fall-Winter	370.5 ± 57.7	25.54 ± 0.58	31.28 ± 1.71	1.7 ± 0.4
SBB	2011-2015	397.3 ± 25.1	24.54 ± 1.56	35.53 ± 0.87	1.1 ± 0.8
	Spring-Summer	395.8 ± 24.9	24.49 ± 1.54	35.49 ± 0.87	1.1 ± 0.8
	Fall-Winter	412.2 ± 22.0	25.31 ± 1.65	36.12 ± 0.64	0.9 ± 0.3
SBS	2011-2015	384.2 ± 34.3	22.03 ± 2.37	33.11 ± 1.97	0.8 ± 0.8
	Spring-Summer	385.2 ± 36.6	21.79 ± 2.30	32.89 ± 1.89	0.9 ± 0.8
	Fall-Winter	378.2 ± 12.0	23.92 ± 2.00	34.81 ± 1.71	0.5 ± 0.4
Offshore	2011-2015	365.9 ± 23.9	22.99 ± 2.50	36.36 ± 0.56	1.2 ± 1.2
	Spring-Summer	367.1 ± 17.9	23.76 ± 2.31	36.26 ± 0.47	0.7 ± 0.8
	Fall-Winter	352.7 ± 7.6	22.51 ± 1.17	36.18 ± 0.24	0.4 ± 0.3

2.3. Database used to reconstruct the distribution of seawater fCO₂

We used monthly mapped products from three different sources, each of which provided one of the main parameters (i.e., SST, SSS or Chla). The 4 km resolution Moderate Resolution Imaging Spectro-radiometer Aqua (MODIS Aqua) products were used to obtain SST, whereas the 1 degree (~111 km) resolution Aquarius products were used for SSS. Both products were obtained from the NASA Ocean Color website (<http://oceancolor.gsfc.nasa.gov/>). The 4 km resolution merged products from the GlobColour project were used for Chla; GlobColour was also used to develop the algorithms (Sec. 2.2) at a monthly temporal resolution. Since the maps for SST, SSS and Chla had different spatial resolutions, the pixel size of the SSS satellite products was adjusted to be the same size as the SST and Chla data. This adjustment did not change any of the SSS data or add any interpolated data.

2.4. Seawater fCO₂ algorithms

The multiple linear regression (MLR) technique with the least squares method was used to develop the seawater fCO₂ algorithms (e.g., Ito et al. 2016; Lencina-Avila et al. 2016; Orselli et al. 2019). Two algorithms considering the seasonal periods of Spring-Summer (September to February) and Fall-Winter (March to August) in the South Hemisphere were obtained. The coefficients (β_0 , β_1 , β_2 , β_3) were found to determine the relationship between seawater fCO₂ (output variable) and SST, SSS, and Chla (input variables). The logarithm form of Chla values (Log (Chla)) were used, thus improving the correlation with seasonal fCO₂ during both seasonal periods. The least squares method was used to determine β values by minimizing the differences between observations and

the regression line, i.e., by minimizing the summed square of the residuals. These algorithms can be expressed as shown by Eq. 1:

$$f\text{CO}_2(\mu\text{atm}) = \beta_0 + \beta_1(\text{SST}) + \beta_2(\text{SSS}) + \beta_3(\log(\text{Chla})), \quad (1)$$

where $f\text{CO}_2$ is the seawater CO_2 fugacity in μatm , SST is the sea surface temperature in degrees Celsius, SSS is the sea surface salinity in practical salinity units, and Chla is the surface chlorophyll-a concentration in mg m^{-3} . To evaluate the representability of the algorithms, *in situ* data with SST, SSS, $f\text{CO}_2$ and Chla (obtained by satellite products) were inserted in the algorithms. The resulting seawater $f\text{CO}_2$ was compared with the respective *in situ* seawater $f\text{CO}_2$ from the dataset used in the algorithms. The comparison between the modeled and predicted seawater $f\text{CO}_2$ was performed by determining the coefficient of determination (r^2) and root-mean-squared error (RMSE). In addition, we applied the Fall-Winter algorithm to determine the distribution of seawater $f\text{CO}_2$ along the FORSA cruise using *in situ* (SST and SSS) and satellite data for Chla.

2.5. Evaluation of the spatial distribution and temporal behavior of seawater $f\text{CO}_2$

The spatial distribution and the temporal time series of the seawater $f\text{CO}_2$ in the South Atlantic Ocean were made by applying the developed algorithms with the input of the satellite products of SST, SSS and Chla to each defined seasonal period. Thus, we produced 47 monthly maps of the distribution of $f\text{CO}_2$'s, i.e., one map for each month of the period from August 2011 to June 2015. We developed an average map of seawater $f\text{CO}_2$ for each month to evaluate the spatial distribution of $f\text{CO}_2$. We also developed monthly averaged maps for each parameter input into the algorithms to improve our understanding of the distribution of $f\text{CO}_2$. To construct the temporal time series of the seawater

$f\text{CO}_2$ between 2011 and 2015, we took the 47 monthly averaged maps and obtained the averaged values for each regional area under investigation. The averaged values of each region were used to obtain the seasonal patterns and annual trends in the analyzed period.

2.6. Drivers of the variability of seawater $f\text{CO}_2$

The distribution of seawater $f\text{CO}_2$ is highly influenced by the spatial patterns of SST and SSS, the composition and concentration of primary producers and changes in Alk and DIC distributions. The main drivers changing the seawater $f\text{CO}_2$ distribution are dependent on specific ocean regions and seasons. Thus, to identify the main drivers of oceanic $f\text{CO}_2$ in each region of the study area, we first obtained the Alk and DIC surface distributions. Alk ($\mu\text{mol kg}^{-1}$) was determined by using two SST- and SSS-dependent algorithms provided by [Lee et al. \(2006\)](#), whereas each algorithm used followed the authors' latitude, SST, and SSS range requirements. We used two algorithms: an algorithm developed for the Subtropics and an algorithm developed for the Southern Ocean (see, for instance, the equations for Zones 1 and 5 provided by [Lee et al. 2006 in their Table 1](#)). The DIC ($\mu\text{mol kg}^{-1}$) distribution was derived using the program CO₂Sys v.1.1 ([van Heuven et al. 2011](#)) by inserting the parameters of Alk, $f\text{CO}_2$, SSS, and SST as input and selecting "Mehrbach refit" for the H₂CO₃ and HCO₃⁻ dissociation constants (K₁ and K₂; [Dickson and Millero 1987](#)); [Dickson \(1990\)](#) was selected for the HSO₄⁻ dissociation constant, and the total borate-salinity relationship proposed by [Uppström \(1974\)](#) was used.

To prevent the proportionally low values of SSS, Alk, and DIC in the region affected by the plume of the Plata River from influencing the averages of each

parameter, we removed the plume-affected dataset from the spatial drivers' analysis. This removal was performed by finding all salinity values lower than 34 (Piola et al. 2005) and excluding them from the subregion analyzed. Because the plume effect has only a localized influence on part of the study region, the analysis of the drivers of seawater $f\text{CO}_2$ in this particular region is shown in the Supplementary Material (Text S6, Fig. S6).

The analysis of the drivers of seawater $f\text{CO}_2$ followed the methodology proposed by Signorini et al. (2013), but we normalized Alk and DIC by the average SSS, producing Alkn and DICn. This normalization removed the effect of dilution of Alk and DIC. The authors used CO₂Sys v.1.1 to obtain the influence of each hydrographic or carbonate system parameter (i.e., SST, SSS, Alkn, and DICn) on the seawater $f\text{CO}_2$ variability. To analyze the spatial drivers, we obtained a map of $f\text{CO}_2$ anomalies in the study region and maps representing the influence of each parameter on these anomalies. To develop the temporal drivers, we produced graphics of the temporal variability of each parameter and the $f\text{CO}_2$ anomaly in each region.

3. Results

3.1. Assessment of the seawater $f\text{CO}_2$ algorithms

The *in situ* parameter with the highest correlation with *in situ* seawater $f\text{CO}_2$ was SST, followed by SSS and Log (Chla), considering both seasonal periods used in this study (Table 2). The r^2 and RMSE values between the *in situ* $f\text{CO}_2$ and other parameters were higher for the Spring-Summer (September to February) algorithm than for the Fall-Winter (March to August) algorithm (Table 3).

Table 2. Correlation coefficients (r) between $f\text{CO}_2$ and the other parameters (SST, SSS and Chla) for Spring-Summer (September to February) and Fall-Winter (March to August). All p -values are <0.05 .

Correlation (r) between $f\text{CO}_2$	SST	SSS	Log (Chla)
Spring-Summer	0.75	-0.24	-0.17
Fall-Winter	0.78	0.26	0.10

Table 3. Algorithms obtained for each seasonal division following Eq. 1: Spring-Summer (September to February); Fall-Winter (March to August). Each β has a specific unit, where β_0 is μatm , β_1 is μatm per $^{\circ}\text{C}$, β_2 is μatm per salinity unit, and $\beta_3 \mu\text{atm}$ per mg m^{-3} of chlorophyll α . Also shown are the coefficient of determination (r^2), root-mean-squared error (RMSE) and number of stations (n) used to develop each algorithm.

Algorithm	β_0	β_1	β_2	β_3	r^2	RMSE	n
Spring-Summer	397.00	8.88	-6.17	-1.40	0.71	13.81	28932
Fall-Winter	330.92	7.39	-3.99	-2.48	0.64	10.05	16731

We used the Fall-Winter algorithm to assess the seawater $f\text{CO}_2$ distribution based on the observations of the FORSA cruise during winter. On average, the seawater $f\text{CO}_2$ algorithm performed well in obtaining the derived fields (Fig. 3). The offset between the seawater $f\text{CO}_2$ observations and the predicted values was $18.9 \pm 1.0 \mu\text{atm}$, with an improvement (average offset of $10.1 \pm 1.6 \mu\text{atm}$) in the representation of the continental shelf regime (Fig. 4). According to FORSA cruise data, this area corresponds to the region where the ocean behavior changes from a strong sink to an environment that is almost in equilibrium with the atmosphere and is a small source of $f\text{CO}_2$. Although the modeled seawater $f\text{CO}_2$ in the FORSA cruise region (which included part of the ACR and offshore regions) was slightly overestimated by an order of magnitude of $\sim 20 \mu\text{atm}$, the difference was small, and the seawater $f\text{CO}_2$ distribution pattern was maintained, which is relevant given the complexity of the ocean dynamics in the region. We

assumed that the Spring-Summer algorithm had similar errors associated with its performance in reproducing the seawater $f\text{CO}_2$ distribution in the study area because the assessed period was expected to present increased mesoscale variability.

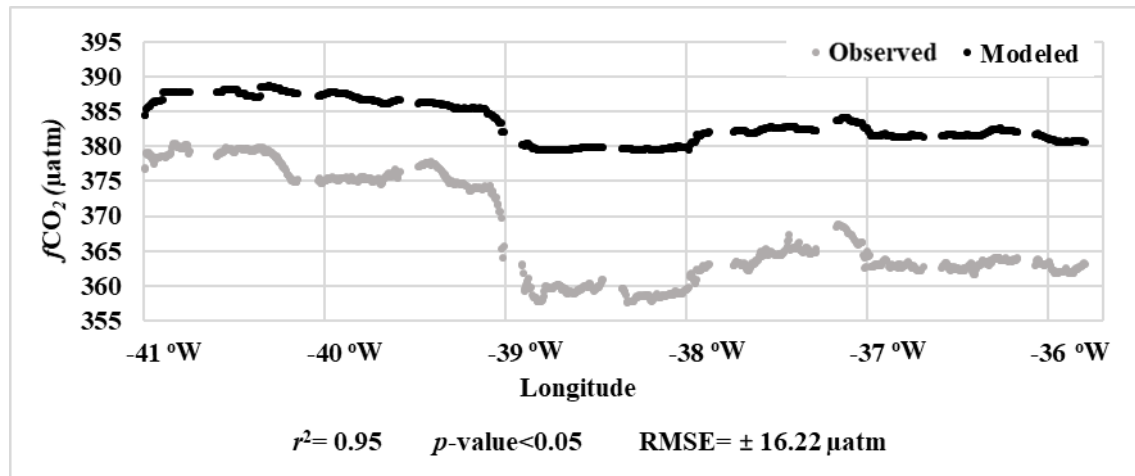


Figure 3. The seawater $f\text{CO}_2$ (μatm) reconstruction along the FORSA cruise section (Fig. 2 in blue dots) using the Fall-Winter algorithm: modeled (black) and observed (gray) data. The values shown are the coefficient of determination (r^2), p-value and root-mean-square error (RMSE) between the predicted and the modeled $f\text{CO}_2$ data.

A sensitive evaluation was performed on the use of the algorithms to verify their influence on the representation of the $f\text{CO}_2$ fields during the last month (i.e., February and August) of each seasonal period (Fig. 4). This evaluation was needed because of the use of two algorithms and the oscillations in the $f\text{CO}_2$ field in the months at the beginning and end of the seasonal periods (see, for instance, Fig. 5). For this, we applied the Spring-Summer (Fall-Winter) algorithm to the August (February) months, even though the algorithms were not originally derived to be applied at that time scale. We found that the averaged difference in seawater $f\text{CO}_2$ between the algorithms for the whole area was $22.34 \pm 0.82 \mu\text{atm}$ for February (Fig. 4a). Higher differences in $f\text{CO}_2$ ($>25 \mu\text{atm}$) were observed over the continental shelf (i.e., SBB and SSB). The averaged difference in $f\text{CO}_2$ of the

algorithms for August (Fig. 4b) was lower than that of the algorithms for February and was estimated to be 15.80 ± 1.03 μatm , with higher differences (>17 μatm) also in the continental shelf region than in the offshore region (Fig. 4b). These values were within the expected order of magnitude (~20 μatm) for the algorithms developed in this study, thus supporting their use to represent the spatial and temporal fields of seawater $f\text{CO}_2$ in the southwestern South Atlantic Ocean.

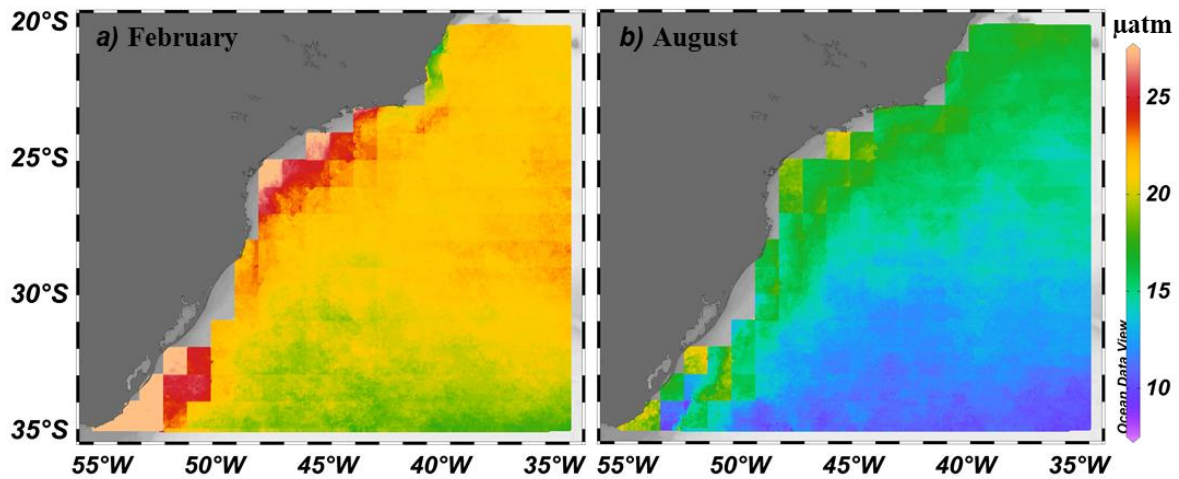


Figure 4. Spatial distribution of the difference in seawater $f\text{CO}_2$ (μatm) between both developed algorithms (i.e., the results obtained with the Spring-Summer algorithm minus the results obtained with the Fall-Winter algorithm) in the two last months of each seasonal period (i.e., February and August). The map (a) shows the absolute seawater $f\text{CO}_2$ difference for February and (b) August, the last months of the Spring-Summer and Fall-Winter periods, respectively.

3.2. Spatial distribution and temporal behavior of seawater $f\text{CO}_2$

The spatial distribution maps show the averaged distribution of the seawater $f\text{CO}_2$ for each month between 2011 and 2015 (Fig. 5). The maps of the spatial distribution of SST, SSS, and Chla in each month used to obtain these $f\text{CO}_2$ values are presented in the Supplementary Material (Figs. S1 to S3, respectively). The highest values of $f\text{CO}_2$ occurred during January and February, with an intensification of up to 425 μatm in the middle region of the SBB and near the inflow of Plata River waters at the SBS (Fig. 5a-b). The change in the

magnitude of the seawater $f\text{CO}_2$ between February and March ([Fig. 5c](#)) was abrupt (an average decrease of 23.66 μatm), with no visible intensification of the seawater $f\text{CO}_2$ near the coast. From March to August ([Fig. 5c-h](#)), the surface $f\text{CO}_2$ was continually decreasing (c.a. $-8.6 \mu\text{atm}$), mainly in the south portion of the region, reaching values below 325 μatm at 35°S. During the winter period ([Fig. 5f-h](#)), there was a marked region with seawater $f\text{CO}_2$ lower than 300 μatm in the southern portion of the SBS. Between August and September ([Fig. 5 h-i](#)), a significant increase in the seawater $f\text{CO}_2$ (14.45 μatm , on average) was observed in the offshore and SBS regions. From September to December ([Fig. 5i-l](#)), the seawater $f\text{CO}_2$ in the entire region gradually increased, with values up to 425 μatm south of the SBS and north of the SBB. Notably, the signal of coastal upwelling (intensifying the development of primary producers and, consequently, lowering seawater $f\text{CO}_2$) that occurred at the ACR was marked during all months. The Spring-Summer months presented higher variability than the Fall-Winter months. The region with the lowest seawater $f\text{CO}_2$ variability occurred at the ACR during the entire period.

The seawater $f\text{CO}_2$ seasonal cycle had the same pattern in all the subregions analyzed here ([Fig. S4](#)). In general, considering the entire study region, there was an increase in the seawater $f\text{CO}_2$ between August and February, followed by a decrease until August ([Fig. S4a](#)). The main difference between the biogeochemical provinces under investigation was related to the magnitudes of seawater $f\text{CO}_2$ ([Fig. S4b-e](#)). The ACR zone presented a lower oscillation in $f\text{CO}_2$ and higher seawater $f\text{CO}_2$ values than the other zones throughout the entire period ([Fig. S4b](#)). The SBS region showed the highest oscillation between warmer (i.e., December, January, and February) and colder

(i.e., June, July, August) months, with variations up to 80 μatm (Fig. S4d). The rapid decrease in seawater $f\text{CO}_2$ between February and March may be associated with changes in the algorithms used for each month, which were not noticeable between August and September.

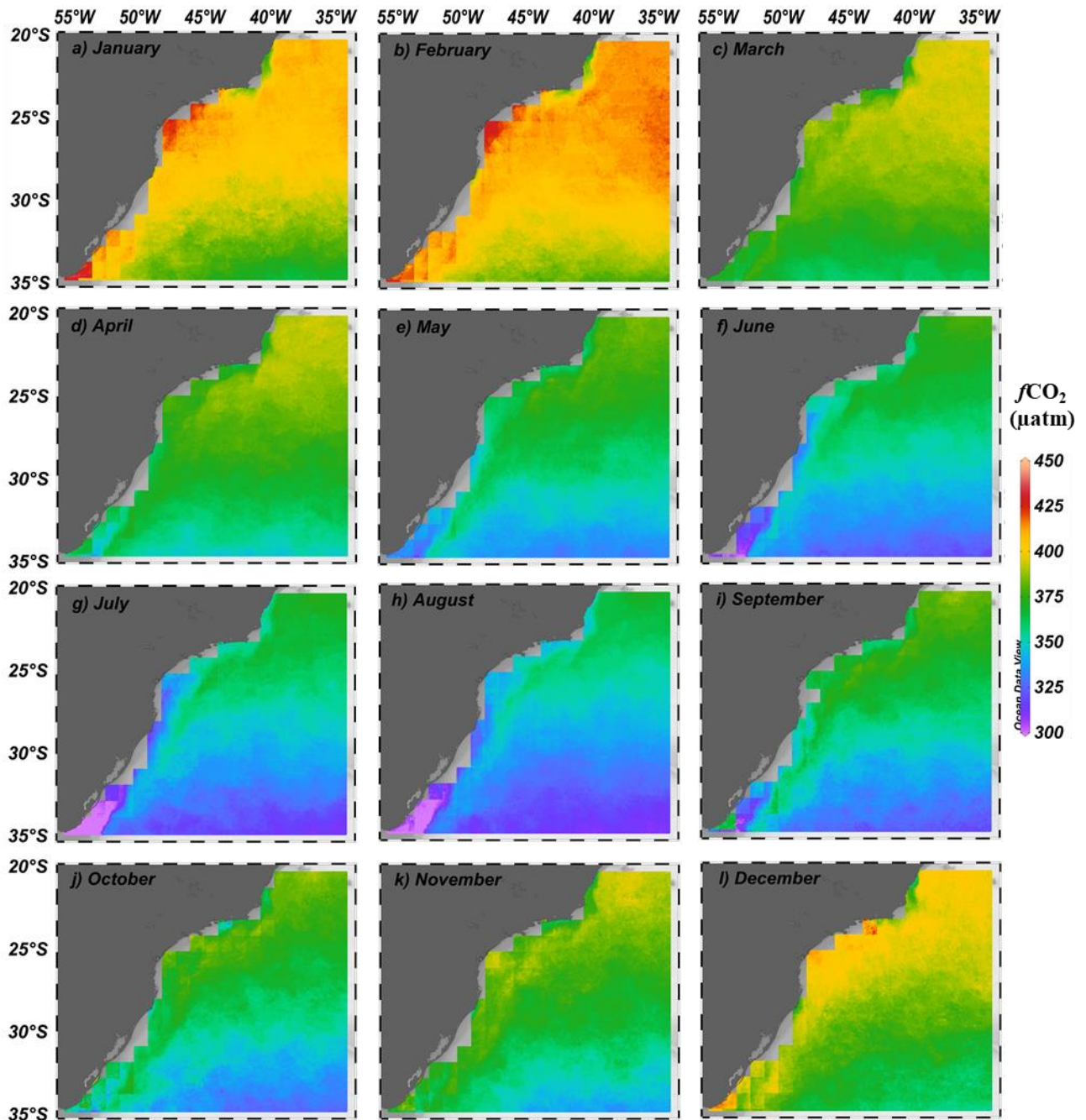


Figure 5. Spatial distribution of the seawater $f\text{CO}_2$ (μatm) in the study region for each month of the year. The panels show the averaged maps from 2011-2015. The exception is July, which was compiled for the period 2012-2015.

The interannual variability of the seawater $f\text{CO}_2$, considering all the biogeochemical provinces investigated, was relatively weak during the analyzed period ([Fig. 6](#)). Higher values of seawater $f\text{CO}_2$ were found during February ($405.66 \pm 6.77 \mu\text{atm}$), and lower values were reported in August ($337.24 \pm 18.2 \mu\text{atm}$). The difference between regions was found at the scale of annual variability. The SBS region presented higher interannual variability (approximately $98.78 \mu\text{atm}$ between February and August) and lower values of seawater $f\text{CO}_2$ ($311.34 \mu\text{atm}$ on August) than the other regions ([Fig. 6d](#)). The variabilities in $f\text{CO}_2$ in both the entire region ([Fig. 6a](#)) and offshore region ([Fig. 6e](#)) were similar in scale ($65.80 \pm 0.88 \mu\text{atm}$ between February and August) and had similar values ($404.14 \pm 0.44 \mu\text{atm}$ in February and $338.33 \pm 0.44 \mu\text{atm}$ in August). The SBB region presented high values of seawater $f\text{CO}_2$ in the Februaries of 2014 ($414.77 \mu\text{atm}$) and 2015 ($416.96 \mu\text{atm}$). The ACR region ([Fig. 6b](#)) presented the smallest oscillation of seawater $f\text{CO}_2$ between the warmer and colder months ($\sim 44.15 \mu\text{atm}$) over the entire analyzed period.

We quantified the seawater $f\text{CO}_2$ trends based on difference in the averaged $f\text{CO}_2$ for each month and the respective monthly averaged $f\text{CO}_2$ for each biogeochemical province. All subregions analyzed showed an increasing trend in seawater $f\text{CO}_2$ between 2011 and 2015 ([Fig. S5](#)). An increase of $+1.04 \mu\text{atm} \text{ y}^{-1}$ in the seawater $f\text{CO}_2$ was reported for in the entire study region in the southwestern South Atlantic Ocean ([Fig. S5a](#)). A higher increasing seawater $f\text{CO}_2$ trend of $+2.08 \mu\text{atm} \text{ y}^{-1}$ was found in the SBS ([Fig. S5d](#)), whereas a lower increasing seawater $f\text{CO}_2$ trend of $+0.77 \mu\text{atm} \text{ y}^{-1}$ was observed in the ACR ([Fig. S5b](#)). The increases in seawater $f\text{CO}_2$ in the offshore region ([Fig. S5e](#)) and the

SBB (Fig. S5c) had a similar magnitude as the increasing trend for the whole area, with values of $+0.98 \mu\text{atm} \text{ yr}^{-1}$ and $+1.09 \mu\text{atm} \text{ yr}^{-1}$, respectively.

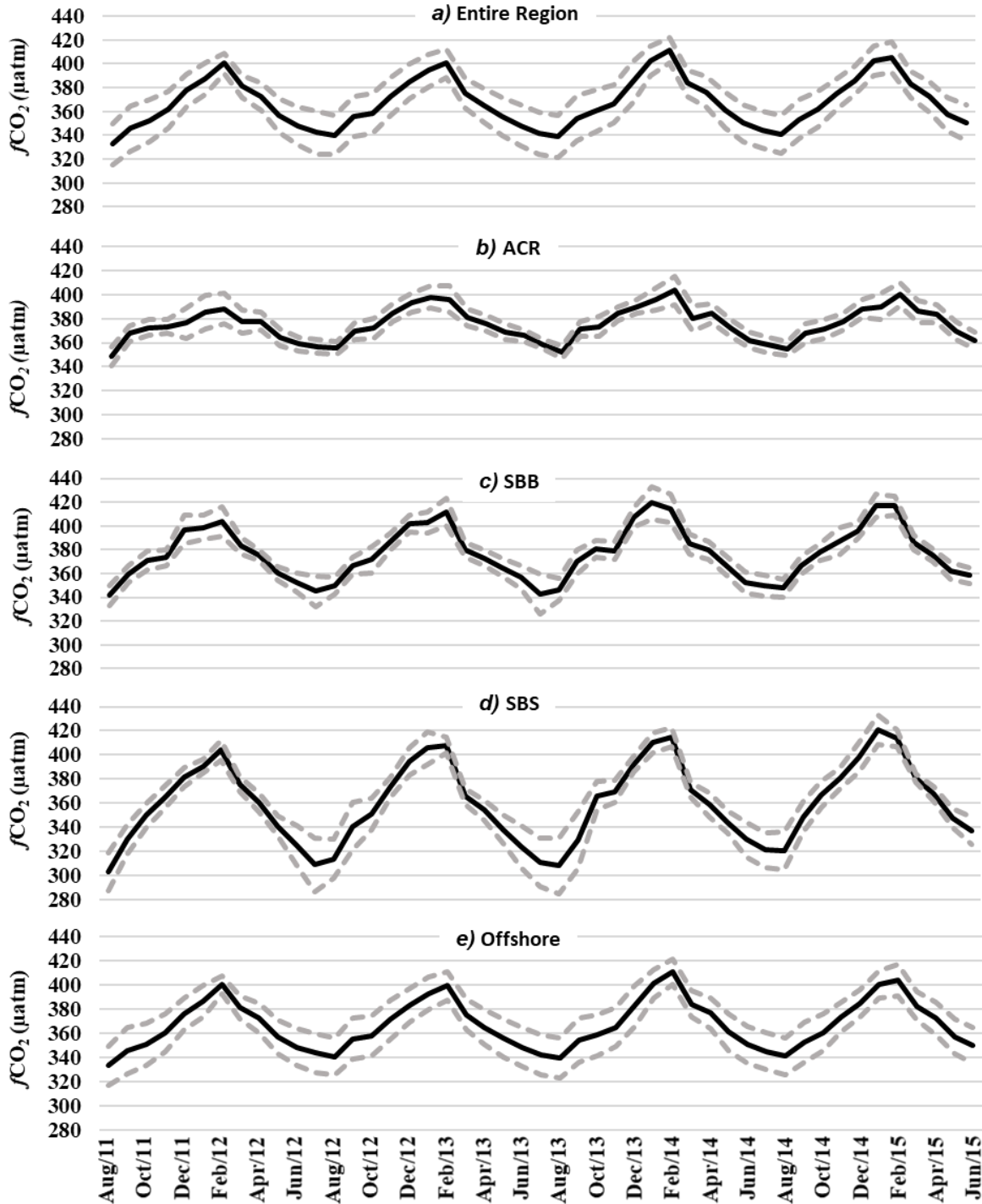


Figure 6. Interannual variability in the seawater $f\text{CO}_2$ (μatm) during the analyzed period (August 2011 to June 2015) for the (a) entire studied region, (b) Abrolhos-Campos Region (ACR), (c) South Brazil Bight (SBB), (d) Southern Brazilian Shelf (SBS), and (e) offshore region. The black line depicts the monthly $f\text{CO}_2$, and the gray dashed lines depict one standard deviation from the monthly averaged $f\text{CO}_2$.

3.3. Spatial distribution of Alk and DIC

The maps in Fig. 7 show the spatial distribution of seawater $f\text{CO}_2$, SST, SSS, Alk, and DIC used to develop the spatial drivers' analysis. The maps for seawater $f\text{CO}_2$ (Fig. 7a), SST (Fig. 7b) and SSS (Fig. 7c) were obtained from averages of the spatial maps of each parameter over the entire period. The maps for Alk and DIC were obtained using the methodology presented in Section 2.6. The distribution map for Alk showed high values ($> 2450 \mu\text{mol kg}^{-1}$) on the upper north portion in both the ACR and offshore region. High Alk values were also presented on the continental shelf break and gradually decreased southward. In the interior of the SBB, there were values of approximately $2300 \mu\text{mol kg}^{-1}$ and there were even lower values ($> 2150 \mu\text{mol kg}^{-1}$) in the south portion of the SBS. The distribution of DIC presented higher values in both the ACR and offshore region ($> 2075 \mu\text{mol kg}^{-1}$) but with less intensity, as shown with Alk. Along the continental shelf break and continental shelf, there were lower values ($> 2050 \mu\text{mol kg}^{-1}$), with the lowest values in the south portion of the continental shelf and adjacent offshore region ($> 1950 \mu\text{mol kg}^{-1}$).

The values of Alk and DIC were divided by each region and the region affected by the plume of the Plata River (Table 4). The region affected by the plume had lower values of both Alk and DIC than the other regions. As mentioned previously in Section 2.6, this region was removed from the entire region, and its spatial driver analysis results are shown in the Supplementary Material.

3.4. Drivers of the variability in seawater $f\text{CO}_2$

The distribution of the DICn had the highest influence on the spatial variability of the seawater $f\text{CO}_2$ in the southwestern South Atlantic Ocean (Fig. 8e). DICn was counteracted on the continental shelf of the SBB and SBS by the salinity (Fig. 8c) and Alkn (Fig. 8d) distributions and was counteracted in the open ocean by SST (Fig. 8b).

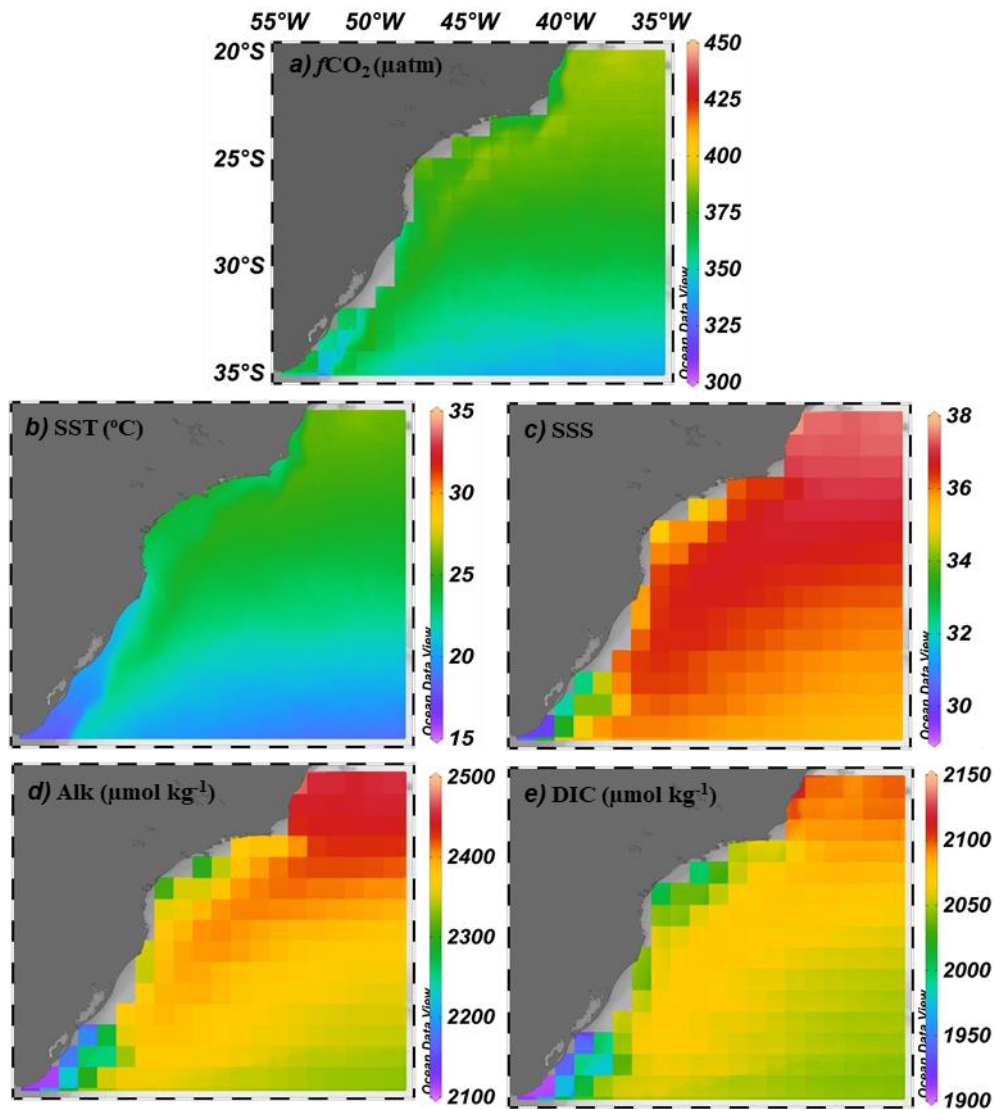


Figure 7. Averaged spatial distribution of the hydrographic and marine carbonate system parameters between 2011-2015: (a) seawater $f\text{CO}_2$ (μatm), (b) SST ($^{\circ}\text{C}$), (c) SSS, (d) Alk ($\mu\text{mol kg}^{-1}$), and (e) DIC ($\mu\text{mol kg}^{-1}$).

Table 4. Regional averages and deviations of Alk ($\mu\text{mol kg}^{-1}$) and DIC ($\mu\text{mol kg}^{-1}$) for each region and the region affected by the Plata River's plume. The Plata plume region was excluded from the other regions.

	Alk ($\mu\text{mol kg}^{-1}$)	DIC ($\mu\text{mol kg}^{-1}$)
Entire Region	2380.48 ± 35.72	2061.56 ± 18.67
ACR	2447.46 ± 12.93	2097.58 ± 8.24
SBB	2354.68 ± 27.91	2039.96 ± 19.16
SBS	2314.77 ± 48.05	2021.56 ± 28.91
Offshore	2383.28 ± 32.25	2063.67 ± 15.25
Plata Plume	2173.51 ± 41.15	1939.15 ± 24.20

The entire study region in the southwestern South Atlantic Ocean had a seawater $f\text{CO}_2$ spatial distribution positively controlled by DICn and SST, with DIC being the main driver (Fig. 9a). This region also experienced a negative influence of SSS. Changes in SSS were the main driver of changes in the seawater $f\text{CO}_2$ distribution in the SBB, with a negative effect on the seawater $f\text{CO}_2$ distribution (Fig. 9c). DICn and Alkn also had a negative impact on the seawater $f\text{CO}_2$ distribution, while SST presented a lower but positive effect. The offshore region was mainly controlled positively by Alkn but also had a positive influence on SSS, DICn, and SST (Fig. 9e). The variability of the seawater $f\text{CO}_2$ at the ACR (Fig. 9b) and the SBS (Fig. 9d) were primarily controlled by changes in the DICn and secondarily controlled by SST distributions. However, the major influence of each parameter changed among the two biogeochemical provinces. The distribution and changes of DICn had a negative (positive) influence on driving the seawater $f\text{CO}_2$ changes in the ACR (SBS). Locally on the coast of the SBS, the variations in seawater $f\text{CO}_2$ were controlled by changes in the distribution of Alkn (Fig. 9d).

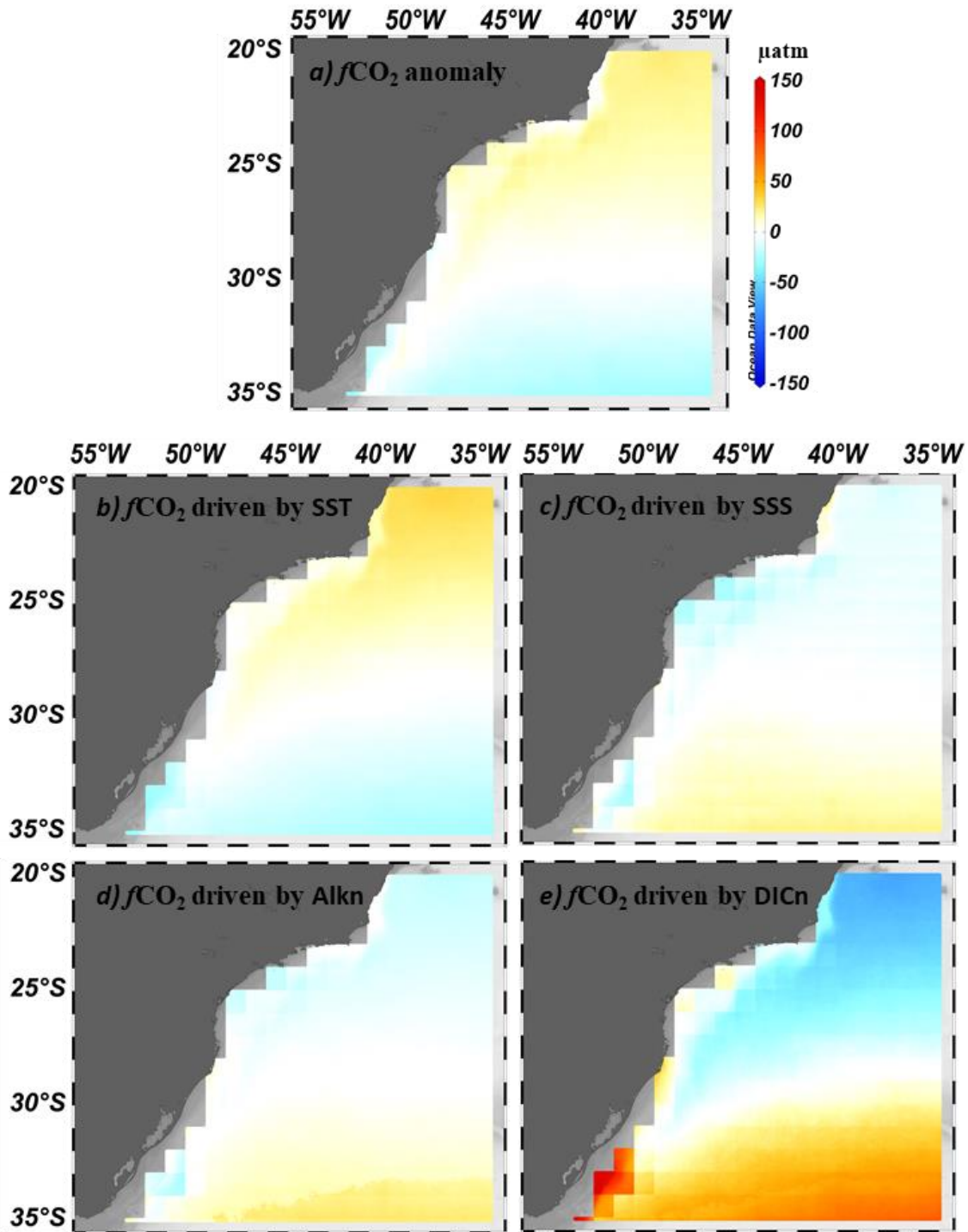


Figure 8. Spatial distribution of the seawater $f\text{CO}_2$ anomalies and parameter drivers of the seawater $f\text{CO}_2$ in the southwestern South Atlantic Ocean (μatm). The panels show the spatial distribution of (a) the seawater $f\text{CO}_2$ anomalies and the driver effect of (b) sea surface temperature (SST), (c) sea surface salinity (SSS), (d) salinity-normalized total alkalinity (Alkn) and (e) salinity-normalized total dissolved inorganic carbon (DICn).

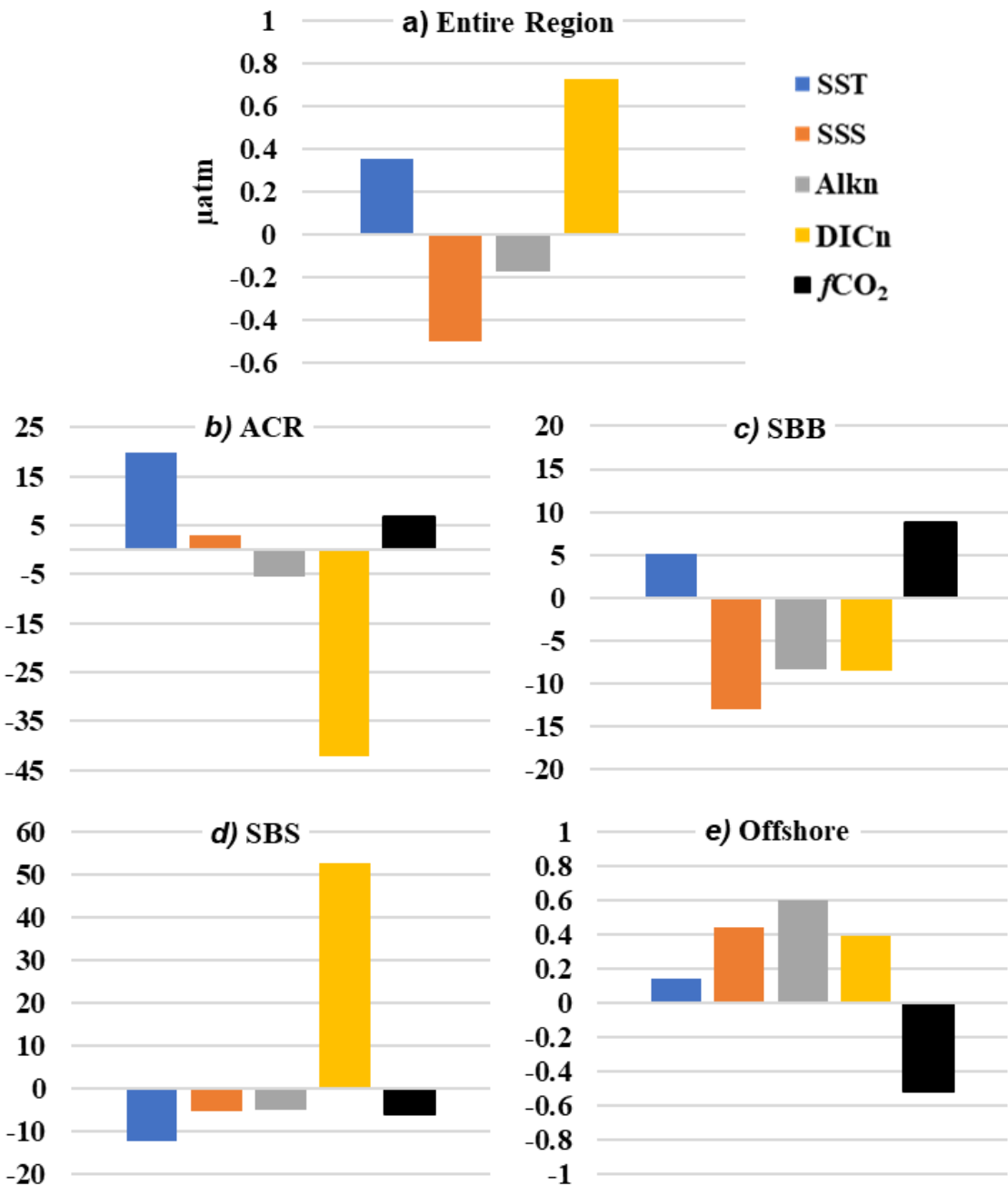


Figure 9. Drivers' influence on the seawater $f\text{CO}_2$ variability in μatm for each biogeochemical province in the southwestern South Atlantic Ocean: (a) entire studied region, (b) Abrolhos-Campos Region (ACR), (c) South Brazil Bight (SBB), (d) Southern Brazilian Shelf (SBS), and (e) offshore region. The bars represent the influence of sea surface temperature (SST, blue), sea surface salinity (SSS, orange), salinity-normalized total alkalinity (Alkn, gray), and salinity-normalized total dissolved inorganic carbon (DICn; yellow) on the spatial distribution of the seawater $f\text{CO}_2$. The black bar represents the sum of the $f\text{CO}_2$ anomalies (i.e., seawater $f\text{CO}_2$ – regional mean $f\text{CO}_2$).

In general, the SST and the combined effect of the other three parameters (i.e., SSS, Alkn, and DICn) have an opposite influence on the seawater $f\text{CO}_2$ variability over the year ([Fig. 10](#)). The change in the major influence of the drivers occurred between May to June and November to December. The influence of SSS, Alkn, and DICn on the seawater $f\text{CO}_2$ variability was reduced starting in September over all the regions analyzed. The temporal behavior of the seawater $f\text{CO}_2$ drivers in the entire region ([Fig. 10a](#)) and only in the offshore region ([Fig. 10e](#)) were similar. The ACR presented the lowest amplitudes (30 to $-30 \mu\text{atm}$) of all parameters controlling the seawater $f\text{CO}_2$ variability and was primarily controlled by DICn ([Fig. 10b](#)). The main temporal driver controlling the oscillation of the seawater $f\text{CO}_2$ in the SBS was DICn, but this region presented the highest amplitude of the analyzed regions, with values for DICn oscillating between $-107.7 \mu\text{atm}$ on February to $115.8 \mu\text{atm}$ on August and $117.5 \mu\text{atm}$ on October ([Fig. 10d](#)). The SBB also presented high amplitudes of DICn, with values ranging from $-51 \mu\text{atm}$ on February to $64 \mu\text{atm}$ on August and $61.9 \mu\text{atm}$ on October ([Fig. 10c](#)).

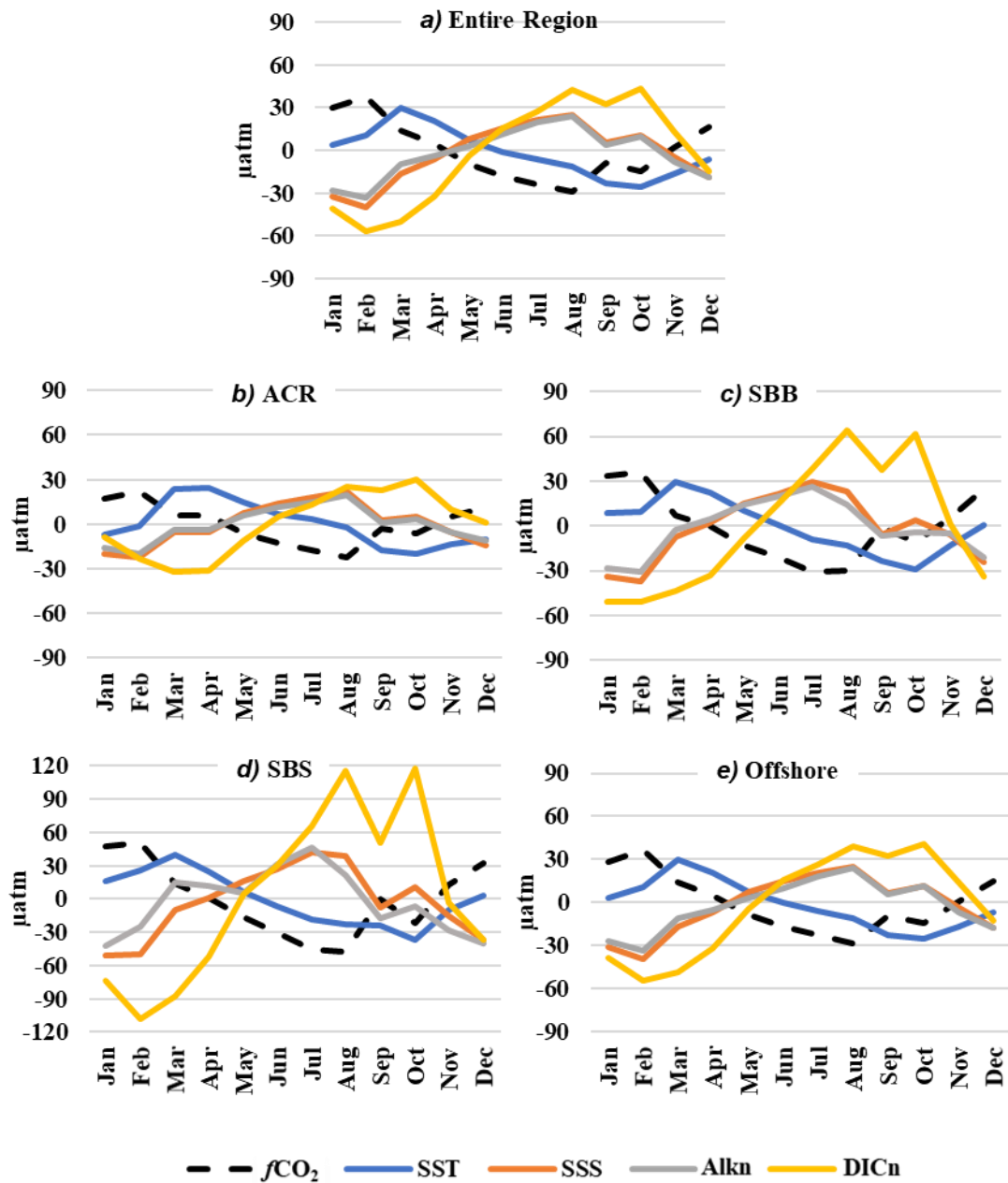


Figure 10. Seasonal cycle of the parameter drivers of the seawater $f\text{CO}_2$ in the (a) entire studied region and each subregion analyzed in this study: (b) Abrolhos-Campos Region (ACR), (c) South Brazil Bight (SBB), (d) Southern Brazilian Shelf (SBS), and (e) offshore region. Temporal anomaly of the seawater $f\text{CO}_2$ (μatm ; black) and the drivers of the seawater $f\text{CO}_2$ (μatm ; in color). The drivers evaluated are sea surface temperature (SST, blue), sea surface salinity (SSS, orange), salinity-normalized total alkalinity (Alkn, gray), and salinity-normalized total dissolved inorganic carbon (DICn, yellow).

4. Discussion

4.1. The performance of the seawater $f\text{CO}_2$ algorithms

A small number of studies have evaluated the seawater $f\text{CO}_2$ or $p\text{CO}_2$ behavior in the southwestern South Atlantic Ocean (e.g., [Ito et al. 2005, 2016](#); [Arruda et al. 2015](#); [Lencina-Avilla et al. 2016](#)). Some of these studies developed algorithms to allow finer spatial and temporal analysis of these parameters ([Table 5](#)). Our algorithms (Spring-Summer and Fall-Winter) achieved reasonable values of r^2 (0.71 and 0.64, respectively) and errors (RMSE = ± 13.81 and $\pm 10.05 \mu\text{atm}$, respectively). In spite of the comparatively low values of r^2 and the high RMSE values, both algorithms performed better at reproducing the spatial and temporal variability of seawater $f\text{CO}_2$ than the algorithms produced in previous works. [Ito et al. \(2016\)](#) developed MLR algorithms for seawater $p\text{CO}_2$ to reproduce the $p\text{CO}_2$ behaviors in the SBS and SBB regions in late spring. Their algorithm presented a good performance ($r^2 = 0.74$, RMSE = $\pm 10.73 \mu\text{atm}$, $n = 640$) and errors close to those presented in this study. [Lencina-Avilla et al. \(2016\)](#) developed MLR algorithms for the southernmost part of our study region during the late spring, two algorithms for the SBS and two for the entire transect of the South Atlantic Ocean. Among the algorithms for the SBS ($n = 550$), the algorithm for seawater $f\text{CO}_2$ presented the best r^2 (0.94) and a low standard error ($\pm 5.6 \mu\text{atm}$), but the algorithm produced by the temperature-normalized $f\text{CO}_2$ ($Nf\text{CO}_2$) fields also presented a good performance ($r^2 = 0.89$, standard error of $\pm 4.8 \mu\text{atm}$). Regarding the transect between the Brazilian and African continental shelf breaks ($n = 7430$), the algorithm for $Nf\text{CO}_2$ presented better results ($r^2 = 0.87$, standard error of $\pm 7.2 \mu\text{atm}$) than the algorithm for $f\text{CO}_2$ ($r^2 = 0.11$, standard error of $\pm 7.4 \mu\text{atm}$).

μatm). Orselli et al. (2019) developed four algorithms ($p\text{CO}_2$, $Np\text{CO}_2$, $f\text{CO}_2$, $Nf\text{CO}_2$) for the entire FORSA cruise ($n = 8650$), which crossed the South Atlantic Ocean in a Southeast-Northwest direction during the winter and reached the SBB. All four algorithms achieved good values of r^2 ($r^2 = 0.81$, 0.91 , 0.86 , and 0.90) and low standard errors for $p\text{CO}_2$ and $f\text{CO}_2$, ($\pm 6.74 \mu\text{atm}$, $\pm 7.37 \mu\text{atm}$, $\pm 6.21 \mu\text{atm}$, and $\pm 6.72 \mu\text{atm}$).

Table 5. List of previous studies that used seawater CO_2 algorithms developed for the southwestern South Atlantic Ocean and their respective performances, sampling periods, evaluated parameters (i.e., $p\text{CO}_2$, $Np\text{CO}_2$, $f\text{CO}_2$, $Nf\text{CO}_2$), correlation coefficient values (r^2), associated errors (i.e., *Root-mean-square error or **Standard Error; μatm), and sample numbers (n). $Np\text{CO}_2$ and $Nf\text{CO}_2$ are the forms of $p\text{CO}_2$ and $f\text{CO}_2$ normalized by the mean sampled temperature, respectively.

References	Studied region	Sampled period	Parameter evaluated	r^2	Associated error	n
This study	Open ocean region and continental shelf	Spring and Summer	$f\text{CO}_2$	0.71	$\pm 13.81^*$	28932
		Fall and Winter	$f\text{CO}_2$	0.64	$\pm 10.05^*$	16731
Ito et al. (2016)	Brazilian Continental Shelf	Late spring	$p\text{CO}_2$	0.74	$\pm 10.73^*$	640
Lencina-Avila et al. (2016)	Brazilian Continental Shelf	Late fall to early spring	$f\text{CO}_2$	0.94	$\pm 5.6^{**}$	550
			$Nf\text{CO}_2$	0.89	$\pm 4.8^{**}$	
Orselli et al. (2019)	Section along 35°S across the open ocean	Winter	$f\text{CO}_2$	0.11	$\pm 7.4^{**}$	7430
			$Nf\text{CO}_2$	0.87	$\pm 7.2^{**}$	
			$p\text{CO}_2$	0.81	$\pm 6.74^{**}$	
			$Np\text{CO}_2$	0.91	$\pm 7.37^{**}$	
	Section along 35°S across the open ocean and continental shelf		$f\text{CO}_2$	0.86	$\pm 6.21^{**}$	8650
			$Nf\text{CO}_2$	0.90	$\pm 6.72^{**}$	

The Fall-Winter algorithm showed a good performance ($r^2 = 0.95$, RMSE = $\pm 16.22 \mu\text{atm}$) in reproducing the FORSA dataset in the southwestern South Atlantic (Fig. 4), with an improved representation over the continental shelf and shelf break. On average, the overall difference between predicted and modeled seawater $f\text{CO}_2$ values was $18.9 \pm 1.0 \mu\text{atm}$, which was reduced in the coastal

regimes of the ACR region ($10.1 \pm 1.6 \mu\text{atm}$). The representation of the spatial variability of seawater $f\text{CO}_2$ was reasonable; however, the mesoscale processes observed by [Orselli et al. \(2019\)](#) would be smoothed by the algorithms from this study. [Orselli et al. \(2019\)](#) noted the occurrence of a change in the sea–air CO_2 fluxes in the region closest to Brazil from CO_2 sink behavior in the oceanic domain to slight CO_2 source behavior over the continental slope and shelf.

4.2. Spatiotemporal distribution of the seawater $f\text{CO}_2$ in the southwestern South Atlantic Ocean

The spatial oscillation pattern of the seawater $f\text{CO}_2$ in the southwestern South Atlantic Ocean followed the seasonal variation in SST, except for in regions influenced by upwelling processes and continental runoff ([Fig. S1](#)). Those regions on the continental shelf domain had the highest variability of Chla ([Fig. S3](#)) and SSS ([Fig. S2](#)). The averaged values of seawater $f\text{CO}_2$ oscillated in the study region between $404.5 \pm 10.0 \mu\text{atm}$ on February to $337.9 \pm 16.3 \mu\text{atm}$ on August ([Fig. 6a](#)). In the climatology presented by [Takahashi et al. \(2014\)](#), the values for February and August in our study region ranged from $381.4 \pm 16.2 \mu\text{atm}$ to $333.6 \pm 16.8 \mu\text{atm}$, respectively, for the reference year 2005. We also observed an annual trend in $f\text{CO}_2$ of $1.0 \mu\text{atm y}^{-1}$ ([Fig. S5a](#)) for the entire study region.

The ACR showed the lowest oscillation of the regions, with mean values of seawater $f\text{CO}_2$ of $396.9 \pm 4.9 \mu\text{atm}$ on February and $352.7 \pm 2.8 \mu\text{atm}$ on August ([Fig. 6b](#)). This low seasonal oscillation in the region may be the cause of the lowest annual trend of the entire studied region ($+0.77 \mu\text{atm y}^{-1}$) ([Fig. S5b](#)). [Ito et al. \(2016\)](#) found values of $p\text{CO}_2$ greater than $400 \mu\text{atm}$ during the early summer period in the ACR, indicating that this region was under the influence of

coastal upwelling and mesoscale cyclonic eddy activity. The lower variability in the seawater $f\text{CO}_2$ found here could be associated with the almost constant levels of primary production in the region over the year (Valentin 2001) or could be associated with the lower resolution of our results in the coastal region than in the offshore region.

The SBB presented great spatial variability on its shelf due to interactions with other regions. The average values of seawater $f\text{CO}_2$ on the SBB oscillated from $411.8 \pm 5.0 \mu\text{atm}$ on February to $346.2 \pm 3.0 \mu\text{atm}$ on July (Fig. 6c). During the entire period evaluated, seawater with relatively low $f\text{CO}_2$ values was identified coming from the ACR (Fig. 5). During warm months, the Brazil Current transported waters with relatively high values of $f\text{CO}_2$ to the inner continental shelf of the region. However, during the winter, this transport decreased, with changes in the intensity of the Brazil Current, and the SBB received waters with low $f\text{CO}_2$ from the northward advance of the STSF along the continental shelf (Fig. 5f-h). In this way, the variability of $f\text{CO}_2$ in the SBB was a product of the intensity of interactions with surface water masses from the ACR, SBS and Brazil Current reaching this province. In previous studies, it was observed that the concentrations of Chla and nutrients in the SBB were higher during the winter than during the summer due to the intrusion of rich cold water transported from the south by a coastal current producing relatively low values of $f\text{CO}_2$ (e.g., Ito et al. 2005; Kampel, 2003). The same behavior was found in this study (see Fig. S3f-h for Chla). Ito et al. (2016) found mean values of $397.5 \pm 22.9 \mu\text{atm}$ for the SBB during November 2010, values close to those found here (Fig. 5k). In addition, the annual increasing trend of $1.09 \mu\text{atm y}^{-1}$ (Fig. S5c) suggests, in

general terms, seawater from the ACR and Brazilian Current has a greater influence than that from the SBS at the SBB.

The SBS had the highest range of seawater $f\text{CO}_2$ of the analyzed regions, with values varying from $410.1 \pm 4.4 \mu\text{atm}$ on February to $311.3 \pm 6.5 \mu\text{atm}$ on August ([Fig. 6d](#)). This region also presented an annual $f\text{CO}_2$ trend of $2.1 \mu\text{atm y}^{-1}$ ([Fig. S5d](#)), the highest value reported in our results. These values can be explained by the extreme seasonal changes in physical parameters caused by the influence of the La Plata River and Patos-Mirim Lagoon plumes ([Lefèvre and Moore, 2000](#)) and the seasonal behavior of the STSF ([Piola et al. 2000](#)). During summer, plumes of relatively fresh water ([Fig. S2a-b, and 2i](#)) with relatively high Chla ([Fig. S3a-b, and 3i](#)) are entrapped south of 32°S by the STSF, and due to values of $\text{SST} > 25^\circ\text{C}$ ([Fig. S1a-b, and 1i](#)), there are high values of $f\text{CO}_2$ ($> 425 \mu\text{atm}$; [Fig. 5a-b and 5i](#)). During winter, cold waters ($\text{SST} < 22.5^\circ\text{C}$; [Fig. S1f-h](#)) are transported up the continental shelf with low-salinity waters ([Fig. S2f-h](#)), causing low values of $f\text{CO}_2$ ($< 350 \mu\text{atm}$; [Fig. 5f-h](#)) in the region.

The offshore region presented a temporal oscillation in seawater $f\text{CO}_2$ from $403.8 \pm 4.5 \mu\text{atm}$ on February to $338.6 \pm 3.16 \mu\text{atm}$ on August ([Fig. 6e](#)). The spatial distribution of the seawater $f\text{CO}_2$ on the eastern portion of the offshore region followed a latitudinal pattern, with relatively high values in the north and low values in the south ([Fig. 5](#)). The area with the relatively high $f\text{CO}_2$ increased southward during summer and decreased during winter. These patterns of variability followed the same seasonal oscillation behavior as SST ([Fig. S1](#)). Near the continental shelf break, the spatial distribution of $f\text{CO}_2$ followed the Brazil Current's seasonal oscillation (e.g., [Ito et al. 2016](#)), with increased intensity during summer and decreased intensity during winter. The annual trend in $f\text{CO}_2$ of the

offshore region was $0.98 \mu\text{atm yr}^{-1}$ (Fig. S5e), which was close to the upper limit found by Lenton et al. (2012). Those authors analyzed a larger portion of the South Atlantic Ocean, between the latitudes of 10°S and 45°S and longitudes of 60°W and 10°E , and showed an increase in $p\text{CO}_2$ of $0.2 \pm 1.0 \mu\text{atm yr}^{-1}$. Lenton et al. (2012) associated this value with the enhanced sink of atmospheric CO_2 driven by biological production and vertical stratification.

4.3 What are the main drivers of seawater $f\text{CO}_2$ in the biogeochemical provinces of the southwestern South Atlantic Ocean?

The analysis of the spatial drivers of $f\text{CO}_2$ showed that the main spatial driver was DICn (Fig. 8e). We found differences in the secondary drivers between the continental shelf and offshore region. SSS and Alkn were secondary drivers on the continental shelf (Fig. 8c, d), and SST had an important role in the offshore region (Fig. 8b). Arruda et al. (2015) analyzed the spatial distribution and temporal behavior of seawater $p\text{CO}_2$ by modeling the entire southwestern South Atlantic Ocean (15° to 55°S , and 70° to 35°W), and they also found that the region is mainly controlled by DICn . Regarding secondary drivers, they found that SST and Alkn counteract DICn . Lenton et al. (2012) analyzed an Atlantic Sector of the Southern Ocean from 2001 to 2008 and found that the main spatial driver of $p\text{CO}_2$ was Alkn , followed by DICn . Although these differences in the results between our work and their works may be associated with the sizes of the studied regions, all studies found that DICn is an important driver of $f\text{CO}_2$ or $p\text{CO}_2$.

The analysis of temporal drivers over the entire region showed that the temporal variability of the seawater $f\text{CO}_2$ was controlled by the alternation between SST and DICn (Fig. 10a). Takahashi et al. (1993), Signorini et al. (2013),

and [Arruda et al. \(2015\)](#) also reported a similar pattern of seasonal oscillation between the drivers of seawater $f\text{CO}_2$ or $p\text{CO}_2$. [Signorini et al. \(2013\)](#) attributed this pattern to winter mixing and spring-summer biological drawdown. The SBB and SBS, regions affected by the seasonal oscillation of the STSW, presented the highest seasonal oscillation between drivers ([Fig. 10c](#) and [Fig. 10d](#)). Both regions presented DICn that was expressively proportional to the other drivers. On the SBB, we found changes driven by DICn ranging between $-51 \mu\text{atm}$ on February to $64 \mu\text{atm}$ on August ([Fig. 10c](#)). This pattern of variability, where surface water masses from the ACR, SBS and Brazil Current have different thermohaline properties, as well as different biological and chemical properties, explains why the SSS changes were the main driver of changes in the seawater $f\text{CO}_2$ distribution in the SBB, followed by DICn and Alkn, in this study ([Fig. 9c](#)). These values were higher than the results reported by [Arruda et al. \(2015\)](#) on the SBB. They found that the contributions of both SST and DICn ranged between -10 to $10 \mu\text{atm}$. In agreement with [Arruda et al. \(2015\)](#), in our work, we observed that the SBS was the region with the highest temporal oscillation of seawater $f\text{CO}_2$ and the region in which DICn exerted the greatest control on $f\text{CO}_2$. Some differences in the results between the two studies may be associated with the different approaches. In this work, we developed our analysis based on MLR algorithms and satellite-derived parameters, while other authors (e.g., [Lenton et al. 2012](#); [Arruda et al. 2015](#)) conducted their analysis based on physical models and climatology.

5. Summary and conclusions

In this study, we investigated the spatial distribution and temporal behavior of seawater $f\text{CO}_2$ in the southwestern South Atlantic Ocean from mid-2011 to mid-2015. We also investigated the drivers of seawater $f\text{CO}_2$ that control its variability. We used an extensive dataset to reconstruct the spatiotemporal variability of seawater $f\text{CO}_2$ through satellite images between 2011 and 2015. Three distinct databases were used (i.e., SOCAT, LDEO and GOAL) to produce two MLR algorithms based on SST, SSS, and Chla for the Spring-Summer and Fall-Winter periods. Both algorithms performed reasonably well (Spring-Summer: $r^2 = 0.71$, RMSE = $\pm 13.81 \mu\text{atm}$, $n = 28932$; Fall-Winter: $r^2 = 0.64$, RMSE = $\pm 10.05 \mu\text{atm}$, $n = 16731$) and demonstrated a good performance ($r^2 = 0.95$; RMSE = $\pm 16.22 \mu\text{atm}$) when compared to an independent dataset. A seawater $f\text{CO}_2$ offset of $18.9 \pm 1.0 \mu\text{atm}$ was found for the entire region evaluated; this offset was reduced to $10.1 \pm 1.6 \mu\text{atm}$ when only the continental shelf region was considered. These algorithms made it possible to reproduce the spatial distribution and temporal behavior of the seawater $f\text{CO}_2$ in a relatively undersampled region of the ocean. Some improvements can be made by improving the sampling rate or by applying other algorithm-development techniques (e.g., feedforward neural networking; e.g., [Moussa et al. 2015](#) and [Benallal et al. 2017](#)).

The spatial-temporal analysis showed that the Brazil Current influenced the seasonal distribution of $f\text{CO}_2$, both in the offshore region and continental shelf. In the ACR, the coastal upwelling system was responsible for the relatively low seasonal changes in seawater $f\text{CO}_2$ and the low annual $f\text{CO}_2$ trend ($0.77 \mu\text{atm y}^{-1}$). The SBB waters seemed to be controlled by the Brazil Current's flow over the

outer shelf, the inflow of low- $f\text{CO}_2$ waters from the ACR in the upper region, and the seasonal oscillation of the front on the southern portion. In the SBS, the seasonal oscillation of the STSW affected the seawater $f\text{CO}_2$ dynamics by controlling the distribution of the Plata River and Patos-Mirim plumes along the shelf. Because these waters present relatively low values of $f\text{CO}_2$, this seasonal oscillation resulted in the SBS being the most variable region in the study region. This part of the shelf presented the highest annual seawater $f\text{CO}_2$ trend ($2.08 \mu\text{atm y}^{-1}$). In the overall region, the spatiotemporal dynamics of seawater $f\text{CO}_2$ were controlled by the opposite relationship between DICn and SST. However, in the SBB and SBS, two regions within the influence of the STSW seasonal dynamics, the DICn showed higher seasonal oscillation.

Acknowledgements

This study contributes to the activities of the Brazilian Ocean Acidification Network (BrOA; www.broa.furg.br) and the Brazilian High Latitude Oceanography Group (GOAL). The oceanographic cruises that compose the GOAL database were sponsored by the Brazilian National Council on Research and Development (CNPq grant no. 558267/2009-2, 445506/2014-8), the Foundation of Research Support to the State of Rio Grande do Sul (FAPERGS grant no. 2075-2551/13-7), the CAPES Foundation (grant no. 23038.001421/2014-30), and the support of the Brazilian Ministry of Science, Technology, Innovation and Communication (MCTIC). We would also like to thank the producers, supporters, collaborators, and distributors of SOCAT, LDEO, NASA, and ACRI-ST for providing high-quality datasets for our work. C.C. Liutti acknowledge CAPES scholarship grant no. 23038.013648/2018-51. R. Kerr acknowledges CNPq researcher grants n°

302604/2015-4 and 304937/2018-5 and CAPES grant nº 88881.195000/2018-01. I. B. M. Orselli acknowledges CAPES/CMAR2 for her Ph.D. funding (CAPES process nº. 23038.001421/2014-30). R. G. Ito acknowledges CNPq DTI-1 grant nº 381207/2011-0. The GOAL and BrOA datasets can be provided by request. We thank researchers and students from LEOC (FURG), LABFITO (FURG) and LAGOM/LABOQUI (UERJ) for help with sampling during the cruise and/or laboratory analysis and data preprocessing. We also thank the Brazilian Navy, especially the officers, crew, and all researchers onboard the vessels RV Cruzeiro do Sul and RV Vital de Oliveira, for providing logistical and sampling support during the GOAL cruises.

Supplementary Material

The Supplementary Material section presents auxiliary materials used to develop this work's results and discussion that are not relevant to the comprehension of the main text but may be interesting to some readers. The maps of the spatial distribution of SST, SSS and Chla for each month used to obtain the maps of the spatial distribution of seawater $f\text{CO}_2$ are shown in Figs S1, S2 and S3, respectively. These maps were used to understand how oscillations of the spatial distribution were controlled by each parameter. We also present the seasonal cycle of seawater $f\text{CO}_2$ for all subregions analyzed in this work ([Fig. S4](#)) and graphics with the linear seawater $f\text{CO}_2$ trend for each region over the analyzed period (2011 to 2015) ([Fig. S5](#)). Both figures are presented in detail in [Section 3.2](#) of the main document. The Supplementary Material section also presents the results of the spatial drivers of the seawater $f\text{CO}_2$ analysis in the La Plata River plume ([Text S6, Fig S6](#)).

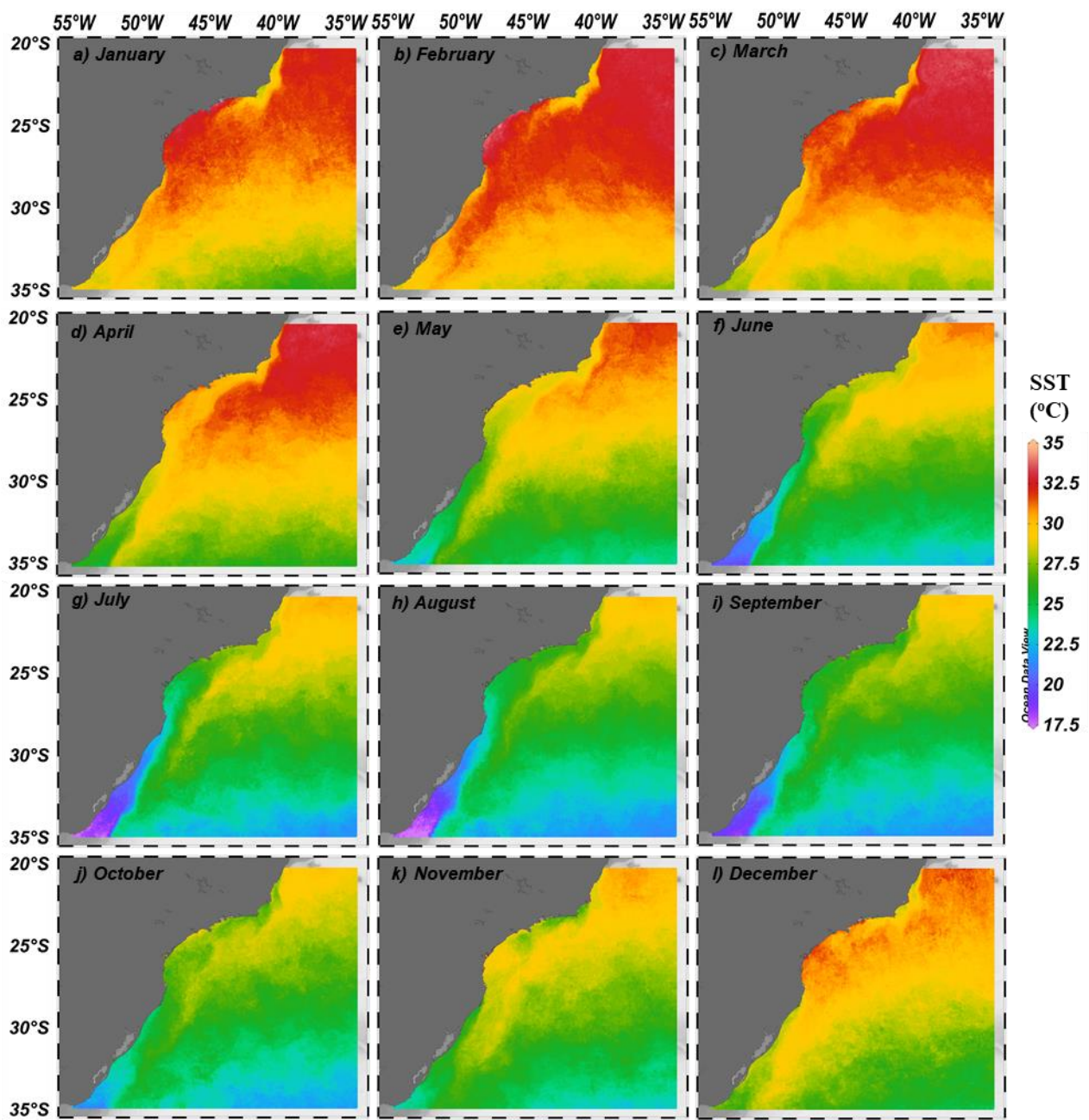


Figure S1. Spatial distribution of the SST ($^{\circ}\text{C}$) of the study region. The panels show the averaged maps for each month from 2011-2015. The exception is July, which was compiled for the period 2012-2015.

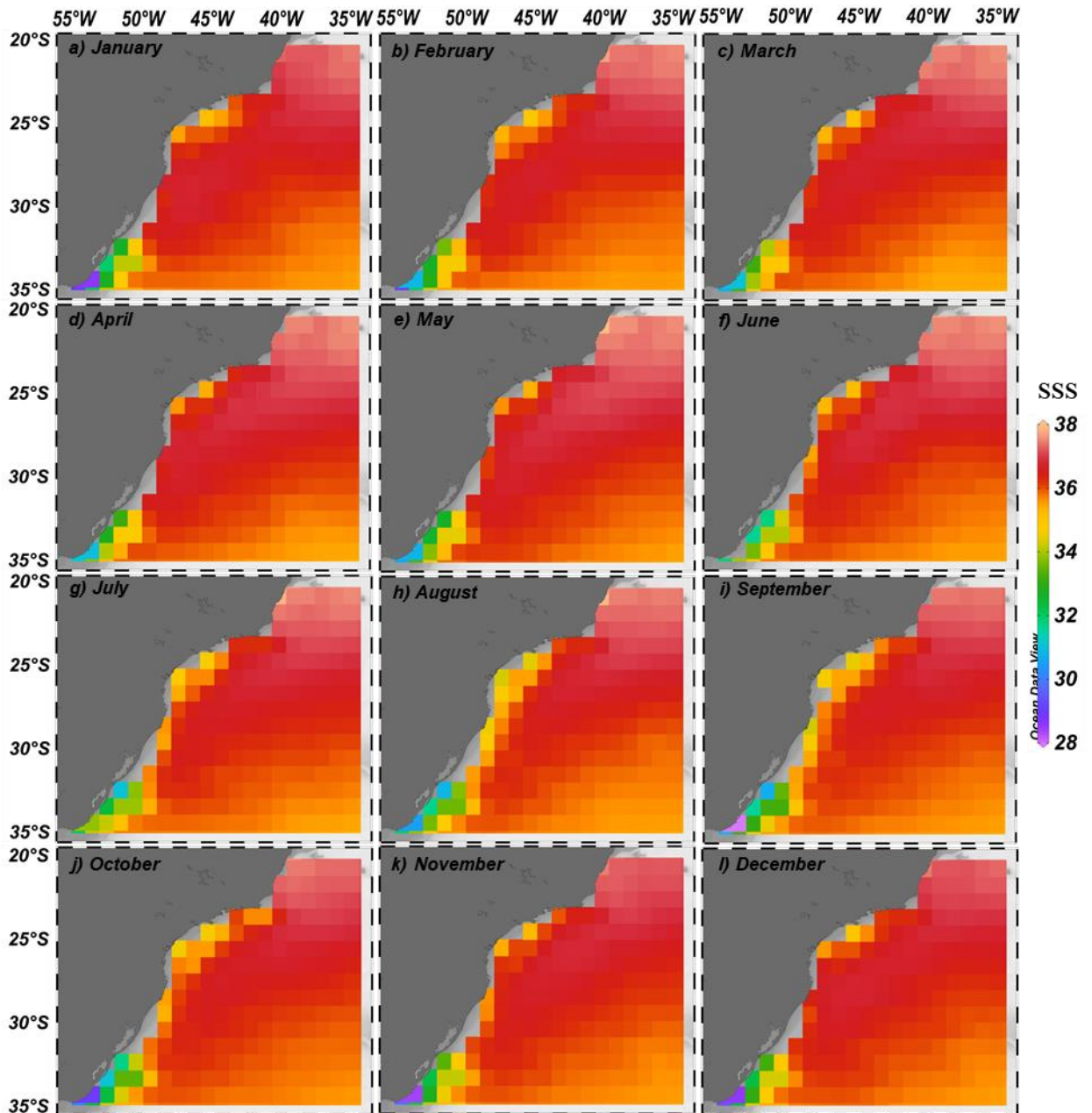


Figure S2. Spatial distribution of the SSS of the study region. The panels show the averaged maps for each month from 2011-2015. The exception is July, which was compiled for the period 2012-2015.

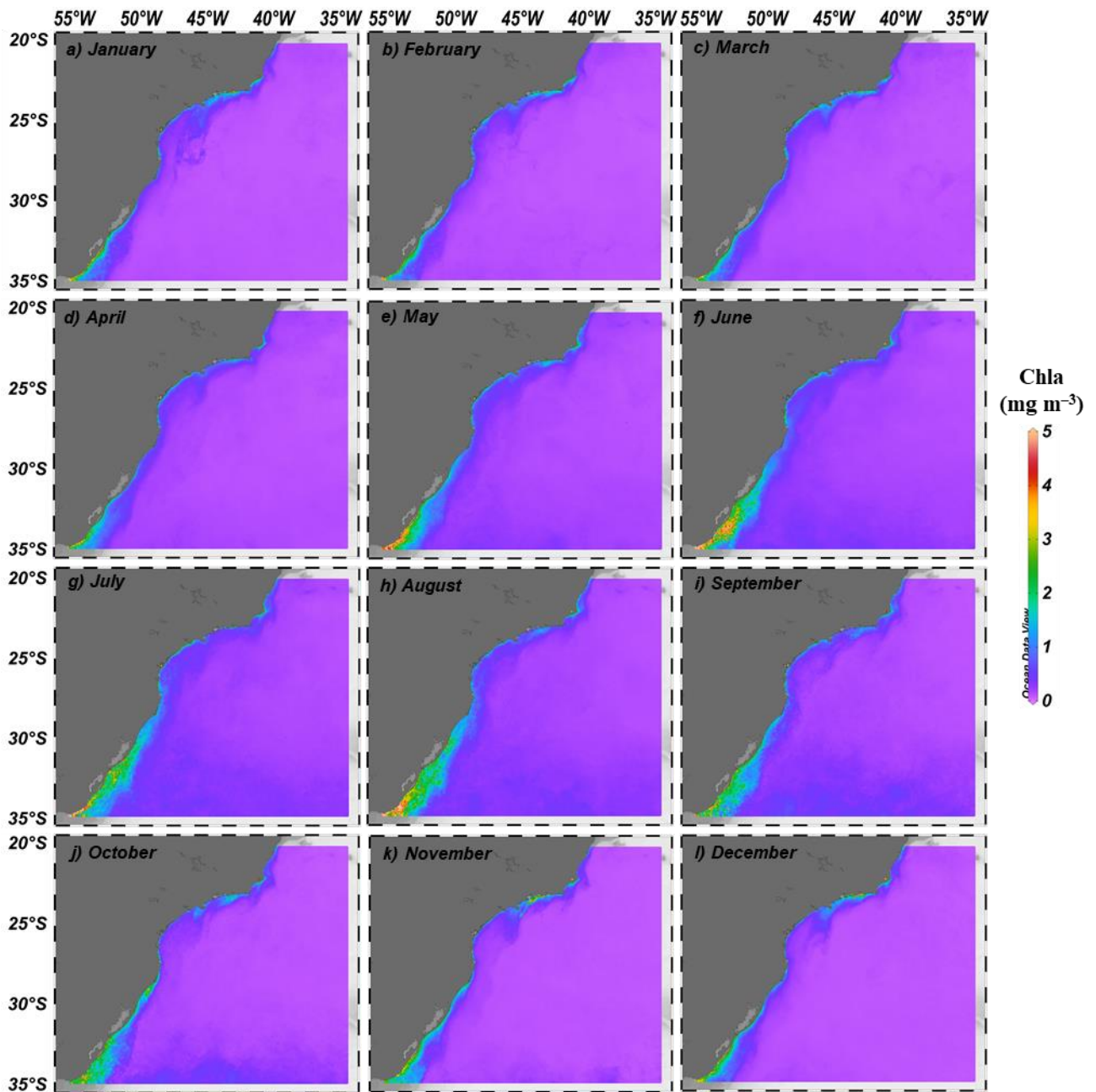


Figure S3. Spatial distribution of the Chla (mg m^{-3}) of the study region. The panels show the averaged maps for each month from 2011-2015. The exception is July, which was compiled for the period 2012-2015.

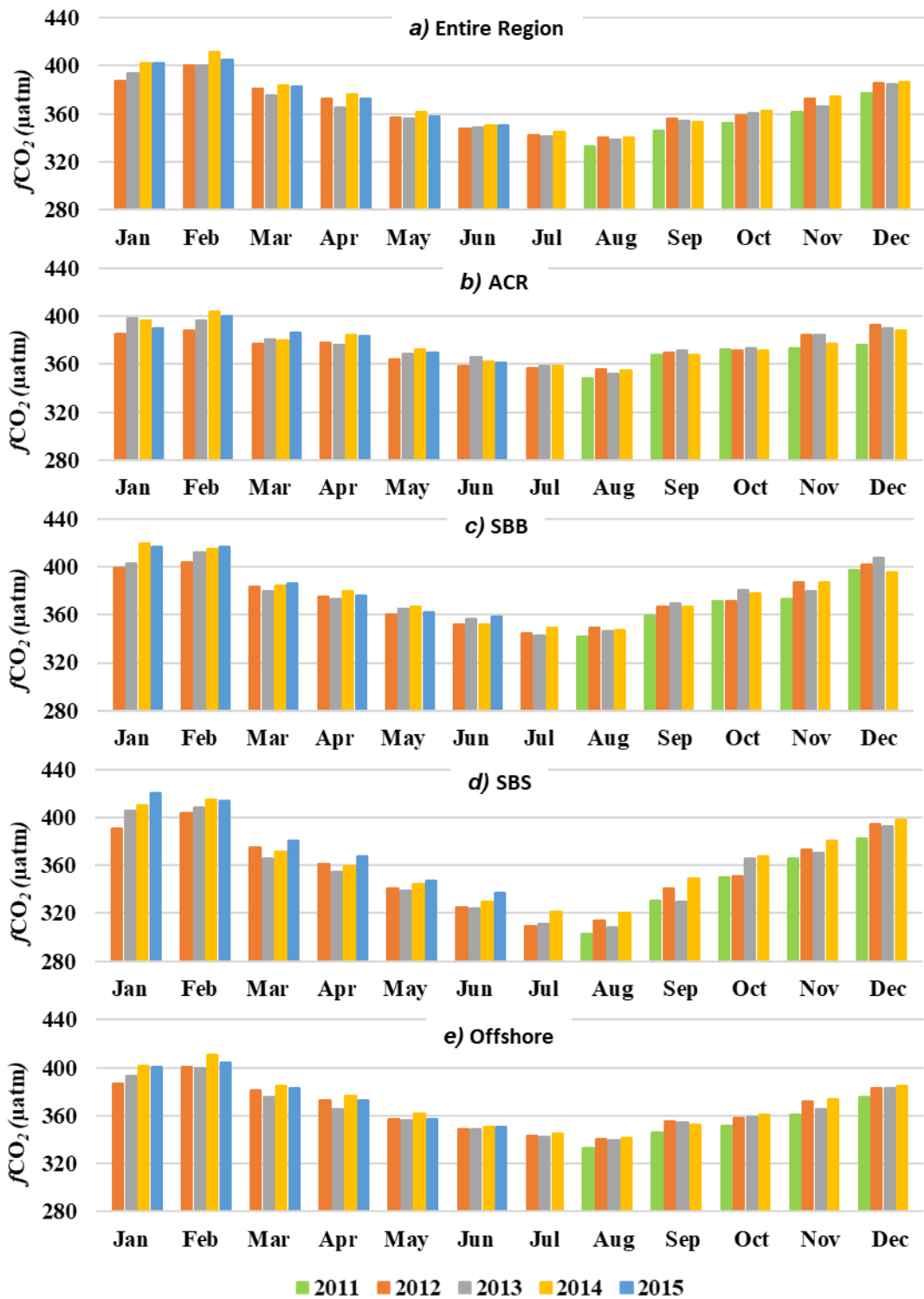


Figure S4. Seasonal cycle of the regional seawater $f\text{CO}_2$ (μatm) during the analyzed period (August 2011 to June 2015) for the (a) entire studied region in the southwestern South Atlantic Ocean, (b) Abrolhos-Campos Region (ACR), (c) South Brazil Bight (SBB), (d) Southern Brazilian Shelf (SBS) and (e) offshore region.

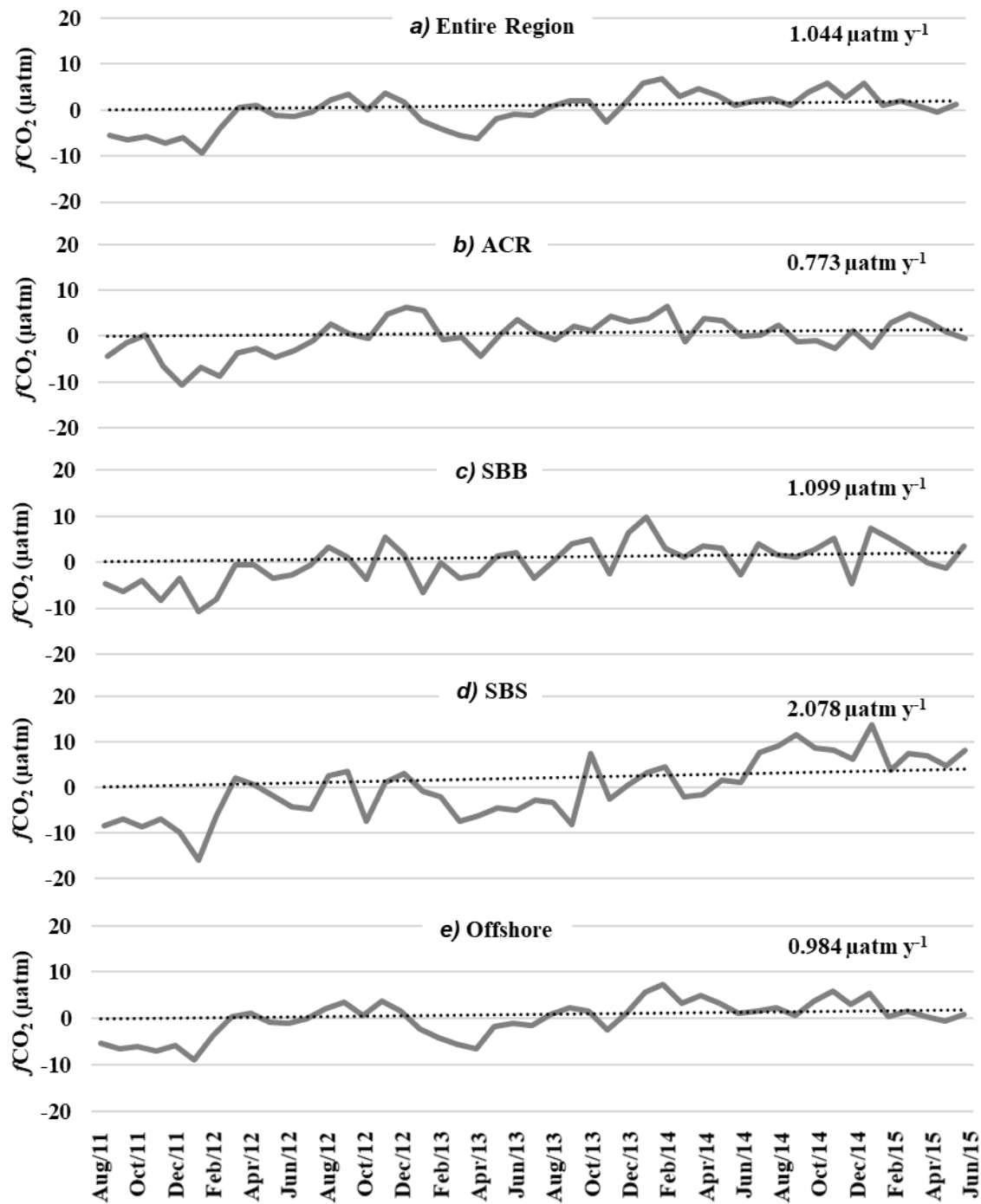


Figure S5. The annual seawater $f\text{CO}_2$ trend (μatm) based on the difference between the $f\text{CO}_2$ in each month and the respective monthly average (gray line) for the (a) entire studied region, (b) Abrolhos-Campos Region (ACR), (c) South Brazil Bight (SBB), (d) Southern Brazilian Shelf (SBS), and (e) offshore region. The annual trend for each biogeochemical province is shown in each panel. The trend is represented by a black dotted line.

Text S6: An analysis of the Plata Plume subregion in the SBS (Fig. S6) indicated that both Alk (Fig. S6d) and DIC (Fig. S6e) have a considerable impact on changes in $f\text{CO}_2$. These two parameters have opposite effects on the $f\text{CO}_2$ distribution. The SST (Fig. S6b) and SSS (Fig. S6c) have similar behaviors and counteract the effect of the DIC.

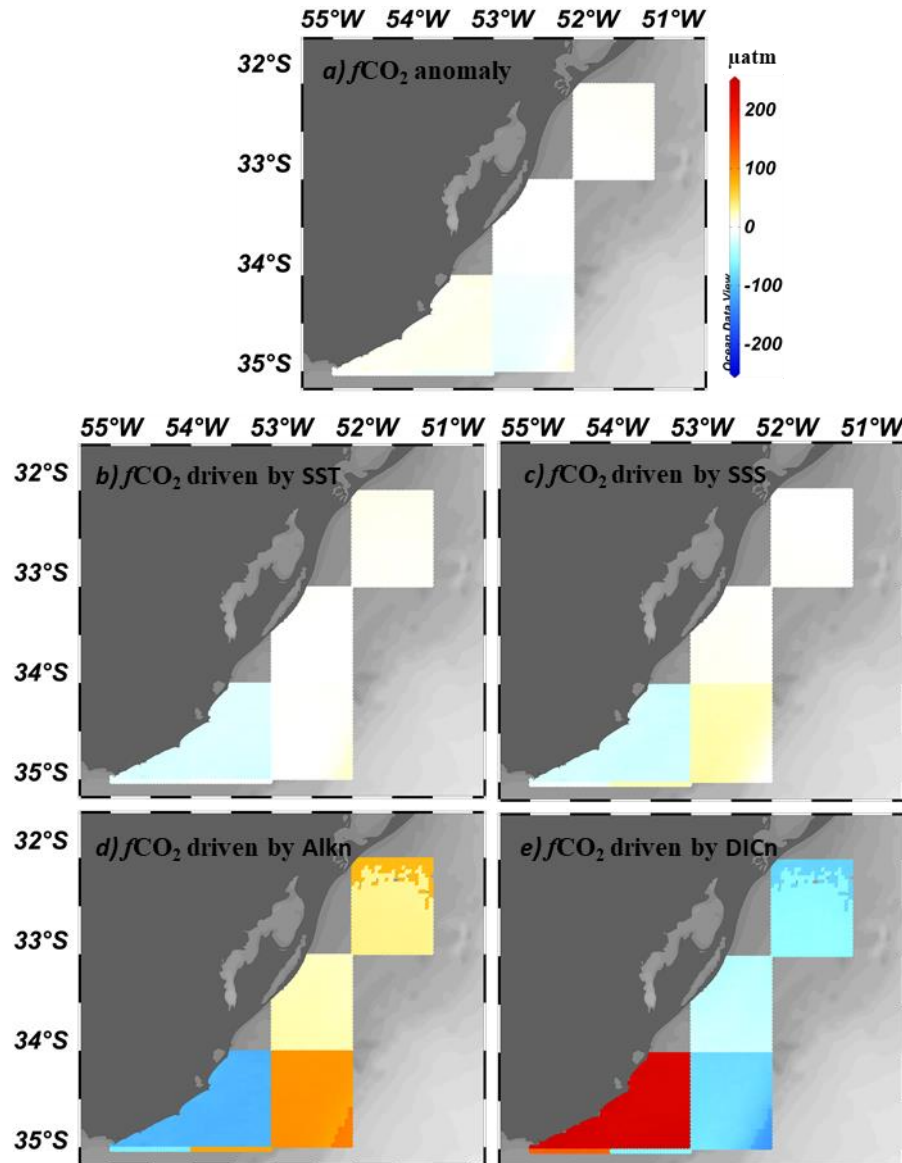


Figure S6. Spatial distribution of the $f\text{CO}_2$ anomalies and $f\text{CO}_2$ drivers in the Plata River Plume region (μatm). Map a) is the spatial distribution of the $f\text{CO}_2$ anomaly; map b) is the spatial distribution of the effect of SST as a driver of $f\text{CO}_2$; map c) is the spatial distribution of the effect of SSS as a driver of $f\text{CO}_2$; map d) is the spatial distribution of the effect of Alk on $f\text{CO}_2$; and map e) is the spatial distribution of the effect of DIC as a driver of $f\text{CO}_2$.

Capítulo IV: Síntese dos resultados e discussão

IV.I – Algoritmos da $f\text{CO}_2$ na água do mar

Dois algoritmos sazonais de $f\text{CO}_2$ na água do mar foram desenvolvidos neste estudo, sendo um para o período de Primavera-Verão e outro para o período de Outono-Inverno. Para o primeiro algoritmo, encontramos os valores de $r^2 = 0.71$ e RMSE = $\pm 13.81 \mu\text{atm}$, e para o algoritmo de Outono-Inverno foram encontrados valores de $r^2 = 0.64$ e RMSE = $\pm 10.05 \mu\text{atm}$. Quando comparados com outros algoritmos desenvolvidos para a região (e.g., [Ito et al. 2005, 2016](#); [Lencina-Avilla et al. 2016](#); [Orselli et al. 2019](#)), os dois algoritmos apresentam valores de r^2 relativamente baixos e RMSE relativamente altos. Porém, nossos algoritmos apresentaram as vantagens de reproduzir a variabilidade da $f\text{CO}_2$ na água do mar em escala espacial superior e não ser limitado sazonalmente, que

são avanços importantes em relação aos algoritmos apresentados em estudos anteriores.

O algoritmo de Outono-Inverno obteve bom desempenho ($r^2 = 0.95$, RMSE = $\pm 16.22 \mu\text{atm}$) no teste de reprodução dos dados do cruzeiro FORSA que estavam inseridos na área de estudo, com melhor desempenho na reprodução dos dados sobre a plataforma continental e talude. No geral, a diferença apresentada entre os valores previstos e modelados de $f\text{CO}_2$ na água do mar apresentaram uma superestimação de aproximadamente 5%, com redução para 3% na região de regime costeiro da ACR. A representação da variabilidade espacial da $f\text{CO}_2$ na água do mar por esse algoritmo foi boa e apresentou uma suavização dos processos de mesoescala observados por [Orselli et al. \(2019\)](#).

IV.II – Distribuição espacial e comportamento temporal da $f\text{CO}_2$ na água do mar

Em geral, a distribuição do $f\text{CO}_2$ na água do mar na região como um todo é controlada pela variação sazonal da SST, com exceção das regiões influenciadas por sistemas de ressurgência e pelo deságue de águas continentais. Em relação a cada região específica, a ACR apresentou a menor oscilação sazonal das regiões estudadas. Essa oscilação menor da $f\text{CO}_2$ na água do mar pode ser associada aos valores quase constantes de produção primária que ocorre ao longo do ano ([Valentin 2001](#)), mas também pode ser associada a baixa resolução dos resultados obtidos na região costeira em comparação à região offshore. A SBB apresentou a maior variabilidade espacial da $f\text{CO}_2$ na água do mar devido a interação que sofre com as outras regiões. Essa região recebe águas com relativamente baixos valores de $f\text{CO}_2$ vindos da

ACR, sofre oscilação sazonal da intensidade do transporte de águas de altos valores de $f\text{CO}_2$ feito pela Corrente do Brasil para a região mais interna da plataforma, e intrusão de águas com baixos valores de $f\text{CO}_2$ vindos da SBS pelo avanço da STSF na direção norte durante o inverno. A SBS foi a região que apresentou a maior oscilação sazonal da $f\text{CO}_2$ e a maior tendência anual. Esses valores podem ser explicados pelas mudanças sazonais extremas nos parâmetros físicos causadas pela influência das plumas do Rio da Prata e da Lagoa Patos-Mirim ([Lefèvre and Moore, 2000](#)), e também pelo comportamento sazonal da STSF ([Piola et al. 2000](#)). A região *offshore* apresentou a distribuição da $f\text{CO}_2$ na água do mar sendo associada a um padrão latitudinal em sua parte mais a leste e sendo altamente influenciada pela oscilação sazonal da Corrente do Brasil na porção mais próxima da quebra de plataforma (e.g., [Ito et al. 2016](#)).

IV.III – Quais são as principais forçantes que controlam a variabilidade da $f\text{CO}_2$ na água do mar na região?

A análise das forçantes responsáveis pela alteração da $f\text{CO}_2$ na água do mar na escala espacial apontaram que o parâmetro com maior influência é o DICn. Em relação aos parâmetros com influência secundária, tanto a SSS e a Alkn se mostraram influentes sobre as águas da plataforma continental, e na região *offshore* esse papel secundário foi atribuído a SST. [Arruda et al. \(2015\)](#) encontraram resultados similares para a forçante principal, porém com papel secundário tanto da SST quanto da Alkn. [Lenton et al. \(2012\)](#) identificaram a Alkn sendo a principal forçante e DICn como a forçante secundária. Apesar das diferenças entre os resultados encontrados neste trabalho e os resultados dos autores citados acima, que podem estar associadas ao tamanho das regiões

analisadas, todos os trabalhos apontaram DICn como um parâmetro importante na variabilidade espacial da $f\text{CO}_2$ na água do mar.

Em relação às forçantes temporais das variações da $f\text{CO}_2$ na água do mar, foi encontrada uma alternância entre SST e DICn. Esse padrão de alternância também foi apontado por [Takahashi et al. \(1993\)](#), [Signorini et al. \(2013\)](#) e [Arruda et al. \(2015\)](#). [Signorini et al. \(2013\)](#) atribuíram essa oscilação aos processos de mistura mais intensos no período de inverno e o declínio biológico que ocorre no período de primavera e verão. A SBB e SBS, as duas regiões afetadas pela oscilação sazonal da STSW, apresentaram as maiores oscilações sazonais das forçantes analisadas, com destaque para a influência exercida pelo DICn em ambas as regiões. A escala da sazonalidade encontrada para a SBB é muito superior à encontrada por [Arruda et al. \(2015\)](#) para todas as forçantes. Para a SBS, foram encontradas as maiores oscilações sazonais para a $f\text{CO}_2$ na água do mar e a maior influência do DICn dentre as regiões analisadas. Esse resultado condiz com o que foi encontrado por [Arruda et al. \(2015\)](#).

Capítulo V: Perspectivas Futuras

Durante o desenvolvimento desse trabalho foram notados certos pontos importantes que podem beneficiar futuros trabalhos na área de estudo do comportamento e distribuição da $f\text{CO}_2$ na água do mar, tanto para a região do sudoeste do oceano Atlântico Sul, quanto para esse tipo de estudo em outras regiões.

- Atualmente, estudos que focaram no desenvolvimento de ferramentas matemáticas para a elaboração de modelos capazes de reproduzir o comportamento e distribuição da $f\text{CO}_2$ e $p\text{CO}_2$ indicaram uma melhor performance de modelos desenvolvidos a partir de *feed-forward neural network* em comparação ao MLR (e.g., [Moussa et al. 2015](#)).
- Nosso estudo utilizou grande parte dos dados *in situ* de $f\text{CO}_2$ e $p\text{CO}_2$ na água do mar disponíveis para a região. Porém, a cobertura espacial e temporal dos dados no hemisfério sul ainda é muito inferior à do hemisfério norte e precisa ser mais desenvolvida, por cruzeiros de pesquisa ou de oportunidade.

Referências Bibliográficas

- Arruda, R., Calil, P. H. R., Bianchi, A. A., Doney, S. C., Gruber, N., Lima, I., and Turi, G. (2015). Air-sea CO₂ fluxes and the controls on ocean surface *p*CO₂ seasonal variability in the coastal and open-ocean southwestern Atlantic Ocean: A modeling study. *Biogeosciences*, 12(19), 5793–5809. <https://doi.org/10.5194/bg-12-5793-2015>
- Bakker, D. C. E., Pfeil, B. Landa, C. S., Metzl, N., O'Brien, K. M., Olsen, A., Smith, K., Cosca, C., Harasawa, S., Jones, S. D., Nakaoka, S., Nojiri, Y., Schuster, U., Steinhoff, T., Sweeney, C., Takahashi, T., Tilbrook, B., Wada, C., Wanninkhof, R., Alin, S. R., Balestrini, C. F., Barbero, L., Bates, N. R., Bianchi, A. A., Bonou, F., Boutin, J., Bozec, Y., Burger, E. F., Cai, W.-J., Castle, R. D., Chen, L., Chierici, M., Currie, K., Evans, W., Featherstone, C., Feely, R. A., Fransson, A., Goyet, C., Greenwood, N., Gregor, L., Hankin, S., Hardman-Mountford, N. J., Harley, J., Hauck, J., Hoppema, M., Humphreys, M. P., Hunt, C. W., Huss, B., Ibánhez, J. S. P., Johannessen, T., Keeling, R., Kitidis, V., Kötzinger, A., Kozyr, A., Krasakopoulou, E., Kuwata, A., Landschützer, P., Lauvset, S. K., Lefèvre, N., Lo Monaco, C., Manke, A., Mathis, J. T., Merlivat, L., Millero, F. J., Monteiro, P. M. S., Munro, D. R., Murata, A., Newberger, T., Omar, A. M., Ono, T., Paterson, K., Pearce, D., Pierrot, D., Robbins, L. L., Saito, S., Salisbury, J., Schlitzer, R., Schneider, B., Schweitzer, R., Sieger, R., Skjelvan, I., Sullivan, K. F., Sutherland, S. C., Sutton, A. J., Tadokoro, K., Telszewski, M., Tuma, M., Van Heuven, S. M. A. C., Vandemark, D., Ward, B., Watson, A. J., and Xu, S. (2016). A multi-decade record of high quality *f*CO₂ data in version 3 of the Surface Ocean CO₂ Atlas (SOCAT). *Earth System Science Data*, 8(2), 383–413. <https://doi.org/10.5194/essd-8-383-2016>
- Benallal, M. A., Moussa, H., Lencina-Avila, J. M., Touratier, F., Goyet, C., El Jai, M. C., Poisson N., and Poisson, A. (2017). Satellite-derived CO₂ flux in the surface seawater of the Austral Ocean south of Australia. *International Journal of Remote Sensing*, 38(6), 1600–1625. <https://doi.org/10.1080/01431161.2017.1286054>
- Bianchi, A. A., Pino, D. R., Perlender, H. G. I., Osiroff, A. P., Segura, V., Lutz, V., Clara, M. L., Balestrini, C. F., Piola, A. R. (2009). Annual balance and seasonal variability of sea-air CO₂ fluxes in the Patagonia Sea: Their relationship with fronts and chlorophyll distribution. *Journal of Geophysical Research*, 114(C3), C03018. <https://doi.org/10.1029/2008JC004854>

Braga, E. S., Chiozzini, V. C., Berbel, G. B. B., Maluf, J. C. C., Aguiar, V. M. C., Charo, M., Molina, D., Romero, S. I., and Eichler, B. B. (2008). Nutrient distributions over the Southwestern South Atlantic continental shelf from Mar del Plata (Argentina) to Itajaí (Brazil): Winter-summer aspects. *Continental Shelf Research*, 28(13), 1649–1661. <https://doi.org/10.1016/j.csr.2007.06.018>

Broecker, W. S. (1974). “NO”, a conservative water-mass tracer. *Earth and Planetary Science Letters*, 23(1), 100–107. [https://doi.org/10.1016/0012-821X\(74\)90036-3](https://doi.org/10.1016/0012-821X(74)90036-3)

Broecker, W. S., and Peng, T.-H. (1982). Tracers in the sea. Lamont-Doherty geological observatory. Palisades, New York.

Cai, W. J., Wang, Z. A., and Wang, Y. (2003). The role of marsh-dominated heterotrophic continental margins in transport of CO₂ between the atmosphere, the land-sea interface and the ocean. *Geophysical Research Letters*, 30(16), 1–4. <https://doi.org/10.1029/2003GL017633>

Calado, L., Gangopadhyay, A., and da Silveira, I. C. A. (2008). Feature-oriented regional modeling and simulations (FORMS) for the western South Atlantic: Southeastern Brazil region. *Ocean Modelling*, 25(1–2), 48–64. <https://doi.org/10.1016/j.ocemod.2008.06.007>

Carvalho, A. da C. de O., Mendes, C. R. B., Kerr, R., Azevedo, J. L. L. de, Galdino, F., and Tavano, V. M. (2019). The impact of mesoscale eddies on the phytoplankton community in the South Atlantic Ocean: HPLC-CHEMTAX approach. *Marine Environmental Research*, 144(2019), 154–165. <https://doi.org/10.1016/j.marenvres.2018.12.003>

Carvalho-Borges, M. de, Orselli, I. B. M., Ferreira, M. L. de C., and Kerr, R. (2018). Seawater acidification and anthropogenic carbon distribution on the continental shelf and slope of the western South Atlantic Ocean. *Journal of Marine Systems*, 187, 62–81. <https://doi.org/10.1016/j.jmarsys.2018.06.008>

Castelao, R. M., and Barth, J. A. (2006). Upwelling around Cabo Frio, Brazil: The importance of wind stress curl. *Geophysical Research Letters*, 33(3), 2–5. <https://doi.org/10.1029/2005GL025182>

de Castro, B. M., and de Miranda, L. B. (1998). Physical oceanography of the western Atlantic continental shelf located between 4 N and 34 S. In *The sea* (11th ed., pp. 209–251). New York: John Wiley & Sons.

Dickson, A. G., and Millero, F. J. (1987). A comparison of the equilibrium constants for the dissociation of carbonic acid in seawater media. Deep Sea Research Part A, Oceanographic Research Papers, 34(10), 1733–1743. [https://doi.org/10.1016/0198-0149\(87\)90021-5](https://doi.org/10.1016/0198-0149(87)90021-5)

Dickson, A. G. (1990). Standard potential of the reaction: $\text{AgCl(s)} + 1/2\text{H}_2\text{g} = \text{Ag(s)} + \text{HCl(aq)}$, and the standard acidity constant of the ion HSO_4^- in synthetic sea water from 273.15 to 318.15 K. The Journal of Chemical Thermodynamics, 22(2), 113–127. [https://doi.org/10.1016/0021-9614\(90\)90074-Z](https://doi.org/10.1016/0021-9614(90)90074-Z)

Fanton d'Andon, O., Mangin, A., Lavender, S., Antoine, D., Maritorena, S., Morel, A., Barrot, G., Demaria, J., and Pinnock, S. (2009). GlobColour—the European Service for Ocean Colour. In Proceedings from 2009 IEEE International Geoscience & Remote Sensing Symposium (IGARSS). IEEE International Geoscience & Remote Sensing Symposium (IGARSS).

Ferreira, A., Stramski, D., Garcia, C. A. E., Garcia, V. M. T., Ciotti, Á. M., and Mendes, C. R. B. (2013). Variability in light absorption and scattering of phytoplankton in Patagonian waters: Role of community size structure and pigment composition. Journal of Geophysical Research: Oceans, 118(2), 698–714. <https://doi.org/10.1002/jgrc.20082>

Howes, E. L., Joos, F., Eakin, M., and Gattuso, J.-P. (2015). The Oceans 2015 Initiative, Part I: An updated synthesis of the observed and projected impacts of climate change on physical and biological processes in the oceans. Studies, (02/15), 52. <https://doi.org/10.3389/fmars.2015.00036>

Ito, R. G., Garcia, C. A. E., and Tavano, V. M. (2016). Net sea-air CO_2 fluxes and modelled $p\text{CO}_2$ in the southwestern subtropical Atlantic continental shelf during spring 2010 and summer 2011. Continental Shelf Research, 119, 68–84. <https://doi.org/http://dx.doi.org/10.1016/j.csr.2016.03.013>

Ito, R. G., Schneider, B., and Thomas, H. (2005). Distribution of surface $f\text{CO}_2$ and air-sea fluxes in the Southwestern subtropical Atlantic and adjacent continental shelf. Journal of Marine Systems, 56(3–4), 227–242. <https://doi.org/10.1016/j.jmarsys.2005.02.005>

Kampel, M. (2003). Estimativa da produção primária e biomassa fitoplânctonica através de sensoriamento remoto da cor do oceano e dados in situ na costa sudeste brasileira. Universidade de São Paulo.

Kerr, R., da Cunha, L. C., Kikuchi, R. K. P., Horta, P. A., Ito, R. G., Müller, M. N., Orselli, I. B. M., Lencina-Avila, J. M., de Orte, M. R., Sordo, L., Pinheiro, B. R., Bonou, F. K., Schubert, N., Bergstrom, E., and Copertino, M. S. (2016). The Western South Atlantic Ocean in a High-CO₂ World: Current Measurement Capabilities and Perspectives. *Environmental Management*, 57(3), 740–752. <https://doi.org/10.1007/s00267-015-0630-x>

Le Quéré, C., Andrew, R. M., Friedlingstein, P., Sitch, S., Hauck, J., Pongratz, J., Pickers, P. A., Korsbakken, J. I., Peters, G. P., Canadell, J. G., Arneth, A., Arora, V. K., Barbero, L., Bastos, A., Bopp, L., Chevallier, F., Chini, L. P., Ciais, P., Doney, S. C., Gkritzalis, T., Goll, D. S., Harris, I., Haverd, V., Hoffman, F. M., Hoppema, M., Houghton, R. A., Hurtt, G., Ilyina, T., Jain, A. K., Johannessen, T., Jones, C. D., Kato, E., Keeling, R. F., Goldewijk, K. K., Landschützer, P., Lefèvre, N., Lienert, S., Liu, Z., Lombardozzi, D., Metzl, N., Munro, D. R., Nabel, J. E. M. S., Nakaoka, S.-I., Neill, C., Olsen, A., Ono, T., Patra, P., Peregon, A., Peters, W., Peylin, P., Pfeil, B., Pierrot, D., Poulter, B., Rehder, G., Resplandy, L., Robertson, E., Rocher, M., Rödenbeck, C., Schuster, U., Schwinger, J., Séférian, R., Skjelvan, I., Steinhoff, T., Sutton, A., Tans, P. P., Tian, H., Tilbrook, B., Tubiello, F. N., van der Laan-Luijkx, I. T., van der Werf, G. R., Viovy, N., Walker, A. P., Wiltshire, A. J., Wright, R., Zaehle, S., and Zheng, B. (2018). Global Carbon Budget 2018. *Earth System Science Data*, 10(4), 2141–2194. <https://doi.org/10.5194/essd-10-2141-2018>

Lee, K., Tong, L. T., Millero, F. J., Sabine, C. L., Dickson, A. G., Goyet, C., G.-H. Park, R. Wanninkhof, R. A. Feely, and R. M. Key (2006). Global relationships of total alkalinity with salinity and temperature in surface waters of the world's oceans. *Geophysical Research Letters*, 33(19), 1–5. <https://doi.org/10.1029/2006GL027207>

Lefèvre, N., and Moore, G. F. (2000). Distribution of the CO₂ partial pressure along an Atlantic meridional transect. *Progress in Oceanography*, 45(3–4), 401–413. [https://doi.org/10.1016/S0079-6611\(00\)00010-0](https://doi.org/10.1016/S0079-6611(00)00010-0)

Legeckis, R., and Gordon, A. L. (1982). Satellite observations of the Brazil and Falkland currents- 1975 to 1976 and 1978. *Deep Sea Research Part A, Oceanographic Research Papers*, 29(3), 375–401. [https://doi.org/10.1016/0198-0149\(82\)90101-7](https://doi.org/10.1016/0198-0149(82)90101-7)

Lencina-Avila, J. M., Ito, R. G., Garcia, C. A. E., and Tavano, V. M. (2016). Sea-air carbon dioxide fluxes along 35°S in the South Atlantic Ocean. *Deep Sea Research Part I: Oceanographic Research Papers*, 115, 175–187. <https://doi.org/10.1016/j.dsr.2016.06.004>

Lenton, A., Metzl, N., Takahashi, T., Kuchinke, M., Matear, R. J., Roy, T., Sutherland, S. C., Sweeney, C., and Tilbrook, B. (2012). The observed evolution of oceanic $p\text{CO}_2$ and its drivers over the last two decades. *Global Biogeochemical Cycles*, 26(2), 1–14. <https://doi.org/10.1029/2011GB004095>

Mahadevan, A., Lévy, M., and Mémery, L. (2004). Mesoscale variability of sea surface $p\text{CO}_2$: What does it respond to?. *Global Biogeochemical Cycles*, 18(1), n/a-n/a. <https://doi.org/10.1029/2003gb002102>

Maritorena, S., D'Andon, O. H. F., Mangin, A., and Siegel, D. A. (2010). Merged satellite ocean color data products using a bio-optical model: Characteristics, benefits and issues. *Remote Sensing of Environment*, 114(8), 1791–1804. <https://doi.org/10.1016/j.rse.2010.04.002>

Matano, R. P., Palma, E. D., and Piola, A. R. (2010). The influence of the Brazil and Malvinas Currents on the Southwestern Atlantic Shelf circulation. *Ocean Science Discussions*, 7(4), 837–871. <https://doi.org/10.5194/os-6-983-2010>

Millero, F. J. (2007). The Marine Inorganic Carbon Cycle. *Chemical Reviews*, 107(2), 308–341. <https://doi.org/10.1021/cr0503557>

Mucci, A., Sundby, B., Gehlen, M., Arakaki, T., Zhong, S., and Silverberg, N. (2000). The fate of carbon in continental shelf sediments of eastern Canada: a case study. *Deep Sea Research Part II: Topical Studies in Oceanography*, 47(3–4), 733–760. [https://doi.org/10.1016/S0967-0645\(99\)00124-1](https://doi.org/10.1016/S0967-0645(99)00124-1)

Olson, D. B., Podestá, G. P., Evans, R. H., and Brown, O. B. (1988). Temporal variations in the separation of Brazil and Malvinas Currents. *Deep Sea Research Part A, Oceanographic Research Papers*, 35(12), 1971–1990. [https://doi.org/10.1016/0198-0149\(88\)90120-3](https://doi.org/10.1016/0198-0149(88)90120-3)

Orselli, I. B. M., Kerr, R., Azevedo, J. L. L. de, Galdino, F., Araujo, M., and Garcia, C. A. E. (2019). The sea-air CO_2 net fluxes in the South Atlantic Ocean and the role played by Agulhas eddies. *Progress in Oceanography*, 170(October 2018), 40–52. <https://doi.org/10.1016/j.pocean.2018.10.006>

Orselli, I. B. M., Kerr, R., Ito, R. G., Tavano, V. M., Mendes, C. R. B., and Garcia, C. A. E. (2018). How fast is the Patagonian shelf-break acidifying? *Journal of Marine Systems*, 178(July 2017), 1–14. <https://doi.org/10.1016/j.jmarsys.2017.10.007>

Padin, X. A., Vazquez-Rodriguez, M., Castaaoo, M., Velo, A., Alonso-Perez, F., Gago, J., Gilcoto, M., Álvarez, M., Pardo, P. C., de la Paz, M., Ríos, A. F., and Perez, F. F. (2010). Air-Sea CO₂ fluxes in the atlantic as measured during boreal spring and autumn. *Biogeosciences*, 7(5), 1587–1606. <https://doi.org/10.5194/bg-7-1587-2010>

Palma, E. D., and Matano, R. P. (2009). Disentangling the upwelling mechanisms of the South Brazil Bight. *Continental Shelf Research*, 29(11–12), 1525–1534. <https://doi.org/10.1016/j.csr.2009.04.002>

Palma, E. D., Matano, R. P., and Piola, A. R. (2008). A numerical study of the Southwestern Atlantic Shelf circulation: Stratified ocean response to local and offshore forcing. *Journal of Geophysical Research*, 113(11), 1–22. <https://doi.org/10.1029/2007JC004720>

Piola, A. R., Campos, E. J. D., Möller, O. O., Charo, M., and Martinez, C. (2000). Subtropical Shelf Front off eastern South America. *Journal of Geophysical Research: Oceans*, 105(C3), 6565–6578. <https://doi.org/10.1029/1999JC000300>

Piola, A. R., Matano, R. P., Palma, E. D., and Mo, O. O. (2005). The influence of the Plata River discharge on the western South Atlantic shelf, 32(1), 4–7. <https://doi.org/10.1029/2004GL021638>

Provost, C., Garcia, O., and Garçon, V. (2008). Analysis of satellite sea surface temperature time series in the Brazil-Malvinas Current Confluence region: Dominance of the annual and semiannual periods. *Journal of Geophysical Research: Oceans*, 97(C11), 17841–17858. <https://doi.org/10.1029/92jc01693>

Rodrigues, R. R., and Lorenzetti, J. A. (2001). A numerical study of the effects of bottom topography and coastline geometry on the Southeast Brazilian coastal upwelling. *Continental Shelf Research*, 21(4), 371–394. [https://doi.org/10.1016/S0278-4343\(00\)00094-7](https://doi.org/10.1016/S0278-4343(00)00094-7)

Sarmiento, J. L., and Gruber, N. (2006). Ocean Biogeochemical Dynamics, Chapter 1. *Ocean Biogeochemical Dynamics*, (January). Retrieved from <http://press.princeton.edu/titles/8223.html>

Schlitzer, R. (2018). Ocean Data View. Retrieved from odv.awi.de

Schuster, U., McKinley, G. A., Bates, N., Chevallier, F., Doney, S. C., Fay, A. R., González-Dávila, M., Gruber, N., Jones, S., Krijnen, J., Landschützer P., Lefèvre N., Manizza M., Mathis J., Metzl N., Olsen A., Rios A. F., Rödenbeck C., Santana-Casiano J. M., Takahashi T., Wanninkhof R., and Watson, A. J. (2013). An assessment of the Atlantic and Arctic sea-air CO₂ fluxes, 1990–2009. *Biogeosciences*, 10(1), 607–627. <https://doi.org/10.5194/bg-10-607-2013>

Signorini, S. R., Mannino, A., Najjar, R. G., Friedrichs, M. A. M., Cai, W. J., Salisbury, J., Aleck Wang, Z., Thomas, H., and Shadwick, E. (2013). Surface ocean pCO₂ seasonality and sea-air CO₂ flux estimates for the North American east coast. *Journal of Geophysical Research: Oceans*, 118(10), 5439–5460. <https://doi.org/10.1002/jgrc.20369>

Stephens, M. P., Samuels, G., Olson, D. B., Fine, R. a., and Takahashi, T. (1995). Sea-air flux of CO₂ in the North Pacific using shipboard and satellite data. *Journal of Geophysical Research*, 100(C7), 13,571–13,583. <https://doi.org/10.1029/95JC00901>

Stramma, L., and Peterson, R. G. (1990). The South Atlantic Current. *Journal of Physical Oceanography*, 20(6), 846–859. [https://doi.org/10.1175/1520-0485\(1990\)020<0846:TSAC>2.0.CO;2](https://doi.org/10.1175/1520-0485(1990)020<0846:TSAC>2.0.CO;2)

Takahashi, T., Olafsson, J., Goddard, J. G., Chipman, D. W., and Sutherland, S. C. (1993). Seasonal variation of CO₂ and nutrients in the high-latitude surface oceans: A comparative study. *Global Biogeochemical Cycles*, 7(4), 843–878. <https://doi.org/10.1029/93GB02263>

Takahashi, T., Sutherland, S. C., and Kozyr, A. (2018). Global Ocean Surface Water Partial Pressure of CO₂ Database: Measurements Performed During 1957–2017 (Version 2017) (Vol. 088). Retrieved from https://www.nodc.noaa.gov/oceanacidification/stewardship/data_portal.html

Takahashi, T., Sutherland, S. C., Wanninkhof, R., Sweeney, C., Feely, R. A., Chipman, D. W., Hales, B., Friederich, G., Chavez, F., Sabine, C., Watson, A., Bakker, D. C. E., Schuster, U., Metzl, N., Yoshikawa-Inoue, H., Ishii, M., Midorikawa, T., Nojiri, Y., Kötzinger, A., Steinhoff, T., Hoppema, M., Olafsson, J., Arnarson, T. S., Tilbrook, B., Johannessen, T., Olsen, A., Bellerby, R., Wong, C. S., Delille, B., Bates, N.R., and de Baar, H. J. W. (2009). Climatological mean and decadal change

in surface ocean $p\text{CO}_2$, and net sea-air CO_2 flux over the global oceans. Deep-Sea Research Part II: Topical Studies in Oceanography, 56(8–10), 554–577. <https://doi.org/10.1016/j.dsr2.2008.12.009>

Takahashi, T., Sutherland, S. C., Chipman, D. W., and Goddard, J. G. (2014). Climatological Distributions of pH, $p\text{CO}_2$, Total CO_2 , Alkalinity, and CaCO_3 Saturation in the Global Surface Ocean Contributed by. <https://doi.org/10.3334/CDIAC/OTG.NDP094>

Uppström, L. R. (1974). The boron/chlorinity ratio of deep-sea water from the Pacific Ocean. In Deep Sea Research and Oceanographic Abstracts (Vol. 21, pp. 161–162).

Valentin, J. L. (2001). The Cabo Frio Upwelling System, Brazil (Vol. 144, pp. 97–105). https://doi.org/10.1007/978-3-662-04482-7_8

Van Heuven, S., Pierrot, D., Rae, J. W. B., Lewis, E., and Wallace, D. W. R. (2011). MATLAB program developed for CO_2 system calculations. ORNL/CDIAC-105b. Carbon Dioxide Information Analysis Center, Oak Ridge National Laboratory, US Department of Energy, Oak Ridge, Tennessee, 530.

Zembruscki, S., 1979. Geomorfologia da margem continental sul brasileira e das bacias oceânicas adjacentes, in: Projeto REMAC. Geomorfologia da margem continental brasileira e das áreas oceânicas adjacentes. PETROBRAS, CENPES e DINTEP (Série REMAC, nº7), Rio de Janeiro, pp. 129–177. In portuguese.

Zhu, Y., Shang, S., Zhai, W., and Dai, M. (2009). Satellite-derived surface water $p\text{CO}_2$ and air-sea CO_2 fluxes in the northern South China Sea in summer. Progress in Natural Science, 19(6), 775–779. <https://doi.org/10.1016/j.pnsc.2008.09.004>